SYNTHESIS OF SUPPPORTED METALLOCENE CATALYSTS AND APPLICATION TO COPOLYMERIZATION OF ETHYLENE WITH 4-METHYL-1-PENTENE

BY

SAGIR ADAMU

A Thesis Presented to the
DEANSHIP OF GRADUATE STUDIES

KING FAHD UNIVERSITY OF PETROLEUM & MINERALS

DHAHRAN, SAUDI ARABIA

In Partial Fulfillment of the
Requirements for the Degree of

MASTER OF SCIENCE

In

CHEMICAL ENGINEERING

MAY 2013

KING FAHD UNIVERSITY OF PETROLEUM & MINERALS

DHAHRAN- 31261, SAUDI ARABIA

DEANSHIP OF GRADUATE STUDIES

This thesis, written by **ADAMU SAGIR** under the direction his thesis advisor and co-advisor, and approved by his thesis committee, has been presented and accepted by the Dean of Graduate Studies, in partial fulfillment of the requirements for the degree of **MASTER OF SCIENCE IN CHEMICAL ENGINEERING**.

Dr. Zuhair Omar Malaibari
(Advisor)

Dr. Usamah A. Al-Mubaiyedh
Department Chairman

Dr. Muhammad Atiqullah
(Co-Advisor)

Dr. Salam A. Zummo
Dean of Graduate Studies

Dr Mamdouh A. Al-Harthi
(Member)

28/5/13
Date

Dr. Mohammad Mozahar Hossain
(Member)

Dr. Shaikh Asrof Ali
(Member)

DEDICATION

To my parents Adamu Salihu and Rabiatu Usman, and my wife Hafiza Musa.

ACKNOWLEDGMENTS

I highly thank my advisor Dr. Zuhair Omar Malyabari for nicely coordinating this work between the Department of Chemical Engineering and the Center of Research Excellence in Petroleum Refining & Petrochemicals (CoRE-PRP); completing the academic formalities, review of the thesis report, and recommendations. I owe a lot of gratitude to my co-advisor Dr. Muhammad Atiqullah (Senior Research Engineer and Full Professor, CRP), who formulated the thesis topic, meticulously guided the entire work, and fully supported the research expense through his project titled *Development of Novel High Performance Supported Catalysts for Ethylene Polymerization* which is sponsored by King Abdulaziz City for Science & Technology (KACST) through the Science & Technology Unit at KFUPM through Project No. 08-PET-90-4 as part of the National Science and Technology Innovation Plan (NSTIP). I also thank my thesis committee members Dr. Mamdouh A. Al-Harthi and Dr. Mohammed Mozahar Hussain (from the Department of Chemical Engineering); and Dr. Shaikh Asrof Ali (from the Department of Chemistry) for their constructive criticism and recommendation on this work. I appreciate Dr. Abdul-Hamid M. Emwas, NMR Core Laboratory, King Abdullah University of Science & Technology (KAUST) for kindly conducting the highly time-consuming NMR analysis of the synthesized polymers.

I am highly thankful to Mr. Anwar Hossaen, CRP for his great help in the overall synthesis work; to Mr. Ikram Hussain, CRP for logistical support, and to Mr. Sarath P. Unnikri of the Department of Chemical Engineering for the Crystaf analysis.

In conclusion, I acknowledge my profound gratitude to CoRE-PRP and KFUPM for offering me research assistantship for my MS study. My special thanks are due to CRP, CoRE-PRP, and the Department of Chemical Engineering for the use of their laboratory instruments.

TABLE OF CONTENTS

LIST OF SCHEMES

LIST OF FIGURES

LIST OF TABLES

LIST OF ABBREVIATIONS

MAO	Methyaluminoxane
$(^{n}BuCp)_2ZrCl_2$	Bis(n-Butyl Cyclopentadienyl) Zirconium Chloride
4-M1P	4-Methyl-1-pentene
TMA	Trimethylaluminum
TIBA	Tiisobutylaluminum
TCB	1,2,4-Trichlorobenzene
$(\eta\text{-}C_5H_5)_2M$	Symmetrical, classical, “sandwich” metallocene structure
Crystaf	Crystallization analysis and fractionation
GPC	Gel permeation chromatography
FTIR	Fourier transforms infrared spectroscopy
^{13}C NMR	Carbon 13 Nuclear magnetic resonance
DSC	Differential scanning calorimetry
SSA	Successive self-nucleation and annealing
LTD	Lamellar thickness distribution
SLD	Sequence length distribution

ABSTRACT (ENGLISH)

Full Name: Adamu Sagir

MS Thesis Title: Synthesis of Supported Metallocene Catalysts and Application to Copolymerization of Ethylene with 4-Methyl-1-pentene

Major Field: Chemical Engineering

Date of Degree: May 2013

In the family of commodity polyolefins, linear low density polyethylene (LLDPE)—a copolymer of ethylene and α-olefin—is the latest addition. LLDPEs have wide applications. Therefore, all the nine (9) Saudi petrochemical industries produce LLDPEs. The total production volume is about 4 million metric tons per annum which places Saudi Arabia as the largest LLDPE producer in the Middle East and within top five in theworld. LLDPEs are mostly produced by low pressure conventional supported catalysts. In this regard, the versatility of catalyst type and polymer synthesis methodology creates new knowledge. This eventually makes new polymeric materials for advanced applications. Metallocenes are a modern innovation in polyolefin catalysis, and have several advantages over the Ziegler-Natta catalysts. Hence, the overall objective of the proposed study is to synthesize various supported metallocene catalysts with varying anions, and apply them to prepare ethylene-1-hexene and ethylene-4-methyl-1-pentene copolymers.

In this work, the supported metallocene catalysts were prepared using the following order: dehydroxylated silica (alone or functionalized with $ClSiMe_2Cl$), methylaluminoxane (MAO) cocatalyst and $(^nBuCp)_2ZrCl_2$). These catalyst systems were applied to homo- or copolymerize ethylene with 4-methyl-1-pentene as well as its isomer 1-hexene, using solution, in-situ, and slurry polymerization trials. In the latter two modes of polymerizations, no MAO was fed separately into the reactor. The variations in the polymerization processes varied the MAO cocatalyst anions. The effects of the resulting cocatalyst anions on polymerization performance and the product properties were elaborately studied by determining the reactor operability and catalyst productivity, and by characterizing the polymers using gel permeation chromatography, Fourier Transform infra-red spectroscopy, ^{13}C NMR spectroscopy, differential scanning calorimetry (DSC), successive self-nucleation and annealing (SSA) thermal fractionation, and crystallization fractionation technique (Crystaf).

This study has advanced the fundamental understanding of supported metallocene catalysis and development of ethylene-α-olefin copolymers as follows. The

functionalizing linker $ClSiMe_2Cl$ did not affect the catalyst productivity. The supported systems showed similar productivity as the solution polymerization which is hardly reported in the literature. The distributive as well as the bulk properties of the polymers varied with the MAO anion design. This understanding produced selected application-specific polymers. The copolymerization mechanism was found to be well predicted by the first order Markovian (terminal) model. $ClSiMe_2Cl$ suppressed chain transfer reactions in the supported catalyst. Microstructural properties, determined using ^{13}C NMR/SSA-DSC, elaborated how supported MAO anions made copolymer backbones with compositional heterogeneity. The nonisothermal Avrami-Erofeev crystallization model well matched the experimental data notably for Avrami-Erofeev index of 2 to 3. This shows bi- and tri-dimensional crystal growth. The apparent crystallization activation energy, predicted by the Avrami-Erofeev crystallization model, did not depend on the cooling rates. This finding, therefore, refutes the concept of *instantaneous variable crystallization activation energy*, articulated in the literature. Furthermore, the crystallization model successfully elaborated the influence of compositional heterogeneity on copolymer crystallization behavior.

So far as product development is concerned, this study shows how to synthesize LLDPEs that are blocky and more degradation-resistant, have improved processability (fairly low melting point and crystallinity), and that can be used for load-bearing applications.

ABSTRACT (ARABIC)

ملخص الرسالة

الاسم الكامل : صغير آدمو

عنوان الرسالة : تركيب الحفازات المدعمة بالميتالوسين و تطبيقها في بلمرة الإثيلين مع 4-ميثيل-1-بنتين

التخصص: الهندسة الكيميائية

تاريخ الدرجة : رجب 1434(مايو 2013)

في عائلة البولي أوليفينات ، يعد البولي إثيلين منخفض الكثافة الخطية (LLDPE)— الذي هو عبارة عن بوليمر مكون من الإثيلين(ethylene) و ألفا أوليفين(α-olefin)—الإضافة الأحدث في هذه العائلة و له العديد من التطبيقات . و لهذا فإن كل شركات البتروكيماويات في السعودية والبالغ عددها تسع شركات تنتج هذا البولي إثيلين. حجم الإنتاج الكلي في المملكة العربية السعودية حوالي 4 مليون طن سنويا مما يجعلها أكبر منتج للبولي إثيلين منخفض الكثافة الخطية في الشرق الأوسط و من الخمس الأوائل عالميا أيضا. تنتج البولي إثيلينات منخفضة الكثافة الخطية غالبا عند ضغط منخفض و بوجود الحفاز . وفي هذا الصدد ، فإن التعدد في نوع الحفاز و طريقة تركيب البوليمر أنشأت معرفة جديدة و الذي في نهاية المطاف ادي الى ايجاد بوليمرات جديدة ذات تطبيقات متقدمة. تعد الميتالوسين قفزة رائدة في صناعة البولي أوليفينات الحفزية و لهذا العديد من الإيجابيات مقارنة بحفازات زيجلر- ناتّا (Ziegler-Natta). يهدف هذا البحث الى تركيب مختلف الحفازات الميتالوسينية باستخدام مختلف الأنيونات (anions) ومن ثم استخدام هذه الحفازات في تحضير بوليمر إثيلين -1-هيكسان و بوليمير إثيلين-4-ميثيل-1-بنتين .

تم في هذه الدراسة تحضير الحفازات المدعمة بالميتالوسين باستخدام الترتيب التالي : السيليكا منزوعة الهيدروكسيل (بمفردها أو مرتبطة بالمركب $ClSiMe_2Cl$) و الحفاز المصاحب الميثيل ألومينوكسان و ($(^nBuCp)_2ZrCl_2$). هذه الحفازات استعملت في بلمرة الإيثيلين مع 4-ميثيل-1- بنتين و أيضا الإيزومير 1-هيكسان ، باستخدام طريقة المحلول الموضعي ، و طريقة البلمرة الشبيهة بالطين (Slurry polymerization) . في الطريقتين الأخيرتين للبلمرة لم تُدخَل مادة MAO منفردة في المفاعل. الاختلافات هى عمليات البملرة غيرت الأنيونات لحفازات MAO . تمت دراسة تأثيرات هذه الأنيونات للحفازات على أداء البلمرة و خصائص المنتجات من خلال تحديد تشغيلية المفاعل و إنتاجية الحفاز و توصيف خصائص البوليمرات من خلال السماحية الهلامية اللونية (GPC)، FTIR الطيفي, ^{13}C NMR الطيفي, المسح الضوئي الحراري(DSC) , التنوية المتتابعة و التليين(SSA), و التقنيية الجزئية لعمل البلورات(Crystaf) .

ولقد ادت هذه الدراسة الى تحسين الفهم الجوهري للحفازات المدعمة بالميتالوسين و تطوير إنتاج البولي أوليفنات المحتوية على(إثيلين –ألفا) كما يلي. لم يؤثر الرابط الوظيفي $ClSiMe_2Cl$ في إنتاجية الحفاز . أظهرت الأنظمة المدعمة إنتاجية مشابهة لتلك من البلمرة المحلولية التي لم تذكر في الأبحاث السابقة إلا قليلا . اختلفت خصائص البوليمرات باختلاف تصميم الأنيونات لـ MAO. أنتج هذا الفهم تطبيقات مختارة للبوليمرات . تم التوصل إلى أنّ تقنية البلمرة يمكن التنبؤ بها باستخدام النموذج الأول لماركوف . اخمد المركب $ClSiMe_2Cl$ سلسلة التفاعلات التحويلية في الحفاز المدعم . أظهرت الخصائص التركيبية الدقيقة و استخدام ^{13}C NMR/SSA-DSC كيف أن الأنيونات لـ MAO المدعم أنشأت دعائم البوليمر الأساسية باستخدام عدم التجانس التركيبي . طابق نموذج أفرامي-إيروفيف غير المتساوي حراريا للتبلر النتائج التجريبية بشكل ملحوظ بمؤشر أفرامي-إيروفيف مقداره من 2

إلى 3 و هذا يظهر نمو بلوري ثنائي و ثلاثي. لم تعتمد طاقة التنشيط الظاهرية للبلورة على معدلات التبريد كما هو متوقع في نموذج أفرامي-إروفيف للتبلر . و لهذا فإن هذه النتيجة تدحض مبدأ طاقة التنشيط البلورية اللحظية المتغيرة المذكورة في الأبحاث السابقة . كما أن نموذج البلورة قد أظهر جليا التأثير التركيبي غير المتجانس على سلوك بلورة البوليمر .

و لإن المهم هو تطوير المنتج فإن هذه الدراسة تظهر كيف أن تركيب البولي إثيلين منخفض الكثافة الممتلئة و التي تقاوم تدهور الخواص ادت الى تحسين عملية المعالجة (انخفاض معتبر في درجة الانصهار و درجة البلورة) و التي يمكن أن تستخدم في التطبيقات التي تشمل مقاومة و تحمل أثقال .

CHAPTER 1

INTRODUCTION

1.1 General Catalyst Background

The versatility of catalyst type and polymer synthesis methodology creates new knowledge. This eventually makes new polymeric materials for advanced applications. In polyolefin thermoplastics, from such a perspective, the following factors are important: (i) the selection of appropriate precatalysts, (ii) the synthesis of supported/heterogeneous catalysts, and (iii) the α-olefin to be used in copolymerization (which is a very multipurpose polymer synthesis route).

In polyolefin catalysis, metallocenes are a modern innovation. Unlike the Ziegler-Natta (Z-N) catalysts, metallocenes have the following advantages. They have remarkable structural variations. This happens through bridge modifications and substitutions in the cyclopentadienyl ligand and its analogues. Consequently, they can regulate the comonomer-introduced composition (branch) distribution, microstructures, and structural/enchainment defects of ethylene-α-olefin copolymers (linear low density polyethylenes LLDPEs) in a highly versatile fashion. LLDPE has density, crystallinity, melting behavior, processing characteristics and thermal, rheological, and mechanical properties that significantly differ from those of low density polyethylene (LDPE) and high density polyethylene (HDPE). Hence, LLDPE has a series of applications superior to those of LDPE and HDPE. Metallocenes, particularly in solution polymerization, show much higher activity than Z-N catalysts [Ewen 1984, Kaminsky 1985a, Kaminsky

1985b, Giannetti 1985, Tsutsui 1988, Schneider 1997, Yano 1999, Chu 2000, Wahner 2003, Lobón-Poo 2006, Kissin 2008a].

Because of the above advantages, aggressive research continues worldwide in metallocene-catalyzed olefin polymerization. However, several challenges face the supported/heterogenized metallocene catalysts. These include the following [Hoff 2010; Thomas 2005, Halatky 2000, Rappe 2000, Coates 2000, Angermund 2000, Helmut 2000, Severn 2005, Severn's book, Janiak 2006, Atiqullah 1997, Atiqullah 2008, Choi and Soares 2012]:

i. Maintain the single-site characteristics of metallocenes upon heterogenization;

ii. Overcome the significant drop in catalyst activity;

iii. Prevent catalyst leaching (that causes severe reactor fouling, and damages the polymer particle morphology); and

iv. Eliminate the separate feeding of the methylaluminoxane (MAO) cocatalyst (which gels and degrades during feeding, and which is very costly).

Therefore, this study focuszsed on the synthesis of supported metallocene catalysts using silica, a combination of unpublished functionalizing linker, MAO, and $(^{n}BuCp)_2ZrCl_2$. Note that the following impregnation order—silica/methylaluminoxane (MAO) cocatalyst/zirconocene—offers, in general, higher catalyst activity than the other two routes ([support/(cocatalyst + metallocenes)], and [silica/metallocenes, activated by feeding cocatalyst during polymerization]) [Hoff 2010; Thomas 2005; Halatky 2000; Rappe 2000; Coates 2000;Angermund 2000; Janiak 2006; Olabisi 1997; Choi and Soares

2012]. MAO will be used because of its very high co-catalyzing performance. However, it will not be used as a separate cocatalyst to avoid some of the disadvantages listed above. Silica will be used as the support because of its stability at high temperatures; availability with varying pore sizes, volumes, and surface areas; low price; and very large volume usage by the industry [Choi and Soares 2012]. On the other hand, $(^{n}BuCp)_2ZrCl_2$ is well known for its stability, commercial availability with reasonable price, capability of polymerizing ethylene with high activity in solution, and considerable use by researchers to synthesize supported metallocene catalysts [Atiqullah 2007, Białek and Czaja 2006, Grieken et al. 2007a, Paredes 2007, Paredes 2011, Lee et al. 2012].

1.2 Problem Statement

The niche for particularly new contributions by the proposed study to the literature is summarized below. This is divided into two parts. The first part concerns the synthesis of new supported $(^{n}BuCp)_2ZrCl_2$s, and the second part addresses ethylene-α-olefin copolymerization.

As far as heterogeneous metallocene catalysts are concerned, the major contribution, in this study, stem from the application of the proposed unpublished functionalizing linker. These can be represented by the general formula M_1Cl_3:Cl~~~M_2~~~Cl where M_1 and M_2 are two varying metallic Lewis acid centers (M_1 has stronger Lewis acidity than M_2); the chloride (Cl) ligand is capable of bonding with the isolated hydroxyl group of silica surface; and ~~~ stands for —$(CH_2)_n$— spacers. In supported metallocenes, a number of technical issues are withstanding. One important item, in this regard, is the exact role that the linker plays. Several views have been expressed, which are listed

below [Kissin 2008b; Hoff 2010; Chen 2000, Pédeutour 2001, Thomas 2005, Halatky 2000, Rappe 2000, Coates 2000, Angermund 2000, Helmut 2000, Severn 2005, Severn 2008, Janiak 2006, Atiqullah 1997, Atiqullah 2008, Atiqullah 2010, Choi and Soares 2012]:

i. The linker vertically partitions the metallocenes which prevents the precatalysts from deactivation;

ii. It minimizes the steric encumberance; and

iii. It regulates the Lewis acidity of Al in MAO;

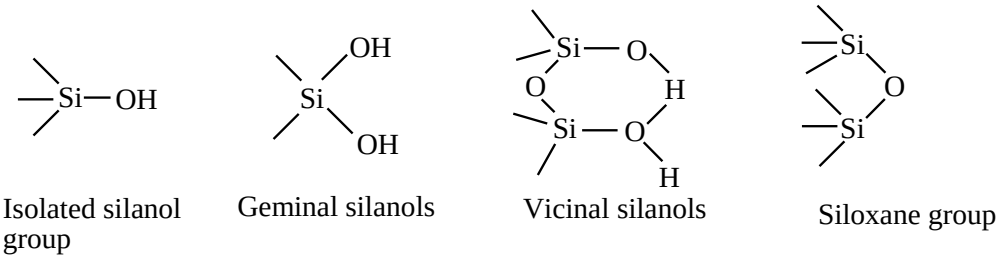

Isolated silanol group | Geminal silanols | Vicinal silanols | Siloxane group

Scheme 1.1: Typical silica surface functionalities.

This study proposes that through ingenious design of the supported MAO anion, the above issue can be better addressed. Accordingly, the linker M_1Cl_3:Cl~~~M_2~~~Cl has been formulated.

Note that silica and MAO are the two major sources of heterogeneity. Silica is amorphous and heterogeneous, comprising tetrahedral SiO_4 units, siloxane bridges $(Si–O–Si)_n$, and silanols RSi–OH (as surface terminations). Siloxane bridges can be typically 6 to 10 member rings, while silanols can be geminal, vicinal, and isolated [Zhuravlev 2006; Gajan 2011]. See Scheme 1.1. On the other hand, MAO is represented by the

formula $(AlOMe)_n \bullet (AlMe_3)_m$ where *n* varies between 6 to 13 while m ranges from 1 and 4. It maintains cage structures having dynamic equilibrium between trimethylaluminum (TMA) and oligomers of methylaluminoxane $(-CH_3OAl-)_n$. The cage structures feature four-coordinate aluminum (Al) and three-coordinate oxygen (O) centers, comprising Al–O and Al–Me bonds [Chen 2000; Zurek 2001a; Zurek 2001b; Zurek 2002a; Zurek 2002b; Negureanu 2006; Linnolahti 2008]. See Scheme 1.2.

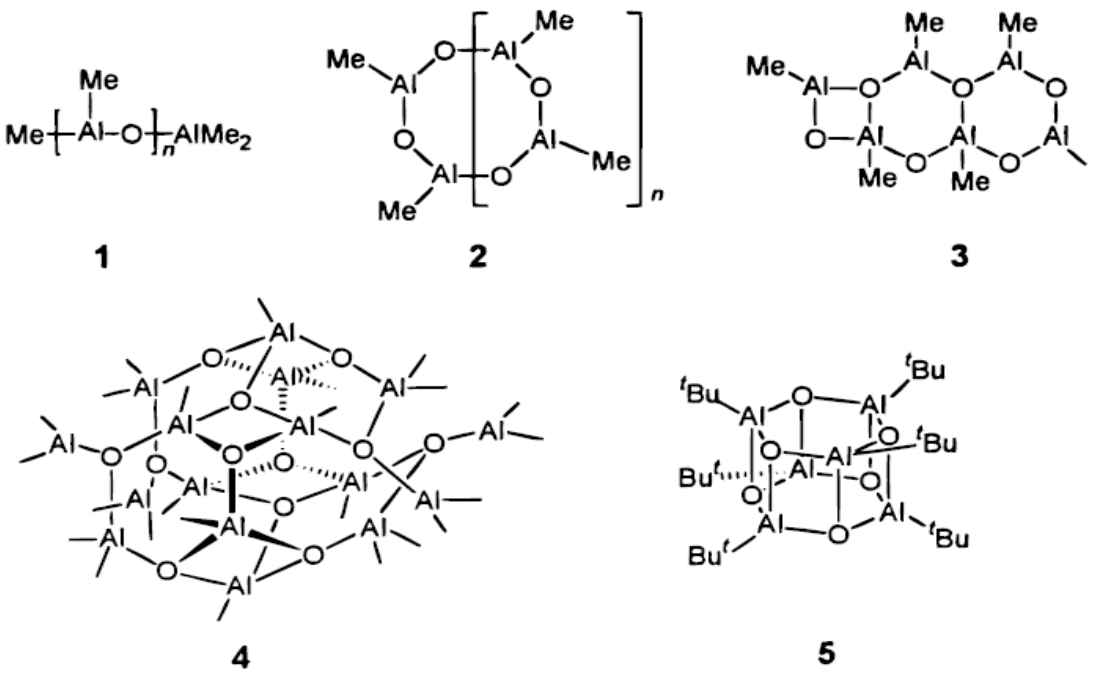

Scheme 1.2: Cage structure of methylaluminoxane (MAO) (4) and tert-butylaluminoxane.

To establish assess the effects of this catalytic characteristic on copolymerization activity, polymerization mechanism, catalyst surface chemistry, comonomer and segregation effects [Atiqullah 1988, 1990, 1993], copolymer microstructures, and their influence on polymer thermal behaviors is, therefore, worth investigation. This will eventually add new insight to this subject and broaden our comprehension. To the best of

our knowledge, this has not been done as we have proposed above though a good number of review reports, book chapters, and books [Kissin 2008b; Hoff 2010; Chen 2000, Pédeutour 2001, Thomas 2005, Halatky 2000, Rappe 2000, Coates 2000, Angermund 2000, Helmut 2000, Severn 2005, Severn 2008, Janiak 2006, Atiqullah 1997, Atiqullah 2008, Atiqullah 2010, Choi and Soares 2012] that discuss various aspects of heterogeneous metallocene catalysis (applied to olefin polymerization) are available.

Now, we discuss the second part—ethylene-α-olefin copolymerization. The review of the literature concerning the application of metallocenes to synthesize ethylene-α-olefin copolymers concludes the following. Metallocenes, both supported and unsupported, have been fairly applied to synthesize ethylene-1-hexene copolymers. However, ethylene-4-methyl-1-pentene (4-M1P) copolymers have not been synthesized using supported/heterogeneous metallocenes [See Chapter 2]. Selected unsupported metallocenes have been used, which are listed in Table 2.6. Note that 4-methyl-1-pentene is branched whereas 1-hexene is linear. The commonality is that they are isomers of each other. See Scheme 1.3. Therefore, it will be very interesting to investigate the branch-induced isomeric copolymerization behaviors.

Structure of 4-methyl-1-pentene

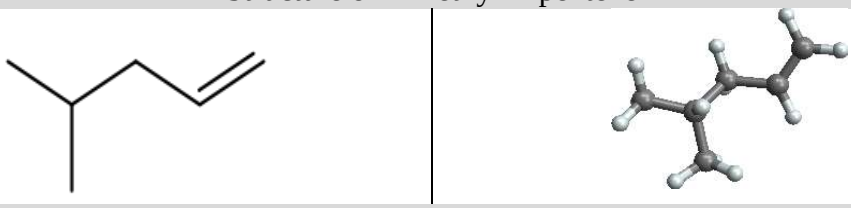

Structure of 1-hexene

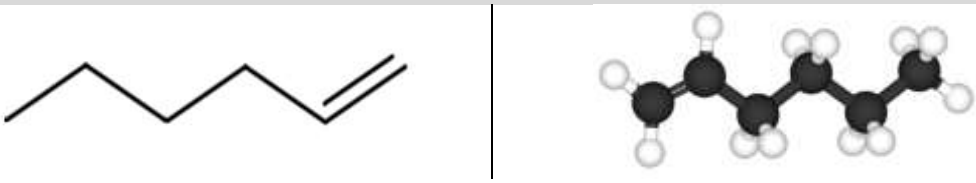

Scheme 1.3: Structural representations of 4-methyl-1-pentene and 1-hexene.

1.3 Objectives

1 Investigate the role that the proposed functionalizing linker is expected to play in context of the present heterogeneous metallocene catalysis.

2 Assess the influence of the proposed supported catalysts on ethylene-4-methyl-1-pentene and ethylene-1-hexene copolymer compositional heterogeneity and highlight the branch-induced isomeric copolymerization behaviors.

3 Evaluate the effects of the design of supported MAO anion on copolymerization activity, copolymerization mechanism comonomer, segregation effects, catalyst surface chemistry and copolymer thermal behaviors.

4 Model the effect of copolymer backbone compositional heterogeneity on the crystallization kinetics and cryallization mechanism.

5 Propose the scope of product development based on the knowledge to be generated herein.

CHAPTER 2

LITERATURE REVIEW

2.1 Ethylene Polymerization Catalysts

Ethylene polymerization catalysts can be broadly divided into Ziegler–Natta, Phillips/Chrome, metallocenes, and post-metallocene catalysts. Ziegler–Natta catalysts manufacture commercial polyolefins since 1956. They mainly comprise $TiCl_4$ supported on $MgCl_2$ and are activated by aluminum alkyl cocatalysts. They show high activity and offer excellent morphology of polymer particle. Processes catalyzed by Ziegler–Natta catalysts include production of low-density polyethylene (LDPE) high-density polyethylene (HDPE), linear low-density polyethylene (LLDPE), and isotactic polypropylene. They widened the properties polyolefin by accuarately controlling their degree of branching as well as polymer chain orientations (Choi and Soares et al., 2012).

The Phillips/Chrome catalysts consist of chromium oxides, mainly supported on silica. It was patented by Hogan and Banks in 1958. Phillips/Chrome catalyst are used to produce more than 30% of the world polyethyelenes. The success of the Phillips polymerization process could be traced to its versatility—producing over 50 different types of LLDPE and HDPE [Groppo et al. 2005]. Furthermore, they work without any cocatalyst (activator). Hence, the catalyst preparation and the consequent production processes are relatively simple. However, they must be treated at high temperatures (temperature range) to become active [Choi and Soares 2012].

Metallocene catalysts are composed of group IV transition metal (commonly Titanium, Zirconium, and Hafnium), substituted cyclopentadienyl ligands and halogen ligands. The metal center is π-bonded to indenyl or cyclopentadienyl ligands, which may have different alkyl or silyl groups. Ziegler–Natta and Phillips catalysts are multi-sited catalysts which give polyolefins having broad molecular weight distributions. On the other hand, Metallocene catalysts are single-sited (in solution) and therefore produce polyethylenes with narrow molecular weight distributions, uniform copolymer composition distributions, and lower polydispersity indices [Choi and Soares 2012].

Post-metallocene catalysts constitute another class of catalysts for olefin polymerization. They were so named to refer to the generation of catalysts following Kaminsky catalysts (metallocenes) discovered in 1980 by Walter Kaminsky. They are made oflate transition metal complexes bearing bulky, neutral, α-diimine (or diketimine) ligands [Johnson et al., 2005].

The current MS thesis proposal concerns the application of metallocene catalysts to copolymerize ethylene with 4-methyl-1-pentene and its isomer, 1-hexene. Therefore, we discuss them in moderate details in the subsequent sections.

2.1.1 Metallocene Precatalysts

Metallocene precatalysts are π-bonded organometallics where a metal is sandwiched between aromatic ligands, such as cyclopentadienyl or indenyl groups. Keally and Panson and Miller et al. discovered ferrocene (from which the general name of metallocenes was derived) simultaneously in 1951. Later, Fischer and Wilkinson

established its structure for which they received the Nobel Prize in Chemistry in 1973. Schemes 2.1a and b show the general representative structures of metallocene

The rings in ferrocene are parallel as in Scheme 2.1a or bent as in Zirconocene (Scheme 2.2)

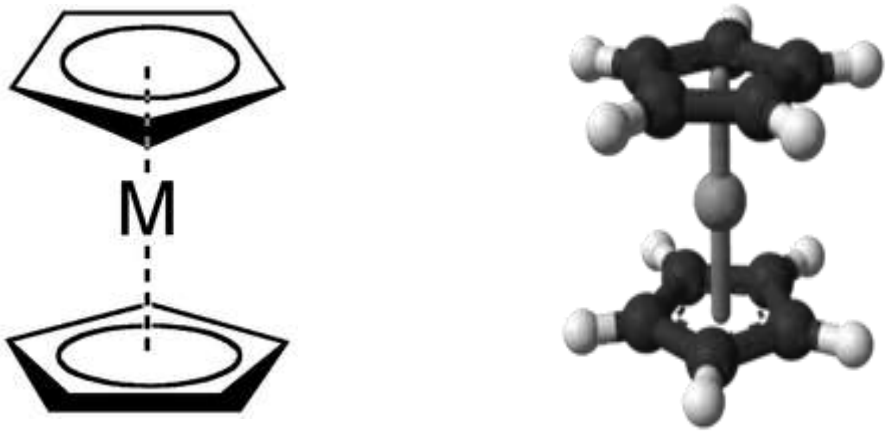

Scheme 2.1: (a) General structure of metallocene (b) Ball and stick structure of metallocene.

In above Scheme, M stands for a metal cation. The ball-and-stick structure shown in 2.1b is typical of metallocene molecule with the metal center (in the middle) sandwiched between the two cyclopentadienyl groups. [http://en.wikipedia.org/wiki/Metallocene *accessed on 28 Feb 2013*]. Table 2.1 lists the general formulae of metallocenes precatalysts.

Table 2.1: General formulae for metallocene precatalysts

General formula	Description
$[(\eta\text{-}C_5H_5)_2M]$	Classical/symmetrical structure
$[(\eta\text{-}C_5H_5)_2ML_x]$	Cp rings tilted by a ligand
$[(\eta\text{-}C_5H_5)ML_x]$	One Cp ring with a ligand

Scheme 2.2(a) and (b) diagrammed bridged and non-bridged metallocenes. In bridged or *ansa*-metallocenes the two cyclopentadienyl ligands bound to the same metal and linked

by the bridging group. The linker group (often $(CH_2)_n$ or R_2Si where R is an alkyl group) hinders rotation of the Cp or indenyl ring, and play substantial role in the structure and reactivity of the metal coordination environment [Wang 2006]. Non-bridged metallocenes do not have such linkers.

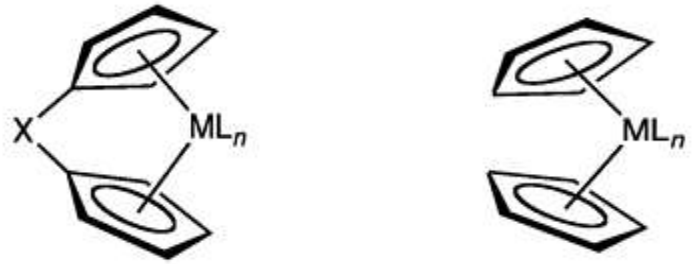

Scheme 2.2: (a) Bridged metallocene. (b) Non-bridged metallocene.

Brintzinger et al. reported that bridged metallocenes exhibit better comonomer incorporation than their corresponding nonbridged analogues in ethylene/α-olefin copolymerization [Brintzinger et al. 1995].

2.1.2 Cocatalysts used in the Activation of Metallocenes

Metallocenes could not be used in polyolefin synthesis with the conventional alkyl aluminums that are used with Ziegler–Natta catalysts. The discovery of methylaluminoxane (MAO) at Hamburg, Germany, by Sinn and Kaminsky, paved the way for metallocene polyolefin catalysis [Kaminsky 1998, Kaminsky 1996]. The structure of MAO consists of aluminum atoms alternating with oxygen atoms while labile methyl subtituents occupy the free valencies. It is obtained when trimethyl aluminum is partially hydrolyzed; and consists of units of basic structure $[Al_4O_3Me_6]$ according to Sinn [Sinn 1995] and Barron [Kaminsky 1998]. Because the aluminum atoms are

coordinately unsaturated, the $Al_4O_3Me_6$ units (usually) four, join together to form the cage structure shown in Scheme 1.2.

Table 2.2 lists the historical development of metallocene in polyolefin synthesis research.

Table 2.2: Historical development of metallocene in polyolefin synthesis research.

Year	Breakthroughs
1952	Fischer and Wilkinson established the structure metallocene using that of ferrocene .
1955	Metallocene as polyolefin catalysts, low activity with conventional metal alkyls cocatalysts
1973	Reichert, Meyer and Breslow used small quantity of water to raised the activity of metallocene/metal alkyls systems
1975	Kaminsky, Sinn and Motweiler attained an unusual increase in activity by adding water in the ratio $Al:H_2O = 1:2$
1977	Kaminsky and Sinn) applied separately synthesized methylaluminoxane (MAO) as cocatalyst for olefin polymerization.
1982	Brintzinger Synthesized *ansa* metallocenes with C_2 symmetry

Another important class of metallocene cocatalysts are arylboranes/borates. Table 2.3 lists selected examples of metallocene activators.

Table 2.3: Examples of activators for metallocenes.

Type	Chemical name	Chemical formula
Aluminoxanes	Methylaluminoxane	$(O\text{-}Al(CH_3))_n$-
	Methylaluminoxane (non-hydrolysis)	$(O\text{-}Al(CH_3))_n$-
	Modified methylaluminoxane type 3	$(O\text{-}Al(CH_3))_m$-(O-Al(Bu-i))n
	Activated Modified methylaluminoxane	(O-Al(CH_3))m-(O-Al(Bu-i))n-
Borane	Polyisobutylaluminoxane	-(O-Al(C_4H_9-i))n-
	Tris(pentafluorophenyl)borane	$B(C_6F_5)_3$
Borates	Dimethylanilinium Tetrakis(pentafluorophenyl)borate	$[PhNH(CH_3)_2]^+[B(C_6F_5)_4]^-$
	Trityl tetrakis(pentafluorophenyl)borate	$[Ph_3C]^+[B(C_6F_5)_4]^-$
	Lithium tetrakis(pentafluorophenyl) borate	$Li^+[B(C_6F_5)_4]^-$

While aluminoxanes are required in high ratio to the precatalyst, boranes may be used in near stoichiometric amounts [Malpass 2010]. The following reactions relate to metallocene activation using a methylaluminoxane and a borate, respectively [Tosoh FineChem Corporation 2012].

$$Cp_2ZrCl_2 + —(O\text{-}Al(CH3))_n— \longrightarrow Cp_2Zr^{+}CH_3l[H_3C\text{-}MMAO]^{-} \quad (1)$$

$$Cp_2Zr(CH_3)_2 + B(C_6F_5)_3 \longrightarrow [Cp_2ZrCH_3]^{+} + [H_3C\text{-}B(C_6F_5)_3]^{-} \quad (2)$$

The next subsection is dedicated to the discussion of supported Metallocene/MAO catalyst systems. This is the system that will be used in this research.

2.1.3 Mechanism of Metallocene Catalysis

There are remarkable differences between the mechanisms of polymerization with metallocenes and their closely related Ziegler-Natta counterparts. Active site generation is the key step in polyolefin catalysis (See Scheme 2.3). The reaction is divided into the following two parts. First, the bridged labile methyl groups of MAO monomethylate a chloride ligand (—Cl) of the precatalyst $L_1L_2ZrCl_2$ where L_1 and L_2 are π-ligands; then another one is abstracted by the strong Al Lewis acidic site of MAO [Chen et al. 2000, Pédeutour et al. 2000, Babushkin et al. 2000,97,98]. This MAO Lewis acid site is attributed to the coordinatively unsaturated Al in an —AlO_2Me— environment (that consists of the tricoordinated Al atoms bridging the tricoordinated oxygen atoms) **[**Eisch et al. 1985 Eisch et al. 1991, John et al. 1993, Eisch et al. 1999, Fusco et al. 1998, Panchenko et al. 1999]. The Cl^{-}ligand-exchanged Me group remains intact. It should be noted that the conversion of $L_1L_2ZrCl_2$ to $L_1L_2ZrMe_2$ by MAO (through complete ligand exchange between Cl and Me) is not supported by visible UV spectroscopy [Babushkin et

al. 2000, Coevoet et al. 1998a, Coevoet et al. 1998b], ^{1}H or ^{13}C NMR spectroscopy [Babushkin et al. 2000]. Consequently, the corresponding ion-pairs (which are the active catalyst centers) are generated [Chen et al. 2000, Pédeutour et al. 2001, Babushkin et al. 2000, Coevoet et al. 1998a, Coevoet et al. 1998b, Pédeutour et al. 2002]. This reaction product is responsible for initiating the polymerization of an α-olefin.

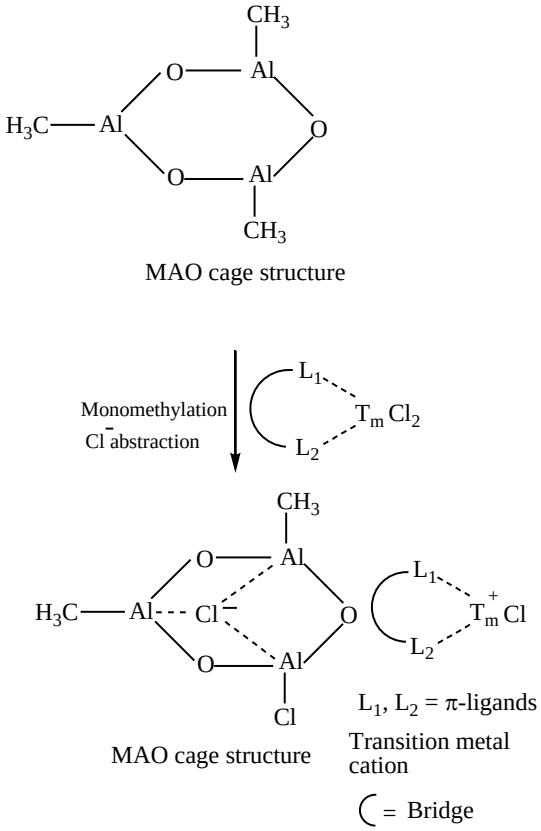

Scheme 2.3: Generation of catalyst ion-pair active center.

It has been shown that the counterion in the ion pair resulting from abstraction must be weakly coordinated to the cationic active center. MAOs, modified MAOs or the accompanying TMAs may also act as the alkylating agents and scavengers of poisons as they do in Ziegler-Natta catalyzed systems [Malpass 2010]. MAO does not have a unanimously agreed upon structure. However, the proposed three-dimensional cage structures characterized with the following—structural similarity with poly(tert-

butylaluminoxane) cages, preferred hexagonal (six-membered ring) faces, and four-coordinate Al and three-coordinate O centers, comprising Al–O and Al–Me bonds—are most widely accepted [Thomas et al. 2005, Chen et al. 2000, Negureanu et al. 2006, Linnolahti et al. 2012, Pédeutour et al. 2001, Ystenes et al. 2000]. See Scheme 1.2.

Chain initiation:

$$Cp_2Zr(CH_3)_2 + MAO \longrightarrow Cp_2Zr^{+}CH_3 + CH_3MAO^{-}$$

$$\downarrow CH_2{=}CH_2 \qquad (3)$$

$$Cp_2Zr^{+}CH_2CH_2CH_3$$

Metallocene and post-metallocene chain-growth process: propagation

This step is very similar to Ziegler-Natta chain-growth process. However, the rate of chain propagation/addition is related to the fundamental current concept of ion-pair separation **[**Wang et al. 2001, Macchioni 2005, Bochmann 2005, Wannaborworn 2011, Ustynyuk 2012]. See Scheme 2.4. The extent of ion-pair separation depends on the required heterolytic dissociation energy, which determines the energy characteristics of the polymerization reactions. For example, a decrease in the heterolytic dissociation energy increases the exothermic effects associated with the reaction(s) of the monomer(s) with the catalyst site types. This eventually decreases the concomitant energy barriers for key polymerization steps, and increases the activity of the related catalyst.

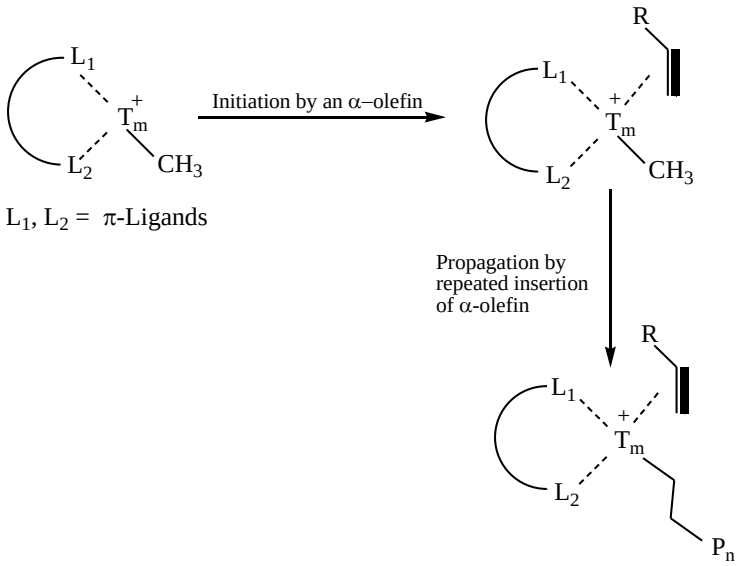

Scheme 2.4: Polymer chain propagation by metallocene catalyst.

The tightness of the cation-anion relatively restricts the access of the bulkier α-olefin to the T_m^+ metal center. Therefore, the rates of monomer insertion and polymer chain growth, and hence the overall catalyst activity decreases with the extent of this ion-pair tightness.

In order to regulate the microstructural characteristics and the resulting poly(α-olefin) properties, a small amount of an additional α-olefin (usually called a comonomer) is added to the mother monomer. This process is typically named copolymerization. Under this condition, comonomer effects are noticed on catalyst activity, as well as on chain termination. What follows summarizes the first part with reference to ethylene-1-hexene copolymerization as a typical example.

The polymerization activity of a given precatalyst increases upon the addition of 1-hexene up to a critical comonomer concentration. This is called positive 1-hexene comonomer effect. This finding (irreversible enhancement of catalyst activity), with reference to ethylene-1-hexene copolymerization, has been widely reported in the

literature [Grieken et al. 2007, Smit et al 2006, Przybyla et al. 1999, de Freitas et al. 1999, Karol et al. 1993, Pasquet et al. 1993, Koivumiiki and Seppala 1993, Schaverien et al. 2001]. The following two explanations or the combination of both have been mostly proposed:

- Fink's filter effect (a physical mass transport or diffusion-limited process) [Grieken et al. 2007, Smit et al 2006, Przybyla et al. 1999, de Freitas et al. 1999]; and

- Activation of the dormant/sleeping catalytic sites [Karol et al. 1993, Pasquet et al. 1993, Koivumiiki and Seppala 1993, Schaverien et al. 2001**,** de Freitas et al. 1999, Chang et al. 1992, Quijada et al. 1997, Chu et al. 1999, Kissin et al. 1999].

The above explanations are being critically reviewed so that one could attain a more insightful comprehension. According to Fink's filter effect, the active sites of a catalyst get coated by a polyethylene inner shell and an ethylene-1-hexene copolymer outer shell because of the difference in monomer molecular size and diffusivity. This is the microscopic view of a typical ethylene-1-hexene copolymer whose overall crystallinity is usually much less than that of the ethylene homopolymer. This increases 1-hexene diffusivity which enhances the catalyst polymerization activity [Przybyla et al. 1999]. However, there are several drawbacks of this explanation which are summarized below.

Copolymerization of ethylene with 1-hexene using unsupported metallocenes is well documented in the literature [Wannaborworn et al. 2011, Koivumiiki and Seppala 1993, Galland et al. 1999, Kim and Ha 2004]. Positive comonomer effect has been noticed under such a situation when the catalyst is soluble but the polymer formed is insoluble in

the polymerization medium. This shows that copolymerization rate enhancement occurs even without Fink's filter effect. Moreover, positive to negative comonomer effects prevail with the increasing concentration of 1-hexene comonomer [Chen et al. 2000, Koivumiiki and Seppala 1993, Jaber 1993, Koppl 2000]. The filter effect does not well accommodate this transitional behavior. Additionally, it does not align with the chain transfer role of 1-hexene that significantly drops the molecular weight through the generation of different vinyl unsaturations in the copolymer backbone. Hence, Fink's filter effect turns out to be less convincing.

On the other hand, the activation of the dormant/sleeping catalytic sites, unlike the filter effect, is an intrinsic chemical phenomenon. In this context, the activation of the dormant/sleeping T_m^+–H catalytic site by 1-hexene is to be specially considered [Karol et al. 1993, Pasquet et al. 1993, Koivumiiki and Seppala 1993, Schaverien et al. 2001, Przybyla et al. 1999, Schaverien et al. 2001, de Freitas et al. 2011, Chang et al. 1992, Quijada et al. 1997, Chu et al. 1999, Kissin et al. 1999]. The genesis of this catalytic site will be addressed in the next section.

Metallocene and post-metallocene chain-growth process: termination

The chain termination/transfer processes for homopolymerization of an α-olefin by Group IV B metallocenes and post-metallocenes are alike to those of Z-N catalysis. The introduction of 1-hexene greatly lowers the weight average molecular weight of the resulting copolymer. Therefore, 1-hexene acts as a strong chain-transfer agent. This happens in addition to incorporation of 1-hexene along the growing polyethylene chain. Consequently, the molecular weights dropped. The growing copolymer chains terminate

following the three simultaneous chain transfer reactions—Route A, Route B, and Route C—shown in Scheme 2.5 [DesLauriers et al. 2005, DesLauriers 2010, Atiqullah et al. 2012]:

- **Route A:** 1, 2 insertion of 1-hexene and generation of vinylidene terminus ($CH_2=CR_1R_2$; $R_1 \neq R_2$) (through β-hydrogen elimination to T_m^+ active sites);
- **Route B:** β-hydrogen transfer to 1-hexene and generation of vinyl terminus ($CH_2=CHR$); and
- **Route C:** 2, 1 misinsertion of 1-hexene, followed by β-hydrogen elimination to the T_m^+ active sites with generation of *trans*-vinylene terminus ($R_1CH=CHR_2$; $R_1 \neq R_2$).

Note that β-hydrogen elimination is the reverse of 1-hexene insertion into the T_m^+–H bond where the less substituted carbon bonds to T_m^+. See Scheme 2.6.

Route A: 1, 2 insertion of 1-hexene

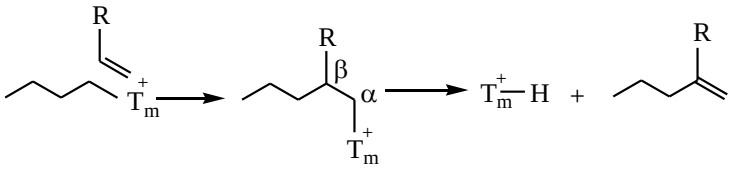

Route B: β-hydrogen transfer to 1-hexene

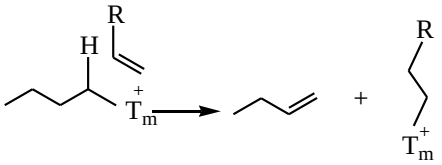

Route C: 2, 1 misinsertion of 1-hexene

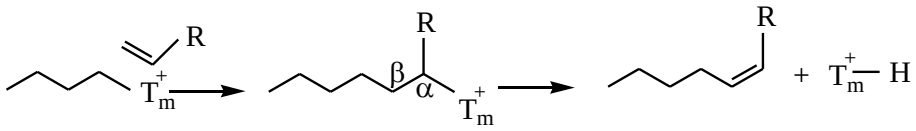

Scheme 2.5: Chain termination by 1-hexene through Routes A, B, and C.

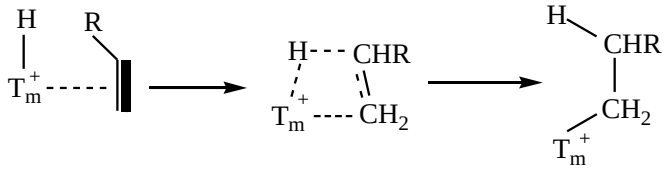

Scheme 2.6: Insertion of 1-hexene into the Tm+–H bond and alternative growth of polymer chain.

2.1.4 Supported metallocene/MAO catalyst systems

Single site catalysts activated by methyl aluminoxanes (MAO) constitute a major class of the heterogeneous single site catalysts for olefin polymerization. We shall discuss the several supporting routes as well as the routes adopted in this work. It is worth noting at this point that unlike homogeneous systems where large Al/Metal ratios (1,000-10,000) are required to prevent deactivation, the carrier in supported system intrinsically eliminate this necessity [Hlatky 2000]. Thus much lower Al/Metal ratio in the order 10 – 10^2 could be used [Chien et al 1999]. The challenges posed by supporting single site catalysts include:

i. Maintain the single-site characteristics of metallocenes upon heterogenization;

ii. Overcome the significant drop in catalyst activity;

iii. Prevent catalyst leaching (that causes severe reactor fouling, and damages the polymer particle morphology); and

iv. Eliminate the separate feeding of the methylaluminoxane (MAO) cocatalyst (which gels and degrades during feeding, and which is very costly).

One of the routes in Metallocene/MAO catalyst system supporting is to first support the MAO and then react it with the metal complex. In this regard, Welborn and Takashi used silica to support MAO in toluene, decanted same, to isolate the solids containing MAO, which they eventually reacted with Cp_2ZrX_2 (Cp = substituted/unsubstituted Cp ligand, X= Cl/Me) to form the supported catalyst which was applied used in gas-phase ethylene homo- and copolymerization. Adding the metallocene to the supported MAO as a solution in toluene or aliphatic hydrocarbon and subsequently subjecting the mixture to microwaves tethered the metal component on the support and reduced reactor fouling [Hlatky 2000]. Alternatively, the metallocene may be dry-blended with the silica support to avoid solubilization of the supported catalyst/cocatalyst system [Hlatky 2000].

2.2 Polyolefins

2.2.1 Brief Introduction

Polyolefins are synthetic polymers that are prepared by the polymerization of olefins. Olefins are hydrocarbons (compounds containing hydrogen H and carbon C) whose molecules contain a pair of carbon atoms linked together by a double bond. They are derived from natural gas or from low molecular weight constituents of petroleum. The most prominent monomers are ethylene and propylene [Brittanica online Encyclopedia]. Polyolefins, in a wide sense, include polyethylene and polypropylene (PP); and they are very popular due to their low cost and wide range of applications. They are classified as

low density polyethylene (LDPE), high density polyethylene (HDPE), and linear low density polyethylene (LLDPE) [IHS 2012].

2.2.2 Polyethylene: History and Classification

Polyethylene is formed from ethylene (C_2H_4). It is a major thermoplastic. Various polymer processes emerged, which produce varieties of polyethylenes with varying properties. They are classified on the basis of their molecular weights, density and the extent of branching as LDPE, HDPE, LLDPE, and so on. The production of these commodity plastics is about 211 million tonnes in 2012 [Sagel 2012].

Polyethylene was first produced, accidentally by Hans von Pechmann in 1898 while working with diazomethane. This white waxy substance which on analysis was found to be made up of $-CH_2-$units was named "polymethylene". In a similar scenario, Eric Fawchett and Reginald Gibson of Imperial Chemical Industries (ICI), in Northwich England produced polyethylene at several hundreds of atmosphere pressure while working with ethylene and benzaldehyde. However, the process was difficult to reproduce as the reaction was initiated by traces of oxygen contaminants. In 1935, Micheal Perrin of the same industry developed a methodology for a high pressure production of polyethylene. This was industrialized in 1939 [newworldencyclopedia 2012].

Several breakthroughs in polyethylene catalysis followed the ICI achievement. In Philips Petroleum, Robert Bands and J. Paul Hogan discovered chromium trioxide in 1951. On the other hand, the German chemist, Karl Ziegler in 1953 developed titanium halides and organoaluminium catalysts compounds for ethylene polymerization. While

Ziegler catalysts were applicable at milder conditions than Philips, the latter was cheaper and much easier to use. Thus, began the commercial production of polyethylene.

Metallocenes, discovered in 1976 in Germany by Walter Kaminsky and Hansjörg Sinn,represent a modern class of olefin catalyst systems. The wide range of polymeric materials available today is partly because of metallocene-catalyzedcopolymerization of ethylene with α-olefins (1-butene to 1-octene) [newworldencyclopedia 2012].

2012 global polymer demand indicates that polyethylene is still the largest commodity thermoplastics at 211million tonnes [Sagel 2012]. See Figure 2.1.

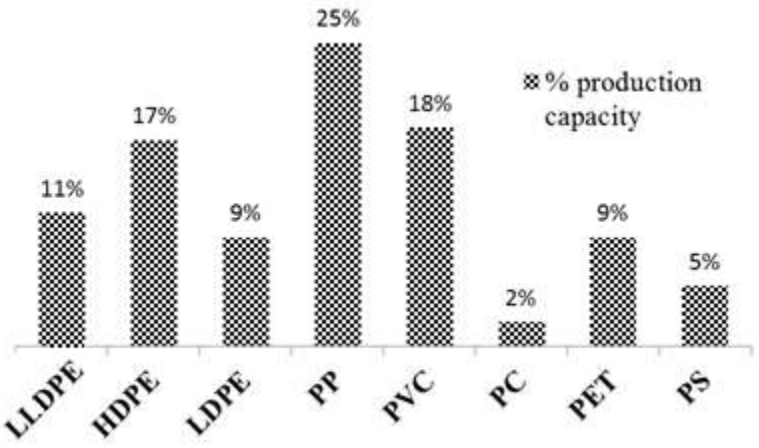

Figure 2.1: Global Polymer demand in 2012. Total = 211 million tonne/annum

2.2.3 Applications of Polyolefins

Polyolefins are usually processed by extrusion, injection molding, blow molding, and rotational molding methods. Thermoforming, calendering, and compression molding are not frequently used. An inherent characteristic common to all polyolefins is a nonpolar, nonporous, and low-energy surface that is not receptive to inks, and lacquers without special oxidative pretreatment. They are the largest group of thermoplastics, often referred to as commodity thermoplastics.

The general applications include wire and cable coating, film, automotive applications, automotive exterior parts, foam, cast film, food packaging, low voltage insulation, and automotive bumper. However, they have such disadvantages as high thermal expansion, poor UV resistance, being subjective to stress cracking, flammable and low use temperature [IDES 2012]. Some specific applications are summarized in Table 2.4.

Table 2.4: Summary of the general applications of some selected polyolefins.

Polyolefins	Applications
LDPE	Cling film, carrier bags, agricultural film, milk carton coatings, electrical cable coating, heavy duty industrial bags.
LLDPE	stretch film, industrial packaging film, thin walled containers, and heavy-duty, medium- and small bags.
HDPE	Crates and boxes, bottles (for food products, detergents, cosmetics), food containers, toys, petrol tanks, industrial wrapping and film, pipes and houseware.
PP	Food packaging, including yoghurt, margarine pots, sweet and snack wrappers, microwave-proof containers, carpet fibres, garden furniture, medical packaging and appliances, luggage, kitchen appliances, and pipes.

In the next section, we particularly focus on the developments related to polyethylenes.

2.3 Polyolefin Process Technologies

2.3.1 High Pressure Process

The first class of polyolefins that was synthesized is low density polyethylene (LDPE). This is produced at a high pressure (1000-3000 atmosphere) and temperatures of between 80-300 $^{\circ}$C [PTLs 2012].

In oxygen-initiated reactions, pressures of 1500 atm and temperature of 200^{o}C at oxygen concentration of 0.03 – 0.1% have been reported. In most cases, the process is continuous in a tubular reactor or continuously stirred tank reactors. Because the reaction is highly exothermic, proper heat dissipation is necessary, the lack of which may formexplosives of carbon hydrogen and methane. Benzene and water have been used as diluents to help in heat exchange and in removing the product from the reactor. Conversions of 10-30% have been reported and the polymer is usually extruded as ribbon and granulated [PTLs 2012].

High pressure is necessary to obtain high molecular weight product. Similarly, high molecular weights are favored by high comonomer concentrations because the radicals have short life and must react within certain period of time. During these high pressure processes, the gas converts into a liquid. The polymer dissolves; bulk polymerization takes place, producing low density polyethylene (LDPE).

$$n\,CH_2 = CH_2 \rightarrow\ [-CH_2 - CH_2 -]_n \tag{5}$$

Results of IR spectrum of LDPE reveal degree of branching of up to 30 methyl groups per 1,000 carbon atoms in the chain. Methyl groups must be terminal but this number is too high to be accounted for by the methyl chain ends in a linear polymer. Hence, branching must be present. The branches are of two types. One type is due to intermolecular chain transfer arising from reactions shown below:

$$R_1CH_2\dot{C}H_2 + R_2CH_2CH_3R_3 \xrightarrow{\substack{intermolecular\ hydrogen \\ transfer}} R_1CH_2CH_3 + R_2\dot{C}HCH_3R_3 \tag{6}$$

The other type of short chain branching is assumed to result from intramolecular chain transfer.

$$RCH_2CH_2CH_2CH_2CH_2\dot{C}H_2 \xrightarrow{\substack{transient\ six\ membered \\ ring\ formation}} RCH_2CH_2CH_2CH_2CH_2\dot{C}H_2$$

$$\xrightarrow{\substack{intramolecular\ hydrogen \\ transfer}} RCH_2\dot{C}HCH_2CH_2CH_2CH_3 \qquad (7)$$

2.3.2 Ziegler Process

These are carried out at pressure ranges of 2-4 atm and temperatures of 50-75^{o}C. Catalysts such as titanium tetrachloride/aluminium alkyl (e.g. diethyl aluminum chloride) components are used for ethylene polymerization. The catalyst preparation may be in-situ by adding the components separately to the reactor as solutions in diluents such as diesel oil, heptanes or toluene. Alternatively, the components may be pretreated and the catalyst may be added as slurry in liquid diluents. These operations must be conducted in an inert atmosphere (argon or nitrogen) because oxygen and moisture reduce drastically, the catalyst activity and may cause explosion. Typically, the process is continuous in feeding ethylene, catalyst and diluents. The polymer is sparingly soluble in the diluents,makinga slurry which is continuously removed. The reaction is quenched by adding alcohols such as methanol, ethanol or isopropanol. The resulting metallic residues are extracted with alcohol and hydrochloric acid. This purification is vital especially for polymer application in high frequency electrical insulation. Lastly, the polymer is centrifuged, dried, extruded, and granulated [PTLs 2012]. Ziegler process produces polyethylenes with a small degree of branching (about 57 ethyl groups per 1,000 carbon atoms).

2.3.3 Phillips Process

Phillips polymerization process uses operating conditions in range between those of high pressure processes and low pressure Ziegler processes. The methodology involves impregnation of support (usually silica or silica alumina) with an aqueous solution of chromium salt, followed by heating in air to temperatures in the range of 400-800^{o}C. Final products containing about 5% of chromium trioxide are normally obtained. In some processes, ethylene is fed along passed in a solvent such as toluene or cyclohexane [PTLs 2012].

The polymer/product may be obtained in the form of slurry or solution, depending on the reaction conditions particularly temperature. Solution processes are normally run at 120-160^{o}C, at which the polymer is soluble in the diluent. Hot polymer solution is continuously taken out of the reactor while unreacted ethylene is vented out and suspended catalyst is removed by filtration or centrifuging. In the slurry processes, polymer granules are formed around each catalyst particles. The operating temperatures are between 90-100^{o}C. The polymer exhibits low solubility in the diluents. After the reaction, the product is treated as in gas phase except that the accompanying small amount of catalyst is not usually removed. The polyethylene so obtained here is almost completely linear without ethyl or butyl branching. However, the number of methyl groups of up to 3 per 1,000 carbon atoms may be greater than the usual number of main chain ends [PTLs 2012].

2.4 Commercial Olefin Polymerization Processes Using Supported Transition Metal Catalysts

Metallocene catalysts have been used industrially mainly for the production of LLDPE and HDPE resins since early 1990s. In the following section, we summarized the most important commercial polymerization processes for the production of LLDPE and HDPE,using supported transition metal catalysts.

2.4.1 Slurry Processes

These are three phase reactors in which the catalysts are always present as porous particles and the monomers are present either as a gas (for ethylene or propylene) or a liquid (for propylene and higher -olefins). If the monomer is gaseous, hydrocarbon solvents like hexane or toluene must also be present to serve as the suspending medium for the catalysts and polymer particles. Hydrogen is often used as a chain transfer agent. There are several slurry reactor technologies available, but they are always designed as either continuous stirred tank reactors (CSTR) or loop reactors. CSTR Ziegler slurry processes are capable of producing any HDPE resins, including bimodal products produced in a series of reactors, each operated at different conditions. Usually, the first reactor in the series produces a high molecular weight copolymer without, or with a small amount of hydrogen. The second reactor in the series is then used to produce the lower molecular weight homopolymer using hydrogen as a chain transfer agent. The reactors may be interchanged so that the low molecular weight homopolymer is produced in the first reactor while the high molecular weight copolymer is synthesized in the second. Furthermore, stirred tank reactor technologies have low fixed costs and operate with the

conventionally cheap and highly active catalysts. Figure 2.2 diagramms a typical Basell CSTR slurry process. Finally, the third reactor in the series converts all the residual monomers to polymers [Choi and Soares 2012].

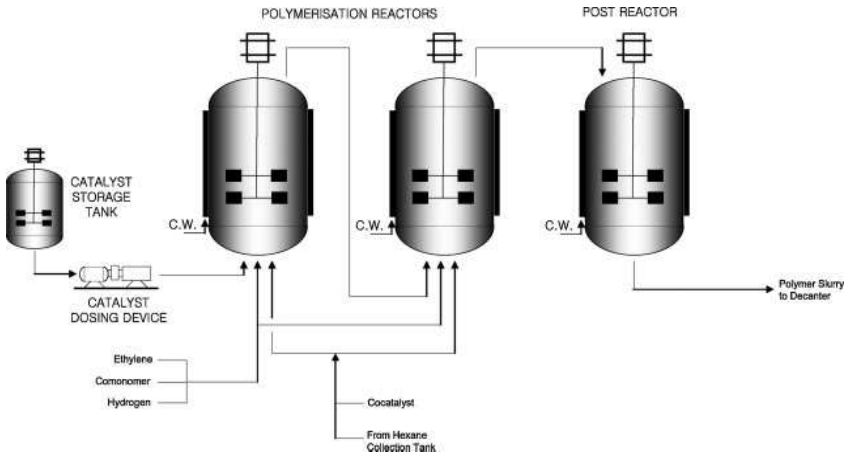

Figure 2.2: Basell (Hostalen) slurry (CSTR) polyethylene process.

Now we shall discuss the loop reactors which account for about 50% of the world's polyolefin resins. They utilize a combination of Phillips/chrome catalysts. Their high length to diameter (L/D) ratio; and high heat transfer surface give them the advantage of excellent heat transfer and allow for accurate temperature control. This is also favoured by high heat transfer coefficients resulting from the high operating flow rates and the concomitant turbulence. This accounts for consistency of the finished product. the Chevron–Phillips reactor is represented in Figure 2.3. This consists of a continuous loop made from the sections of a pipe and equipped with an axial flow pump, which circulates all the components. The RTDs of commercial loop-type reactors are comparable to those of CSTRs because of their high recirculation ratios [Choi and Soares 2012].

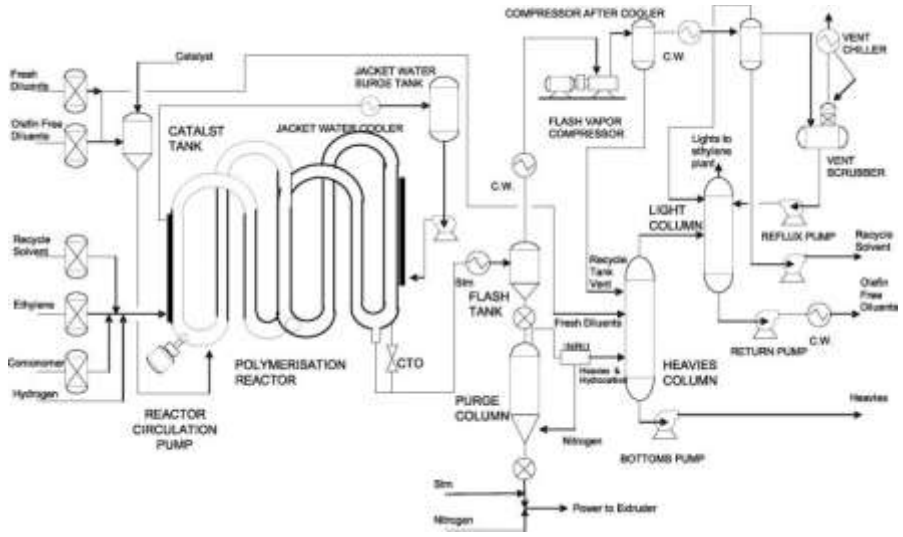

Figure 2.3: Phillips slurry (loop) polyethylene process.

2.4.2 Gas-Phase Processes

These processes utilize two-phase reactors, where the injection of liquid monomers plus inert materials to remove the heat of polymerization by latent heat of evaporation, otherwise called condensed mode of operation is involved. The catalyst is in the form of a porous particle and the monomers are in gaseous phase. They serve as a cheaper (in terms of both process economy and energy efficiency) alternative to slurry polymerizations. Gas-phase reactors offer such advantages as: (1) Elimination of no diluent recycling since no of diluents is present, which enables an efficient design of large-scale reactors; (2) The absence of solubility limits (often encountered with slurry reactors) allow for the production of polymers with a wide range of comonomer incorporation, and molecular weight distributions. (3) They could be used with a variety of catalysts types—Ziegler–Natta, Phillips Metallocenes and Post-metallocenes. (4) They are relatively insensitive to catalyst leaching unlike the slurry reactors. The configuration of gas-phase reactors in the form of a fluidized-bed is illustrated in Figure 2.4 [Choi and Soares 2012].

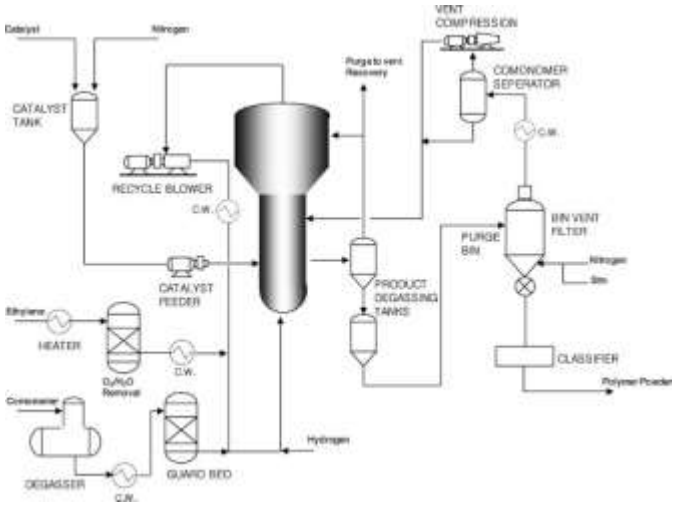

Figure 2.4: Unipol gas-phase (fluidized bed) process for polyethylene production.

2.4.3 Comparison of properties of polyethylenes from different commercial processes

Polyethylenes obtained from various commercial processes differ in their degree of branching, which reduces the ability of polymer chains to pack closely and regularly, that is, to crystallize. Thus, the different types of polyethylenes have varying properties with the highly branched polymer exhibiting lower density, crystalline melting point, stiffness, surface hardness and softening temperature and greater permeability to gases and vapors. Other physical properties may depend not only on degree of branching but also on average molecular weight, molecular weight distribution, and so on. Table 2.5 lists some of the properties of commercial grade polyethylenes.

Polyethylenes have good electrical insulation properties as may be expected of a non-polar substance. Similarly, the dielectric constant and power factor are almost independent of frequency and temperature. Polyehtylene is chemically inert high molecular weight paraffin. It is crystalline and has no solvent at room temperature because there is no specific interaction with any solvent. However, at high temperature, it

dissolves in such solvent as toluene, xylene and dichloro ethylene. Temperatures of 60-80^{o}C are high enough to dissolve polyethylene in a given solvent; with most crystalline requiring higher temperatures within this range [PTLs 2012].

Table 2.5: Properties of polyethylenes produced by various processes.

Property	High pressure PE	Ziegler PE	Philips PE
Molecular weight (M_n)	20,000	15,000	15,000
Methyl groups/1000 Carbon atoms	30	5 – 7	< 0.15
Density (g/cm^3)	0.92	0.95	0.96
Crystalline melting point (^{o}C)	108	130	133
Stiffness (lb/in^2*10^3)	25	90	125

Polyethylene is resistant to most acids alkalis and aqueous solutions. However, nitric acid and concentrated solutions of hydrogen peroxide are able to oxidize it, thereby, deteriorating its mechanical properties. Resistance to these reagents increases as density increases due to diminishing permeability. Oxidation of polyethylene also occurs in air when exposed to UV light and/or high temperature [PTLs 2012].

2.5. Copolymerization of Ethylene with 4-methyl-1-pentene

2.5.1 Applications of metallocenes to synthesize ethylene/4-methyl-1-pentene

Ivanchev et. al. carried out homo- and copolymerization of 4-methyl-1-pentene with ethylene using different zirconocenessuch as $[(CH_3)_2C(Ind)_2]ZrCl_2$, $[(CH_3)_5Cp]ZrCl_3$, $[(CH_3)_2Si(Ind)_2]ZrCl_2$, $[(CH_3)_2C(Cp)_2]ZrCl_2$, $[(C_6H_5)(C_2H_5)C(Ind)_2]ZrCl_2$, $[(Ph)_2C(Cp)(Flu)]]ZrCl_2$, and $[(CH_3)_2C(CH_3Cp)(Flu)]ZrCl_2$. Their results indicated that unsymmetrical, bridged metallocenes have the highest activity. They also determined the best operating conditions of the copolymerization of 4-methyl-1-pentene with ethylene to

form a linear low density polyethylene with a variable content of 4-methyl-1-pentene, and also established the effect of the molar ratio of MAO/Zr on the yield and composition of the resulting copolymer.

Xu and Cheng [2001] used seven (7) different metallocene/MAO catalyst systems to homo- and copolymerize ethylene with 4-methyl-1-pentene. They studied the effect of ligand substitution pattern in catalyst on the activity, comonomer incorporation, as well as the copolymer microstructure. They found that the monocyclopendienyl amido catalysts had higher catalytic activity than biscyclopentadienyl amido catalyst; and produced polymers of higher molecular weight with better comonomer incorporation. Furthermore, they used fluorenyl titanium and fluorenyl zirconium to ascertain the effect of the metal on the catalysis. They established that the metal type of titanium complexes has a noticeably different higher catalyst activity than those of zirconium. They showed about triple productivity, and better comonomer incorporation.

Losio et al. [2008] prepared highly stereoregular and the completely regioregular LLDPEs with 4-methyl-1-pentene comonomer with content ranging between 1 to 35 mol% using the metallocene precatalyst *rac*-$CH_2(3\text{-}t\text{BuInd})_2ZrCl_2$. However, with the constrained geometry catalyst [$Me_2Si(\eta^5\text{-}Me_4C_5)\text{-}(\eta^1\text{-N-tBu})TiCl_2$], activated with methylalumoxane, Losio et al. [2009] obtained copolymers which showed low regio- and stereoregularity and nearly random comonomer distribution.

Mauler et al. [1996] studied the effect of pressure in the reaction of ethylene and 4-methyl-1-pentene using $Et[Ind]_2ZrCl_2$/MAO catalyst system. They found that the catalyst activity is independent of the comonomer concentration. On the other hand, increase in

ethylene pressure resulted in an increase in the productivity while the activity showed some extent of decay. When the copolymers were characterized, it was observed that those produced at higher pressure have higher degree of crystallinity due to lower comonomer incorporation [Mauler et al. 1996].

Boragno et al correlated the microstructure of ethylene/4-methyl-1-pentene copolymers synthesized using isospecific metallocene catalyst with their melt crystallization behavior. They fund that the isospecific catalyst formed homosequences of ethylene and 4M1P due to facileness of isospecific propagation of the □-olefin. By applying Markov second order model, they reported that the presence of sterically hindered 1-olefin, a penultimate unit effect is responsible for the copolymers blocky microsture even with the isospecific cataslyst.

Awudza and Tait [2007] compared the commoner effect in the homogeneous and silica supported Cp_2ZrCl_2/MAO catalyst system copolymerizations of ethylene with 1-butene, 1-hexene, 4-methyl-1-pentene and 1-octene. The general rate depression with homogeneous catalysts at 70^oC was ascribed to reduction in the active center distribution; while the rate enhancement in the case of silica supported catalyst at 70^oC, and for both catalytic systems at 50^oC was ascribed to the increase in the propagation rate coefficient Earlier, same authors reported rate enhancement in Ethylene/4-Methyl-1-pentene copolymerizations at 60^oC using homogeneous Cp_2ZrCl_2/MAO catalyst at high Al/Zr ratio of $5.8x10^4$:1[Awudza and Tait 2007].

Irwin [2004] reported homo- and copolymerization of ethylene with 4-methyl-1-pentene, 1-octene using a metallocene homogeneous catalyst system which is a sterically

expanded zirconium fluorenyl-amido complex with an activity and □-olefin incorporation ability far exceeding those of even most Ziegler-Natta catalyst systems. Their results indicated that catalyst activity and 4-methyl-1-pentene incorporation are proportional to comonomer concentration as contrary to the general trend of increase in activity with the introduction of the comonomer(the comonomer effect), followed by a decrease in activity with increase in concentration as observed with the conventional Ziegler-Natta catalsysts.

Galimberti et al. [2010] copolymerized ethylene with 4-methyl-1-pentene using non-living insertion copolymerizations with five different isospecific homogeneous catalysts systems. They described the copolymers by second order Markovian copolymerization model and proposed data to correlate the formation of 1-olefin sequences with catalytic site isospecificity. They observed a penultimate unit effect with [rac-H_2C-(3-^{t}BuInd)$_2$ZrCl_2, and showed for the first time that moderately isospecific catalysts based on metallocenes with C_2 symmetry gives rise to blocky Ethylene/4-Methyl-pentene copolymers having segments rich in ethylene content and another rich in 1-olefin content along the polymer backbone.

Leone et al. [2012] also used homogeneous α-diimine Ni(II)/Et_2AlCl system to synthesis ethylene/4-methyl-1-pentene copolymers.

Kakinuki et al. [2009] copolymerized ethylene with various pentenes including 4-methyl-1-pentene, using different titanocenes.

Table 2.6 lists the recent works related to the copolymerization of ethylene with 4-methyl-1-pentene.

Table 2.6: List of catalysts used for ethylene/4-methyl-1-pentene co-polymerization.

Reference	Catalyst
Mauler et. al. 1996	$Et[Ind]_2ZrCl_2$/MAO
Chen, 1997	$Me_2Si(\eta^5\text{-}Me_4C_5)(^tBuN)MR_2$/MAO
Ivantech et. al 2000	$[(CH_3)_2C(Ind)_2]ZrCl_2$, $[(CH_3)_5Cp]ZrCl_3$, $[(CH_3)_2Si(Ind)_2]ZrCl_2$,$[(CH_3)_2C(Cp)_2]ZrCl_2$, $[(C_6H_5)(C_2H_5)C(Ind)_2]ZrCl_2$, $[(Ph)_2C(Cp)(Flu)]]ZrCl_2$, and $[(CH_3)_2C(CH_3Cp)(Flu)]ZrCl_2$.
Xu and Cheng 2001	$[\eta^5\text{: }\eta^1\text{-}(2,3\text{-}Me_2Benz[e]Ind)SiMe_2N^tBu]TiCl_2$/MAO
Irwin 2004	$Me_2\text{-}Si(\eta^5\text{-}2\text{-}Me\text{-}benz[\eta]Ind)(\eta^1\text{-}N\text{-}t\text{Bu})TiCl_2$/MAO
Mosia, 2004	$Me_2C(Cp)(Flu)ZrCl_2$/MAO
Awudza and Tait 2007	Cp_2ZrCl_2/MAO and Silica/Cp_2ZrCl_2/MAO
Losio, 2008	$[Me_2Si(\eta^5\text{-}Me_4C_5)\text{-}(\eta^1\text{-N-tBu})TiCl_2]$/MAO
Kakinuki, 2009	$Cp^*TiCl2(N=C^tBu_2)$, $Cp^*TiCl_2(O\text{-}2,6\text{-}^iPr_2C_6H_3)$ & $[Me_2Si(C_5Me_4)(NtBu)]TiCl_2$/MAO
Losio 2009	$rac\text{-}H_2C\text{-}(3\text{-tBuInd})_2ZrCl_2$
Galimberti 2010	$[Me_2Si(Me_4Cp)(N\text{-tBu})TiCl_2]$/MAO,TMA [Solution & Slurry]
Boragno et. al. 2010	[*rac*-(EBTHI)$ZrCl_2$]
Leone, 2012	α-diimine Ni(II)/Et_2AlCl

From the ongoing, we see that it is only in the work of Awudza and Tait that supported metallocene/MAO catalysts systems were used to copolymerize ethylene with 4-methyl-1-pentene. However, they didn't investigate the effect of MAO anion design on copolymerization mechanism, thermal properties, copolymer compositional heterogeneity or crystallization kinetics. These have been covered in this work.

2.5.2 Uses of ethylene/4-methyl-1-pentene copolymers

Because the copolymers of ethylene with 4-methyl-1-pentene are LLDPEs, we expect them to share same general applications of the LLDPEs. They are mainly used to make power cables, control cables, optical cables, and telephone cables as well as signal cables outer sheath. BP Innovex is a commercial producer of ethylene-4-methyl-1-pentene copolymers. The various grades with their properties and applications are given in Table 2.7 [bp.com/chemicals].

Table 2.7: BP Innovex ethylene-4-methyl-1-pentene copolymers.

Product	**Density (g/cm^3)**	**Applications and key characteristics**
LL6130AA	0.920	Cast stretch with high impact and low gels, low deposits and high throughput.
LL6208AF	0.920	Rich blends in heavy duty sacks and thin films e.g. mulch film, refuse sacks, liners, deep freeze. Good processibility and high mechanical performance.
LL6608AF LL6608LJ	0.928	Medium density thin film with low gels. Typical applications are liners, refuse sacks, co-extrusion, bread bags, produce bags.
LL6910AA LL6910KJ	0.936	High density blown grade with low gels for lamination and thin films, where stiffness is required.
L8109AA LL8109KJ	0.918	Super strength blown grade with good processibility and high mechanical performance. (Talc antiblock).
LL6930AA	0.936	Cast grade for cast stretch and GP blending film, low gels with good impact.
LL6430AA	0.924	Cast grade for cast stretch and GP blending film, low gels with good impact.
LL6430AA	0.924	Cast grade for cast stretch and GP blending film, low gels with good impact.

CHAPTER 3

METHODOLOGY

3.1 Catalysts Synthesis

3.1.1 General Considerations

All the manipulations were done under argon using standard Schlenk technique. The solvents used (n-hexane and toluene) were dried using 4A molecular sieve, which was regenerated by subjection to 120 ºC for 2 h and then 220 ºC again for 2 h.

Silica was dehydroxylated at 250 ºC for 4 h using a Thermocraft furnace equipped with a vertical quartz glass tube, a digital temperature indicator and a controller, a gas flow meter, and a vacuum pump. The silica was continuously fluidized during dehydroxylationusing nitrogen during the process. Upon completion of dehydroxylation, it was stored in an inert glove box.

3.1.2 Catalysts for Solution polymerization (Catalyst Ia and Catalyst Ib)

Catalyst Ia consist of untreated mixture of 1g of dehydroxylated silica, 25.7mg of (nBuCp)2ZrCl2 and 0.9ml of MAO. The precatalyst and silica were taken from the glove box under argon. MAO was added to this mixture under argon and the whole mixture diluted with 10ml toluene to enable transfer into the reactor. The silica is used to reduce fouling in the reactor. Catalyst Ib consist in addition to Ia, dicholorodimethylsilane ($ClMe_2SiCl$).

3.1.2 Catalysts for In-situ polymerization (Catalyst IIa and Catalyst IIb)

Catalyst IIa and IIb were prepared by slurring the dehydroxylated silica with de-moisturized (dried) toluene in a specially designed Schlenck flask followed by 20ml of toluene. MAO was added to this mixture dropwise under argon and under constant stirring at room temperature. This was followed by refluxing at 110 ^{o}C for 4 hours. The solvent was eventually dried using vacuum pump and the supported cocatalyst saved in a glove box. Catalyst IIa consist of the supported cocatalyst and the untreated $(^{n}BuCp)_2ZrCl_2$ precatalyst. For catalyst IIb, the silica was first functionalized with dicholorodimethylsilane ($ClMe_2SiCl$). This was done at 110 ^{o}C and refluzed for 20 h. At the end, the solvent was evaporated, and the dried functionalized silica was used to support the MAO as in IIa. Therefore, catalyst IIb consist of the functionalized silica supported MAO and untreated $(^{n}BuCp)_2ZrCl_2$.

3.1.3 Catalysts for slurry polymerization (Catalyst IIIa and Catalyst IIIIb)

Catalyst IIIa was prepared by supporting MAO on dehydroxylated silica as in IIa above. However, $(^{n}BuCp)_2ZrCl_2$, dissolved in dried toluene, was reacted with the above mixture for 1h. The synthesized catalyst was dried under vacuum and upon drying it was saved in a glove box.

Similarly, catalyst IIIa was prepared by supporting MAO on dehydroxylated silica as in IIb; and the remaining steps and the remaining catalyst synthesis procedure followed those of Catalyst IIIa.

3.2 Polymerization Trials and Synthesis of Polymers

Ethylene was homo- and copolymerized using a computer-interfaced, AP Miniplant laboratory-scale reactor set up. This consists of a fixed top head and a one-liter jacketed Büchi glass autoclave. The glassreactor was baked for two hours at 120 °C. Then it was purged with nitrogen four times at the same temperature. The reactor was cooled from 120 °C to 40 °C. About 200 ml of dried n-hexane was transferred to the reactor. Then 1.0 ml of 1.0 M triisobutylaluminum (TIBA) was added to scavenge the impurities that may poison the catalyst. The mixture was stirred for 10 min. n-hexane was dried by contacting it with 4A molecular sieves at room temperature over night that will decreased the moisture level to less than 10 ppm. The molecular sieve was activated at 230 °C. At this stage, for the copolymerization, 15 mL 1-hexene or 4-methyl-1-pentene was added. The resulting mixture was stirred at 50 rpm for 10 min.

The experimental catalyst was slurried in 50 ml n-hexane. The whole volume was siphoned into the reactor under mild argon flow. Ethylene was polymerized by passing it through oxygen- and moisture-removing columns and finally feeding it into the reactor at 5000Nml/min. The polymerization temperature and stirrer speed was set at 50 °C and 750 rpm, respectively. The trial took place for 1 h. Stopping the ethylene flow and venting the post-polymerization ethylene (in the reactor) to the atmosphere quenched the polymerization. Then, the data acquisition was stopped, the stirrer speed was reduced to about 100 rpm, and the reactor was cooled gradually to room temperature.

Upon completion of the polymerization trials as described above, the reactor was opened; and the resulting polymer was dried under ambient conditions in a hood, and was

weighed to obtain the yield. This was used subsequently to determine the corresponding catalyst activity. With each catalyst, one homo- and one copolymer each of 1-hexene and 4-methyl-1-pentene were synthesized, the morphology of which was evaluated as follows.

3.3 Molecular Weights and Polydispersity Indices

The synthesized ethylene homo- and copolymers were characterized in terms of molecular weight properties. That is weight average molecular weight (M_w) and polydispersity index (PDI) using Waters styragel gel permeation chromatography (GPC) (HT3 (500-30000), HT6E (5000-10mln). The column temperature was kept constant at 135 $^{\circ}$C.

The stabilizer Santanox-R, was added to 1,2,4 trichlorobenzene (TCB solvent) to prevent the polymer samples from degrading. Then, 1.0 mg of polymer sample was taken in a 1 mL vial, which was then dissolved in 1.0 mL stabilized TCB as follows. The polymer-containing sample vials was placed in the warming compartment of the GPC instrument at 135 $^{\circ}$C for about 5 hr. During this period, the vials were shaken very well to completely dissolve the polymers.

Before injecting the samples, the differential refractive index (DRI) detector was purged for 4 h using TCB (1 mL/min) to obtain stable baseline. On the other hand, the inlet pressure (IP) and the differential pressure (DP) outputs were purged for 1 hr.

The flow rate of TCB was 1.0 ml/min and each sample was analysed for 35 min. The instrument was calibrated using nine polystyrene standards whose peak molecular

weights ranged from 580 to 3.79 mln. The polystyrene calibration curve was used to obtain the equivalent polyethylene calibration curve using the Mark-Houwink constants: K = 0.0004, α =0.74 for PE and K = 0,00012, α = 0.707 for PS.

3.4 Thermal Properties and Thermal Fractionation

The thermal properties of the experimental resins and the films were measured in terms of peak melting point (Tpm) and % crystallinity, using a differential scanning calorimeter (DSC Q2000, Texas Instrument), which was calibrated using indium.

About 4.5 mg of each sample was taken in an aluminum pan, which was then sealed tightly with a lid. An empty sealed aluminum pan was used as a reference. The samples and the reference were put in the experimental carrousel and nitrogen flow rate was set at 50 ml/min. The temperature was equilibrated at 25 °C and then heat was applied at the rate of 10 °C/min until temperature to 160 °C (Cycle 1). This was followed by isothermal heating for 5 min so as to remove any thermal history, and/or unmelted crystals that may results in heterogeneous crystallization. They were cooled from 160 °C to 25 °C at the same heating rate (Cycle 2) and maintained at this temperature for 5 min. Finally, the samples were re-heated at 10 °C/min to 160 °C (Cycle 3).

The data for each cycle was acquired and handled using the TA explorer software. The peak melting temperature (T_{pm}) and the percent crystallinity were determined from the third Cycle whereas the peak crystallization temperature (T_{pc}) was obtained from the second. The thermogram under Cycle 3 fusion endotherm was integrated to obtain the heat of fusion (H_f) which is proportional to the crystallinity of the sample. The

percent crystallinity was determined using ΔH_f (J/g)/ΔH_{std} (J/g), where ΔH_{std} is the heat of fusion per repeat unit for a perfectly crystalline polyethylene; this equals to 290.0 J/g [Atiqullah et al. 2012; Wignall 2000]. The material density d_{polym} was calculated using T_{pm} [Chai 2003].

The polymers were thermally fractionated using the above DSC instrument, and following the successive self-nucleation and annealing (SSA) experimental procedure reported in the literature [Müller et al. 1997; Czaja et al. 2002; Müller and Arnal 2005; Białek et al. 2005; Lorenzo et al. 2006; Ga´scue et al. 2011]. We applied seven annealing steps. Details are available in Czaja et al. 2002.

3.5 Copolymer Composition Distribution

The chemical composition distribution of the copolymers was determined by crystallization fractionation technique *Crystaf*. The fractionation principle is summarized as follows. The dissolved polymer was sampled at even time interval, and the polymer solution concentration was measured, while the solution is cooled at a constant rate. A copolymer having a lower amount of comonomer crystallizes from the solution at a higher temperature than the one having a higher comonomer content (more short chain branches). The *Crystaf* crystallization profile shows the comonomer incorporation level in a copolymer, as well as the way in which the comonomer is distributed along the backbone [Monrabal 1994; Monrabal 1996; Sarzotti et al. 2002].

For measuring the composition distribution, Polymer Char CRYSTAF 100 was used. Sample solution of concentration 0.1% (w/w) in 1, 2, 4 trichlorobenzene (TCB) was prepared at 160 °C under stirring for 1 h. The solution was equilibrated at 95 °C for 45

min. This was crystallized subsequently from 95 °C to 35 °C at a cooling rate of 0.5 °C/min. The qualitative differential composition distribution ($\frac{dw}{dT}$ versus T) was obtained by numerical differentiation of the integral analogue. This was converted finally into the quantitative version using a calibration curve developed in our laboratory.

3.6 Copolymer Microstructure and Sequence Length Distribution

The microstructural parameters, including average short chain branch content and 1-hexene mol% in the synthesized copolymers, were determined using ^{13}C NMR spectroscopy. For this purpose, a Bruker 600 MHz AVANAC III spectrometer (Bruker BioSpin, Rheinstetten, Germany) was used. This instrument is equipped with a Bruker 5-mm broadband observe (BBO) multinuclear probe.

About 50-60 mg of each polymer sample was dissolved in about 0.55 ml of deuterated 1, 2, 4-trichlorobenzene (TCB) at a temperature of 130 °C, using the standard 5 mm NMR tube. The spectra were recorded using DEPT 135 pulse sequence, and analyzed using Bruker Topspin 2.1 software (Bruker BioSpin, Rheinstetten, Germany). The receiver gain was set at 203. Exponential line broadening of 1 Hz was applied before Fourier transformation.

We calculated the copolymer microstructural parameters following the well-known publications of Hsieh and Randall [1982] and Seger and Maciel [Seger and Maciel 2004]. In this matter, the identification of the triad sequences in the ^{13}C NMR spectrum forms the basis, which we did by applying the peak assignment procedures. First, we determined the various triad mole fractions using the Seger-Maciel algorithm and the

associated collective peak assignment regions. The advantages are documented in Seger and Maciel [2004]. The regions associated with the various chemical shifts assignment are tabulated below.

Table 3.1: Chemical shifts assignment for the ethylene/1-hexene copolymer system.

Assignment region	^{13}C chem shift range	Carbon type(s)	Contributing *n*-ads
A	42.0-39.5	αα	HHHH+EHHH+EHHE
B	38.1	CH(EHE)	EHE
C	36.0-33	CH(EHH) CH(HHH) $4B_4$ αγ $\alpha\delta^+$	EHH HHH EHE+EHH+HHH EHEH+HEHH EEHE+EEHH
D	31.0-28.5	γγ $\gamma\delta^+$ $\delta^+\delta^+$ $3B_4$	HEEH EEEH $(EEE)_n$ EHE+EHH+HHH
E	27.5-26.5	$\beta\delta^+$	EEHE+EEHH
F	25.0-24.0	ββ	EHEHE+EHEHH+HEHEH
G	23.4	$2B_4$	EHE+EHH+HHH
H	14.1	$1B_4$	EHE+EHH+HHH

Hsieh and Randall [1982] related the integrated intensities of the various collective assignment regions of Table 3.1 to the concentrations of the triads as follows [Seger and Maciel 2004].

$$k[EHE] = B \tag{3.1}$$

$$k[EHH] = 2(G - B - A) \tag{3.2}$$

$$k[HHH] = 2A + B - G \tag{3.3}$$

$$k[HEH] = F \tag{3.4}$$

$$k[EEH] = 2(G - A - F) \tag{3.5}$$

$$k[EEE] = {}^{1}/_{2}\,(A + D + F - 2G) \tag{3.6}$$

Next, we calculated the monad and diad mole fractions. Finally, we estimated the copolymer microstructural parameters of our interest by using the entries summarized above. The Necessary relationships for ethylene/1-hexene copolymers are given in Table 3.2 as in [Seger and Machiel 2004].

Table 3.2: Necessary relationships for ethylene/1-hexene copolymers.

Type	Necessary relationship
Monad—monad	[E]+[C]=1
Diad—diad	[EE]+ [EC]+ [CC]=1
Triad—triad	[EEE]+ [EEC]+ [CEC]+ [ECE]+ [ECC]+ [CCC]=1
Monad—triad	[E]=[EEE]+ [EEC]+ [CEC] [C]=[ECE]+[ECC]+ [CCC]
Diad—triad	[EE]=[EEE]+1/2[EEC] [EC]=[EEC]+2 [CEC]

The peak areas that give the triad relations are related to the signal intensity as given in [Kimura 1984] are as follows:

$$S_{PPP} = \sum_{a=0}^{a=n} aS_{EP(P)_aPE} = (I_{26.1} - I_{44.89} - I_{45.46})/k \quad (3.7)$$

$$S_{EPP}+S_{PPE} = 2\sum_{a=0}^{a=n} S_{EP(P)_aPE} = I_{45.46}/k \quad (3.8)$$

$$S_{PEP} = I_{24.29}/k \quad (3.9)$$

$$S_{EPE} = I_{44.89}/k \quad (3.10)$$

$$S_{EEP} + S_{PEE} = 2\sum_{b=0}^{b=n} S_{PE(E)_bEP} = 2\sum_{b=1}^{b=n} S_{PE(E)_bEP} + 2S_{PEEP} = (I_{30.49} + I_{30.98})/k \quad (3.11)$$

$$S_{EEE} = 2\sum_{b=1}^{b=n} bS_{PE(E)_bEP} = \frac{I_{29.99}}{2k} + \frac{I_{30.49}}{4k} \quad (3.12)$$

We modeled the sequence length distribution as follows. The normalized weight fraction w_n of the sequence of n ethylene units, according to Flory model, is related to the ethylene perpetuation probability p as follows [Flory 1955; Hosoda 2011]:

$$w_n = n(1-p)^2 p^{n-1} \tag{3.13}$$

For a statistical copolymer with very long chains, p is related to experimental reactivity ratio product $<r_E r_H>$ and ethylene mole fraction X_E as follows [Allegra 1992; Hosoda 2011]:

$$p = 1 - \frac{1-[1-4(1-<r_E r_H>)X_E(1-X_E)]^{\frac{1}{2}}}{2(1-<r_E r_H>)X_E} \quad <r_E r_H> \neq 1 \tag{3.14}$$

$$p = X_A = X_E \quad <r_E r_H> = 1 \tag{3.15}$$

3.7 Vinyl Unsaturations

The determination of vinyl unsaturations is divided into two parts. First, we made make bubble-free polymer films; then, we characterized them using FTIR spectroscopy. The film-making process is summarized below.

About 100 mg of the copolymer sample was placed in the sample holder of a Universal film maker (Spectra Tech Incorporated, Model No. 0016-030). Then the temperature was increased to 145 °C. A compressive load of 1.5×10^3 kg was applied to the molten polymer samples for about 4 min; and then the temperature was decreased gradually to 60 °C. Finally, the pressure was released, and the fabricated films taken out. The measured thickness of the resulting films is expected to vary between 200 to 300 μm.

The vinyl unsaturation N_{vunsat}, in terms of number of unsaturations per 1000 C atom, in the as-synthesized polyethylenes was determined using the following relationship and FTIR spectroscopy [Blom et al. 1994]:

$$N_{vunsat} = \frac{(-CH = HC-)\ number}{1000\ C} = FW_{methylene} \times \frac{A(2x_H + 1)}{\rho\ t\ \varepsilon} \tag{3.16}$$

where A is the integrated absorbance corresponding to the types of vinyl unsaturations—terminal vinyl, vinylidene, and *trans*-vinylene (internal vinyl). They are shown at 908 cm^{-1}, 888 cm^{-1}, and 964 cm^{-1} FTIR wave numbers, respectively. $FW_{methylene}$ is the formula weight of methylene that equals to 14. ρ is the film density in gcm^{-3} and t is its thickness in cm, and ε is the molar extinction coefficient in $mol^{-1}lcm^{-1}$ for a specific vinyl unsaturation. Values of $\varepsilon$are available in the literature [Blom et al. 1994; Kim and Chang-Sik 2003; Hoáng et al. 2006; Anton 1994]. The term ($2x_H$ + 1) accounts for incorporation of 1-hexene into the copolymer backbone; where x_H is the mole fraction of 1-hexene in the ethylene-1-hexene copolymer.

3.8 Modeling of Lamellar Thickness Distribution

Polyethylenes, like other members of polyolefins, are semi-crystalline materials. Assuming an orthogonal frame work, and that a chain-folding crystallization mechanism dominates, the melting point T_m could be thermodynamically related to the dimensions of a crystal lamella (crystallite) through the famous Gibbs-Thomson equation [Kim and Chang-Sik 2004; Hoáng et al. 2006].

$$T_m = T_m^0 \left[1 - \frac{2}{\Delta H_f^0}\left(\frac{\sigma_1}{L_1} + \frac{\sigma_2}{L_2} + \frac{\sigma_3}{L_3}\right)\right] \tag{3.17}$$

where T_m^0 is the equilibrium melting temperature of an infinitely thick (perfect) crystal; σ_1, σ_2, and σ_3 are the basal specific surface free energies of the crystal lamella, which are associated with the crystallization chain folding process; L_1, L_2, and L_3 represent the

dimensions of the three orthogonal directions. ΔH_f^0 is the heat of fusion per unit volume of a perfect crystallite. Let us make the following assumptions:

- The lateral and transverse dimensions of the framework are much longer than the lamellar thickness. This implies that L_2 and $L_3 >> L_1$, which leads to $L_1 = L_{lamella}$ (folded crystal lamellar thickness), and $\sigma_1 = \sigma_{ssfe}$

- The crystallite parameters do not depend on temperature T and lamellar thickness $L_{lamella}$ over the temperature range considered.

Then Equation 3.17 simplifies to the following expressions [Hoáng et al. 2006; Anton et al 1994; Simha and Branson 1994]:

$$T_m = T_m^0 \left[1 - \frac{2\sigma_{ssfe}}{\Delta H_f^0 L_{lamella}}\right] \tag{3.18}$$

$$L_{lamella} = \frac{2\sigma_{ssfe}}{\Delta H_f^0}\left(\frac{T_m^0}{T_m^0 - T_m}\right) \tag{3.19}$$

Equation 3.19 shows that T_m decreases as $L_{lamella}$ decreases; and vice versa; and $T_m \to T_m^0$ as $L_{lamella} \to \infty$. T_m^0 is the equilibrium melting temperature of a crystalline homopolymer. Note that Equation 3.19 is the variant of the Gibbs-Thompson equation for a lamellar crystallite of large lateral dimensions and finite thickness. For a random copolymer *with comonomer excluded from the lamellar/crystallization thickness (that is, chain fold/stem),* T_m^0 in Equation 3.19 should be substituted by the corresponding copolymer equilibrium melting temperature $T_{m,copolym}^0$ which can be determined using

the Flory model [Stockmayer 1945; Soares 2007; Alghyamah and Soares 2009a; Alghyamah and Soares 2009b; Anantawaraskul et al. 2009]:

$$\frac{1}{T^0_{m,copolym}} = \frac{1}{T^0_m} - \frac{R}{\Delta H_u} lnX_A \tag{3.20}$$

Where ΔH_u is the heat of fusion of ethylene repeat unit and X_A is the mole fraction of ethylene in the random copolymer.

The calculation procedure for lamellar thickness distributions and chain fold length is outlined as follows. Use is made of the Cycle 3 DSC melting phase transformation endotherm. We assume further that the rate of heat flow, at a given temperature, is directly proportional to the mass of a crystallite with a lamellar thickness in the range $L_{lamella}$ and $L_{lamella} + dL_{lamella}$, and chain fold $-CH_2-$ repeat unit between n and $n + dn$ that has melted during dT [Hoáng et al. 2006;Anton et al. 1994]. Therefore, the melted crystallite mass fraction χ_i corresponding to time t_i and temperature T_i can be written as:

$$\chi_i(t) = \frac{\int_{t_0}^{t+dt}\left(\frac{dH}{dt}\right)_{i+1} dt - \int_{t_0}^{t+dt}\left(\frac{dH}{dt}\right)_i dt}{\int_{t_0}^{t_f}\left(\frac{dH}{dt}\right) dt} \left(t_0 \le t \le t_{f;} T_0 \le T \le T_{f;}\right) \tag{3.21}$$

Where t_0 and t_f are the times that correspond to the beginning and completion of melting; and T_0 and T_f are the temperature analogues, respectively.

The weightaverage lamellar thickness, *for a continuous distribution*, is given by [Soares 2007]:

$$L_{wav\ DSC\text{-}GT} = \frac{\sum_{i=1}^{n} L_{lamella,i}\, \chi_i \left(L_{lamella,i+1} - L_{lamella,i}\right)}{\sum_{i=1}^{n} \chi_i \left(L_{lamella,i+1} - L_{lamella,i}\right)} \tag{3.22}$$

The width of the lamellar distribution is given by the root mean square lamellar thickness $L_{\sigma DSC\text{-}GT}$, which is defined as follows.

$$L_{\sigma DSC-GT} = \sqrt{\frac{\sum \chi_i \left(L_i - L_{wav\,DSC-GT}\right)^2}{\sum \chi_i}} \tag{3.23}$$

CHAPTER 4

RESULTS AND DISCUSSIONS

4.1 Elucidation of MAO Anions and Catalyst Performances

The following matrix gives the polymerization trials carried out with various catalyst systems listed in Schemes 4.1 through 4.6.

Table 4.1: List of Polymerization trials

Category		Catalyst	Ethylene Homo-polymerization	Ethylene/1-hexene Copolymerization	Ethylene/4M1P Copolymerization
I	I(a)	Solution: DH SiO_2 +(^{n}BuCp)$_2ZrCl_2$+MAO	AS 16	AS 17	AS 18
	I(b)	Solution: DH SiO_2 +(^{n}BuCp)$_2ZrCl_2$+MAO +$ClMe_2SiCl$	AS 23	AS 29	AS 30
II	II(a)	In situ: Supported MAO+(^{n}BuCp)$_2ZrCl_2$	AS 32	AS 36	AS 35
	II(b)	In situ: Supported MAO+(^{n}BuCp)$_2ZrCl_2$ +$ClMe_2SiCl$	AS 40	AS 38	AS 39
III	III(a)	Supported (^{n}BuCp)$_2ZrCl_2$/MAO	AS 5	AS 7	AS 6
	III(b)	Supported (^{n}BuCp)$_2$ $ZrCl_2$/ MAO/$ClMe_2SiCl$	AS 11	AS 9	AS 10

Polymerization conditions: Temperature = 50^{o}C; Flow rate = 5000Nml/min; Time = 1hr; Catalyst concentration [Zr] = 0.264mmolZr/(L *n*-hexane); Cocatalyst:Catalyst ratio = 48:1

Generation of the MAO anions

Schemes 4.1 and 4.6 illustrate the MAO anions generated during solution, in-situ and slurry polymerizations without and with dicholorodimethylsilane. For solution polymerization, Silica was not functionalized, but rather used as a carrier to prevent

MAO from gelling and choking the feeder, and to ensure its unifiorm distribution within the reaction volume. It also served as an exothermic carrier to prevent reactor fouling, and ensure to the formation of polymer particles.

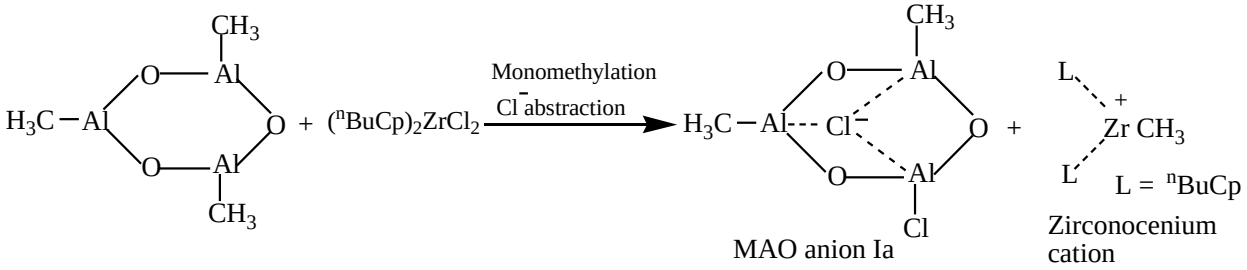

Scheme 4.1: MAO anion Ia generated during solution polymerization (without silane).

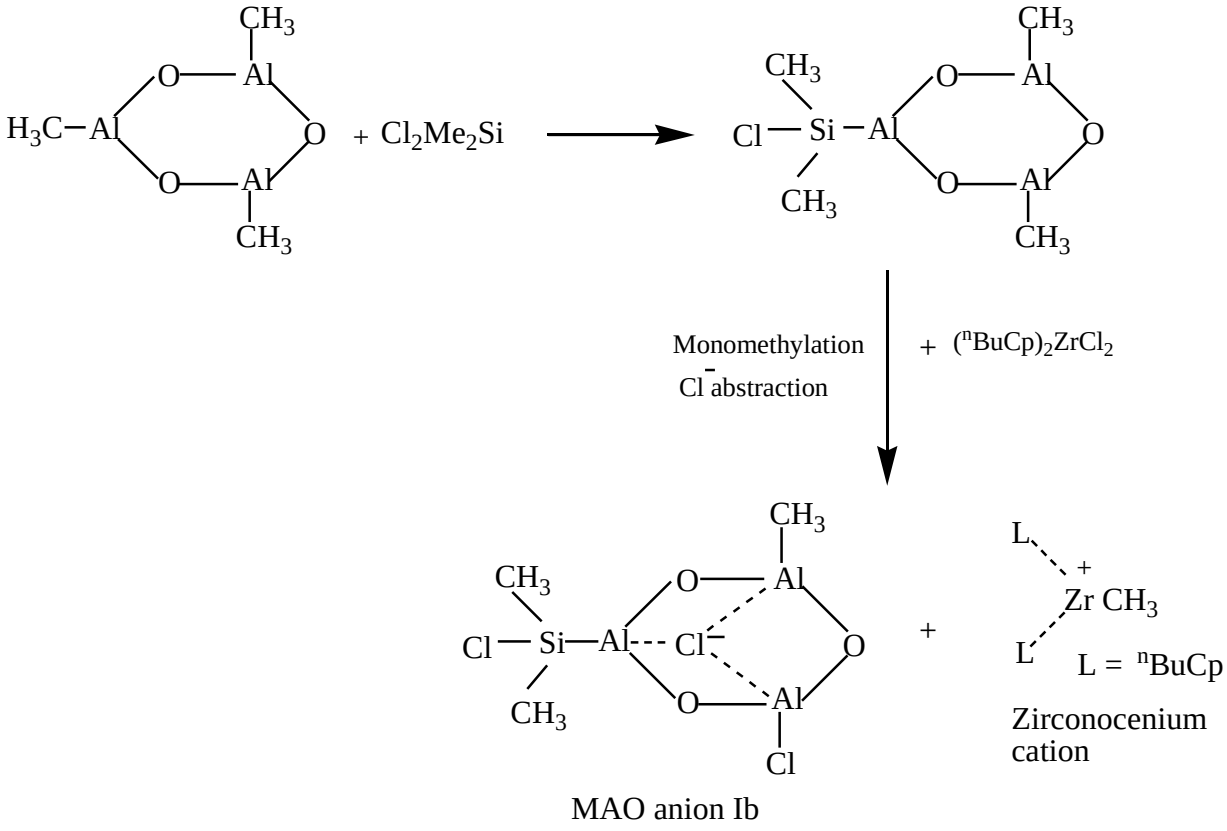

Scheme 4.2: MAO anion Ib generated during solution polymerization (with silane).

While contacting silica with MAO, the following reaction occurs (Schemes 4.3 to 4.6). The isolated —OH Brönsted acid group reacts with the labile basic bridging methyl group (—CH_3) of MAO [Chen et al. 2000, Negureanu et al. 2005, Linnolahti et al. 2008, Pédeutour et al. 2001, Babushkin et al. 2000, Ystenes et al. 2000]. Note that MAO does not have a unanimously agreed upon structure. However, the proposed three-dimensional cage structures characterized with the following—structural similarity with poly(*tert*-butylaluminoxane) cages, preferred hexagonal (six-membered ring) faces, and four-coordinate Al and three-coordinate O centers, comprising Al–O and Al–Me bonds—are most widely accepted [Thomas et al. 2005, Chen et al. 2000, Negureanu et al. 2005, Linnolahti et al. 2008, Pédeutour et al. 2001, Ystenes et al. 2000, Atiqullah et al. 2006].

For MAO anoins IIb and IIIb, in particular, during functionalization of silica, the isolated —OH Brönsted acid group reacts with the chloride ligand (—Cl) of $ClMe_2SiCl$ [Atiqullah and Marmaduke 2008, Kaivalchatchawal et al. 2012], generating HCl that gets stripped during drying of the synthesized catalyst under very high vacuum. The resulting modified silica (Si–O– Me_2SiCl) next contacts MAO. Here, the following ion-pair ($[Si–O– Me_2Si]^{\delta+}[MAOCl]^{\delta-}$) is postulated to form through chloride abstraction by the partial consumption of the strong Al Lewis acidic site of MAO. See Schemes 4.4 and 4.6. This MAO Lewis acid site is attributed to the coordinatively unsaturated Al in an —AlO_2Me— environment (that consists of the tricoordinated Al atoms bridging the tricoordinated oxygen atoms) [Eisch et al. 1985, Eisch et al. 1991, John et al. 1993, Fusco et al. 1998, Panchenko et al. 1999, Talsi et al. 1999]. Therefore, the Lewis acid strength of MAO anions IIb and IIIb partially decreases. Thus $ClMe_2SiCl$ plays a dual role; it modifies silica as well as MAO.

During impregnation of $(^{n}BuCp)_2ZrCl_2$ on SiO_2/MAO (Schemes 4.3 and 4.5) and SiO_2- $ClMe_2SiCl$/MAO (Schemes 4.4 and 4.6), the following two reactions occur. First, the bridged labile methyl groups of the silica-supported MAOs monomethylate a chloride ligand (—Cl) of $(^{n}BuCp)_2ZrCl_2$; then another one is abstracted by the strong Al Lewis acidic site of MAO [Chen et al. 2000, Pédeutour et al. 2001, Babushkin et al. 2000, Coevoet et al. 1998a, Coevoet et al. 1998b]. The Cl-ligand-exchanged Me group in $(^{n}BuCp)_2ZrCl_2$ remains intact. Consequently, the corresponding solid-state electrostatic ion-pairs (which are the active catalyst centers) are generated [Chen et al. 2000, Pédeutour et al. 2001, Babushkin et al. 2000].

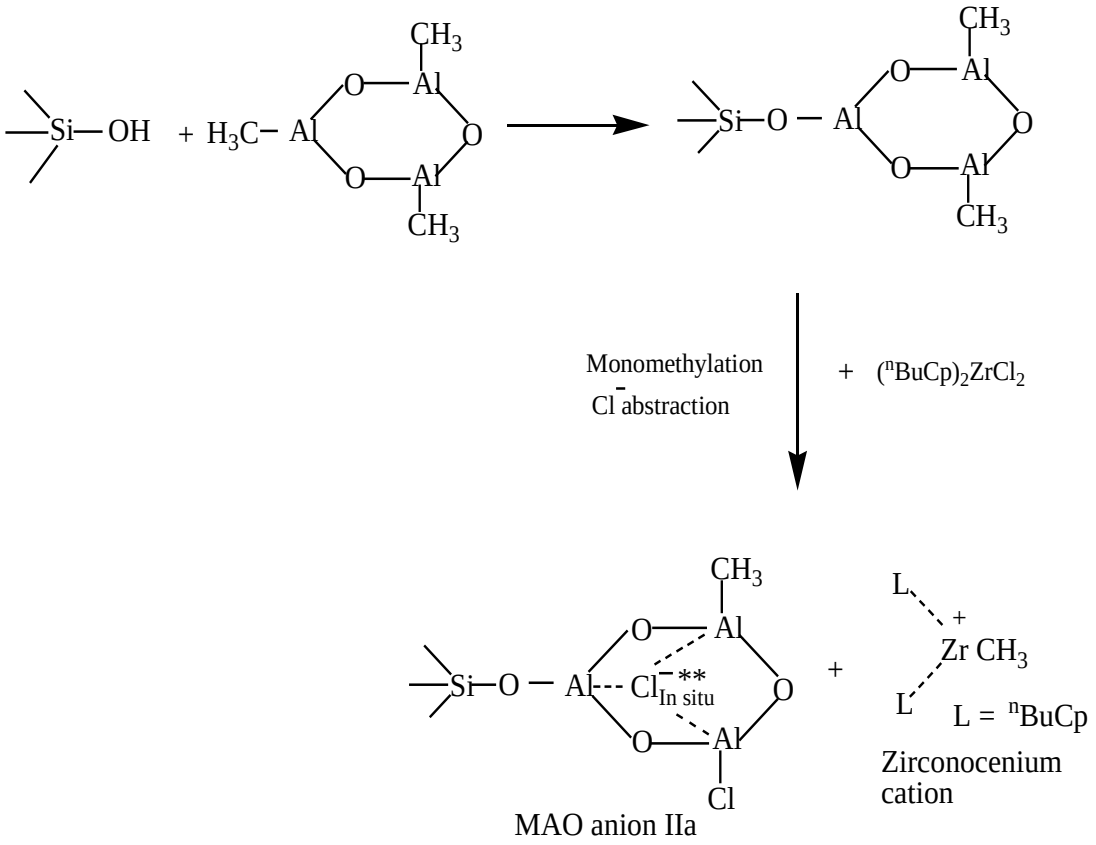

Scheme 4.3: MAO anion IIa generated In-situ (without silane).

** Generated in the reactor from the reaction of MAO supported on dehydroxylated silica and $(^{n}BuCp)_2ZrCl_2$, in the presence of n-hexane, TIBA, ethylene, and comonomer (1-hexene or 4M1P) in the case of copolymerization.

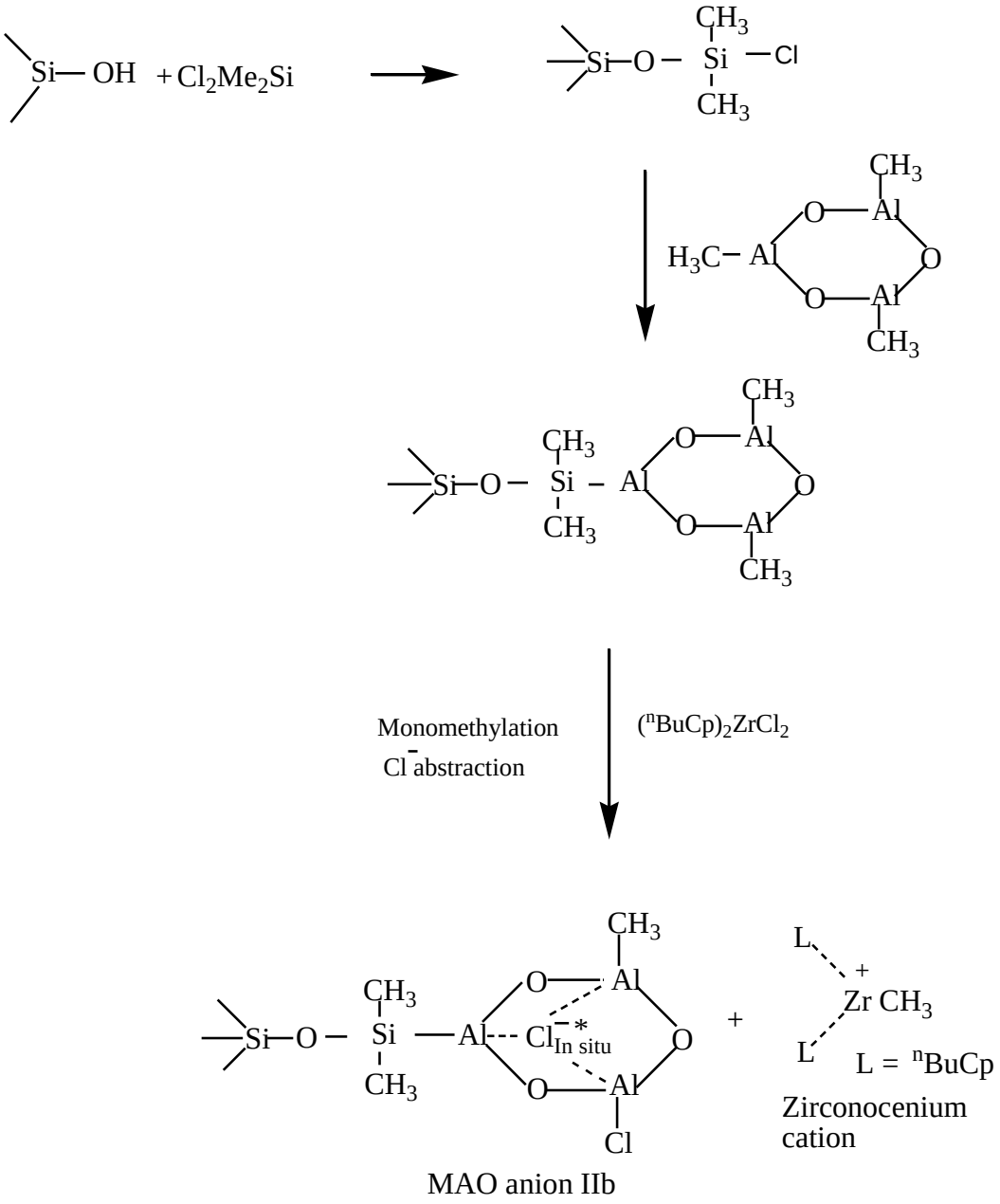

Scheme 4.4: MAO anion IIb generated In-situ (with silane).

** Generated in the reactor from the reaction of MAO supported on $ClMe_2SiCl$—treated dehydroxylated silica and $(^nBuCp)_2ZrCl_2$, in the presence of n-hexane, TIBA, ethylene, and comonomer (1-hexene or 4M1P) in the case of copolymerization.

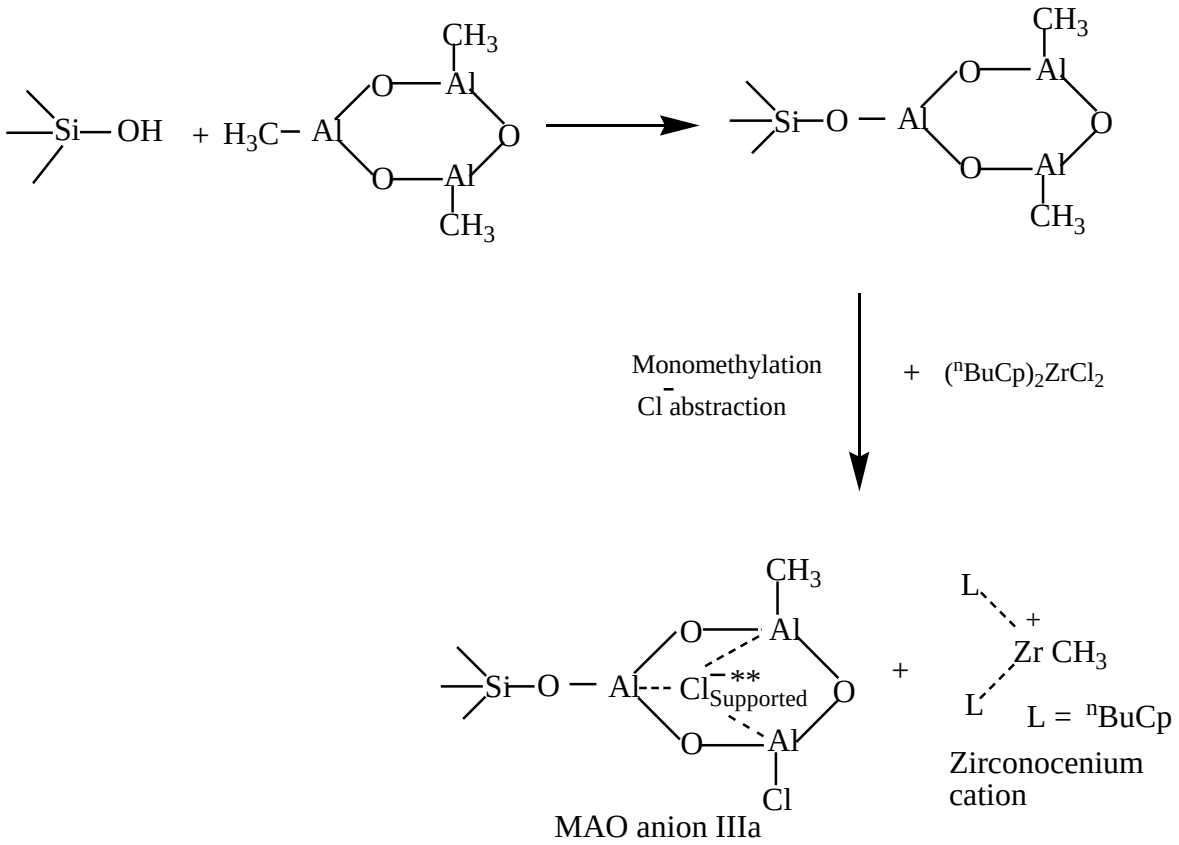

Scheme 4.5: Supported MAO anion IIIa (without silane).

**Generated during catalysts preparation after supporting MAO on dehydroxylated silica followed by $(^{n}BuCp)_2ZrCl_2$.

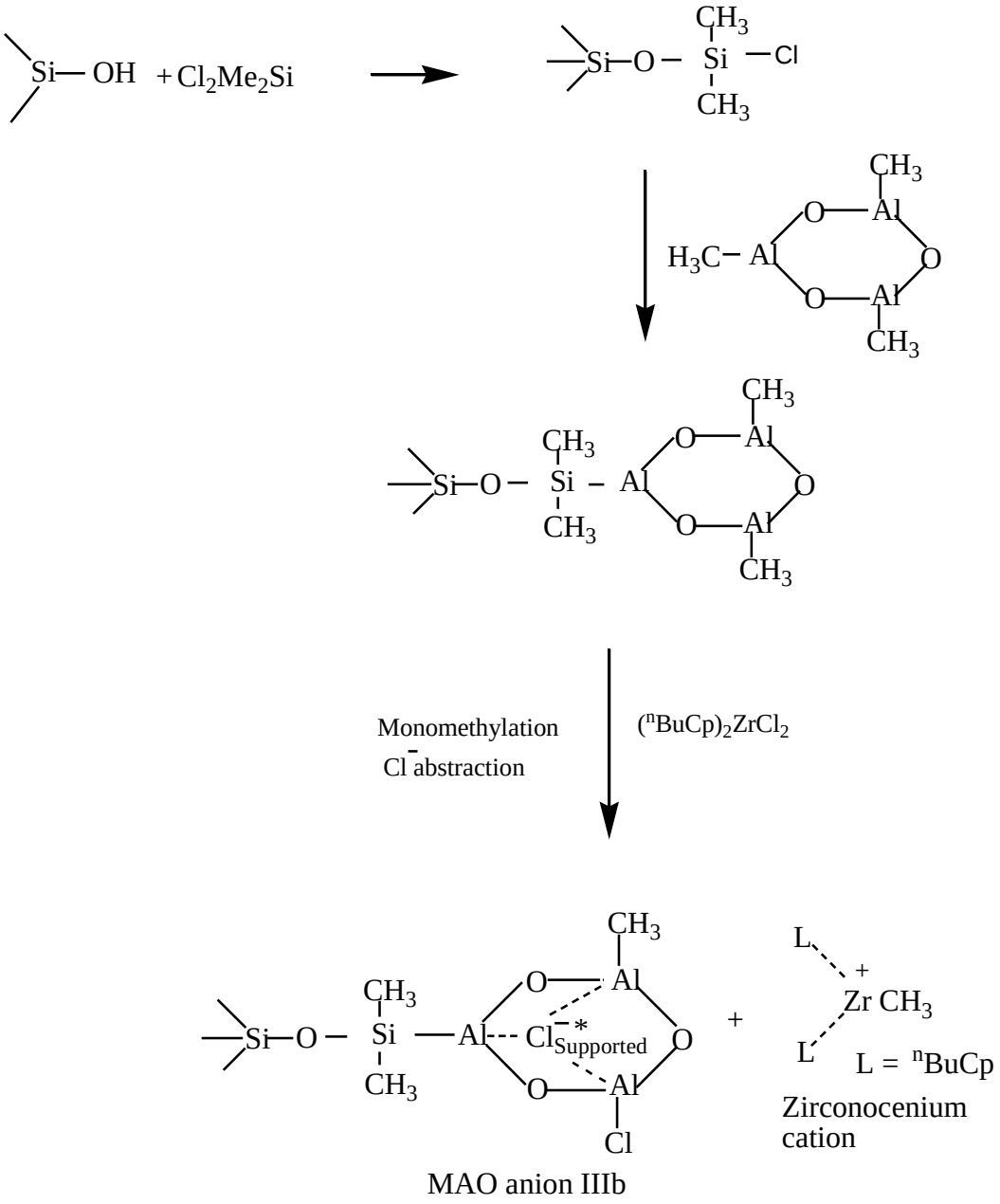

Scheme 4.6: Supported MAO anion IIIb (with silane).

*Generated during catalysts preparation after treating dehydroxylated silica with $ClMe_2SiCl$ and supporting MAO followed by $(^nBuCp)_2ZrCl_2$.

Catalyst performances

Figure 4.1 illustrates the productivity of the various catalyst systems. The linker $ClMe_2SiCl$ showed a negligible effect on the catalysts activity. This is vivid in the similar heights of the bars for the corresponding cases with and without silane. In-situ homo- and copolymers gave much lower productivities. Interestingly, the supported systems exhibited similar productivity with the Solution systems. Therefore, we conclude that we did not experience a drop in catalyst activity upon supporting.

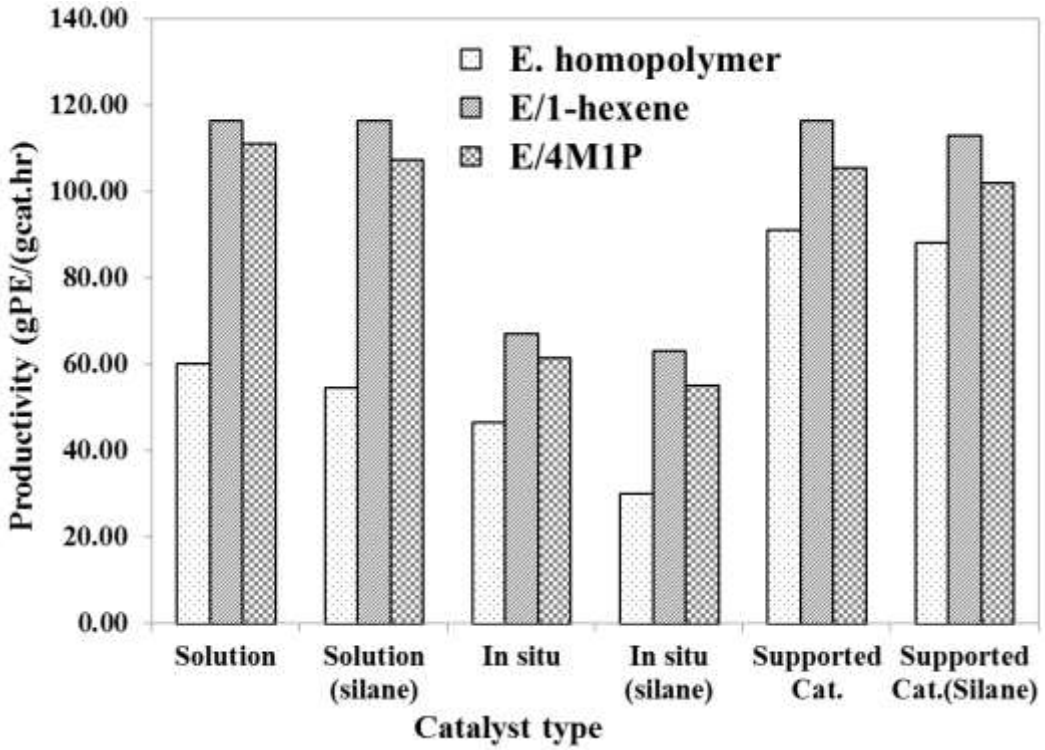

Figure 4.1: Catalyst Performance: Productivity obtained using various catalyst systems.

The copolymerizations showed positive comonomer effect which is most pronounced with the solution polymerizations. Positive comonomer effect has been reported for such situations under which the catalyst is soluble in polymerization medium, but not the

polymer. This shows that copolymerization rate enhancement occurs even in the absence of Fink's filter discussed by [Przybyla et al. 1999]. Moreover, positive to negative comonomer effects prevail with the increasing concentration of 1-hexene comonomer [Chen and Marks 2000, Koivumiiki and Seppala 1993, Jaber and Harmon 1993, Koppl 2000]. The filter effect does not well accommodate this transitional behavior. Additionally, it does not align with the chain transfer role of 1-hexene that significantly drops the molecular weight through the generation of different vinyl unsaturations in the copolymer backbone.

On the other hand, the activation of the dormant/sleeping catalytic sites, unlike the filter effect, is an intrinsic chemical phenomenon. In this context, the activation of the dormant Zr^{+}–H catalytic sites by 1-hexene is to be specially considered [Karol et al. 1993, Pasquet and Spitz 2003, Koivumiiki and Seppala 1993, Schaverien et al. 2001, de Freitas et al. 2011, Chang et al. 1992, Quijada et al. 1997, Chu et al. 1999, Kissin et al. 1999]. Note that these Zr^{+}–H sites originate through Route A and Route B of Scheme 2.5. The combination of Zr^{+}–CH_3 and Zr^{+}–H is considered to be a single family of active center. However, in the first case, the initiation starts with the insertion of ethylene whereas in the latter case, it begins with 1-hexene [Kissin et al 1999]. Consequently, the less substituted carbon bonded to Zr^{+}. See Scheme 2.6.

4.2 Solution Polymerization Results

4.2.1 Bulk properties: Mw, PDI, thermal properties, microstructural properties and vinyl unsaturations

Table 4.2 shows the catalyst productivity weight average molecular weights and the polydispersity indices for the solution homo- and copolymers. Positive comonomer effects were observed in both E/1-hexene and E/4M1P copolymerizations. The low values of PDI in the homopolymerizations indicate that most of product was formed by the same or very similar active site types. The broadening of the PDI in the copolymerization however indicates the participation of many active sites type in the copolymerizations.

Table 4.2: Solution homo- and copolymers: Catalyst productivity, Mw and PDI.

Anion type	Polymer type	Catalyst productivity (gPE/gcat.hr)	M_w (g/mol)	PDI
MAO anion Ia	Ethylene homopolymer	60.00	329,664.00	1.43
	E/1-hexene copolymer	72.73	291,092.00	2.42
	E/4M1P copolymer	110.91	181811.00	2.61
MAO anion Ib	Ethylene homopolymer	54.55	339487.00	1.63
	E/1-hexene copolymer	116.36	179561.00	3.81
	E/4M1P copolymer	103.64	262112.00	3.50

Table 4.3 below shows the thermal properties of solution homo- and copolymers. With MAO anion Ia, 1-hexene units in the LLDPE backbone decreased the melting point, crystallinity and density from 134 to 115 ^{o}C, 58 to 36 % and 0.95 to 0.91 g/mL respectively. Similar trend is seen with MAO anion Ib, where the crystallinity was decreased to as low as 43%.

Table 4.3: Solution homo- and copolymers: Thermal properties.

Anion type	Polymer type	T_{mp} (^oC)	T_{pc} (^oC)	Percent crystallinity (%)	Material density(g/cm^3)
MAO anion Ia	Ethylene homopolymer	133.93	116.76	58.29	0.952
	E/1-hexene copolymer	114.97	103.25	35.87	0.911
	E/4M1P copolymer	118.01	104.06	44.53	0.918
MAO anion Ib	Ethylene homopolymer	132.62	116.97	59.64	0.952
	E/1-hexene copolymer	118.11	104.11	43.32	0.918
	E/4M1P copolymer	118.93	105.96	44.87	0.920

However, the short chain branching impaired the high melting point, density and crystallinity values of ethylene/4-Methyl-1-pentene copolymers. Thus, we conclude that while both copolymers will have better processing properties than PE homopolymer, ethylene/4-Methyl-1-pentene LLDPE of MAO anion Ia will show a relatively higher use temperature than that of ethylene/1-hexene copolymer.

Table 4.4 illustrates the corresponding microstructural properties of the copolymers.

Table 4.4: Solution copolymers: Microstructural properties.

Parameter	MAO anion Ia		MAO anion Ib	
	E/1-hexene copolymer	E/4M1P copolymer	E/1-hexene copolymer	E/4M1P copolymer
E	0.90	0.96	0.85	0.96
C	0.10	0.04	0.15	0.04
$\mathbf{r_E}$	21.78	37.26	15.59	63.72
$\mathbf{r_C}$	0.39	0.02	0.33	0.24
$\mathbf{<r_E r_C>}$	8.41	0.59	5.15	15.21
$\mathbf{r_E r_C}$ **Markov1**	8.03	0.58	4.73	15.19
$\mathbf{n_E}$	14.26	24.71	9.00	36.90
$\mathbf{n_C}$	1.61	1.02	1.59	1.42
$\mathbf{\chi R}$	0.69	1.02	0.74	0.73

10% 1-hexene was incorporated with MAO anion IIa, which led to an average ethylene sequence length of 14 units. Similarly, 4% of 4M1P incorporated with the same MAO anion (Ia) gave to an average ethylene sequence length of 25 units. With MAO anion Ib, the percentage incorporation and average ethylene sequence length were 15% and 9 units respectively for E/1-hexene and 4% and 37 units respectively for E/4M1P. It is logical that the relationship between the percentage comonomer incorporation and the average ethylene sequence length is an inverse one. The experimental reactivity ratio products compare well with those calculated using First order Markov's copolymerization model. Therefore we conclude that the mechanism is well predicted by this model.

Table 4.5 shows the chain end unsaturations determined using Fourier Transform Infrared (FTIR) spectroscopy.

Table 4.5: Solution homo- and copolymers: vinyl unsaturations (FTIR) (units per 1000 Carbon atoms)

MAO Anion	Polymer type	$N_{vinylidene\ unsat.}$	$N_{terminal\ vinyl\ unsat.}$	$N_{Transvinylene\ unsat.}$	N_{Total}	Vinylidene: *Trans*-vinylene : Terminal vinyl
MAO anion Ia	E-homop	0.13	1.12	0.25	1.50	0.11 : 0.22: 1
	E/1-hex	1.35	0.27	0.08	1.69	5.08 : 0.28:1
	E/4M1P	1.89	0.05	0.04	1.98	36.04 : 0.84:1
MAO anion Ib	E-homop	0.01	0.48	0.04	0.54	0.03: 0.08:1
	E/1-hex	1.79	0.23	0.03	2.05	7.86 : 0.13: 1
	E/4M1P	1.83	0.16	0.01	1.99	11.55 : 0.04 :1

With MAO anion Ia, the synthesized ethylene homopolymer showed vinyledene ($CH_2=CR_1R_2$, $R_1 \neq R_2$), *trans*-vinylene ($R_1CH=CHR_2$, $R_1 \neq R_2$), and terminal vinyl (CH2=CHR) unsaturations. The ratio of these unsaturations was 0.11:0.22:1. This

indicates that the concentration of *terminal* vinyl unsaturations is the highest while that of vinyledene is the lowest. However, the three types of chain end unsaturations are present as opposed to earlier reports that only and *trans*-vinyl unsaturations are present in unsupported metallocene catalysts [Thorshaug 1997, 1998, 2000; Wigum 2000; Lehmus 2000; Bruaseth 2005; Bialek 2010; Mehdabadi 2012]. In the presence of dichlodimethylsilane, the homopolymer has a negligible amount of vinyledene unsaturation. The copolymers showed higher vinyledene unsaturation in all cases.

Schemes 4.7 to 4.9 illustrate the mechanisms of formation of these backbone unsaturations.

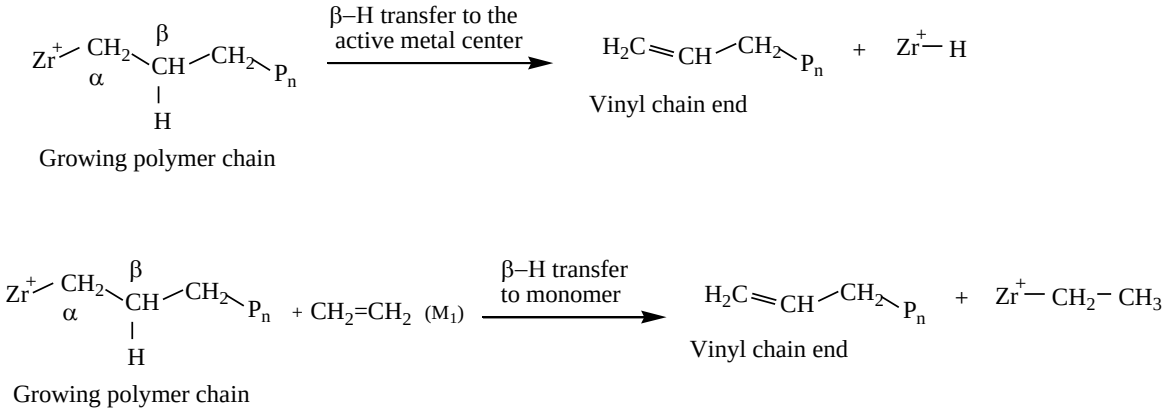

Scheme 4.7: β-H transfer to metal centre followed by β-H transfer to metal monomer.

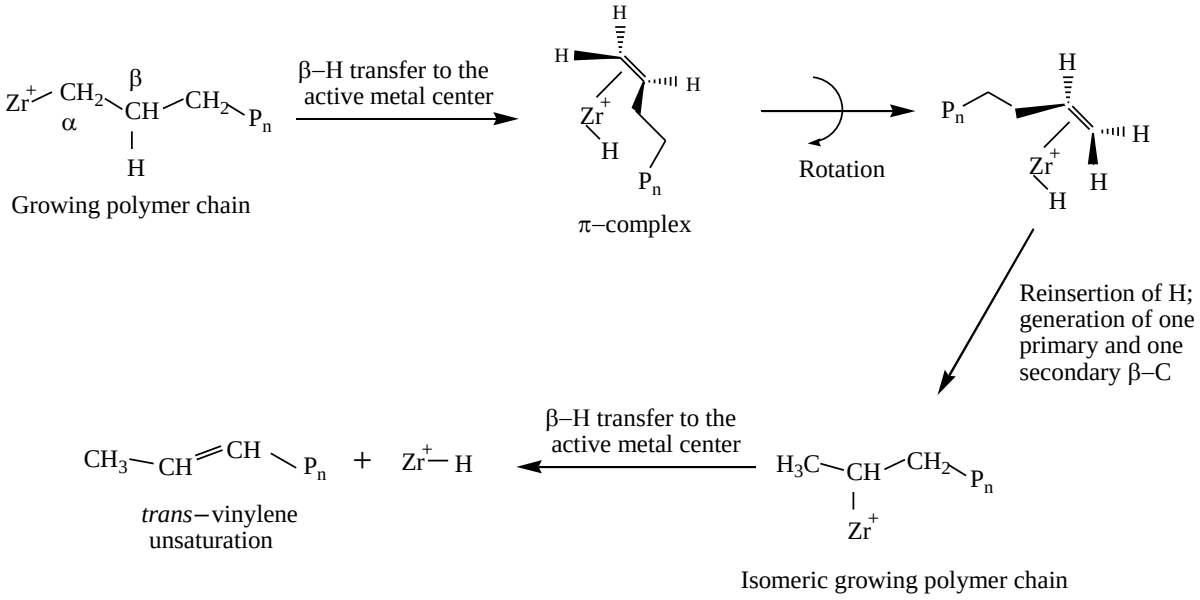

Scheme 4.8: β-H transfer to metal centre followed by termination.

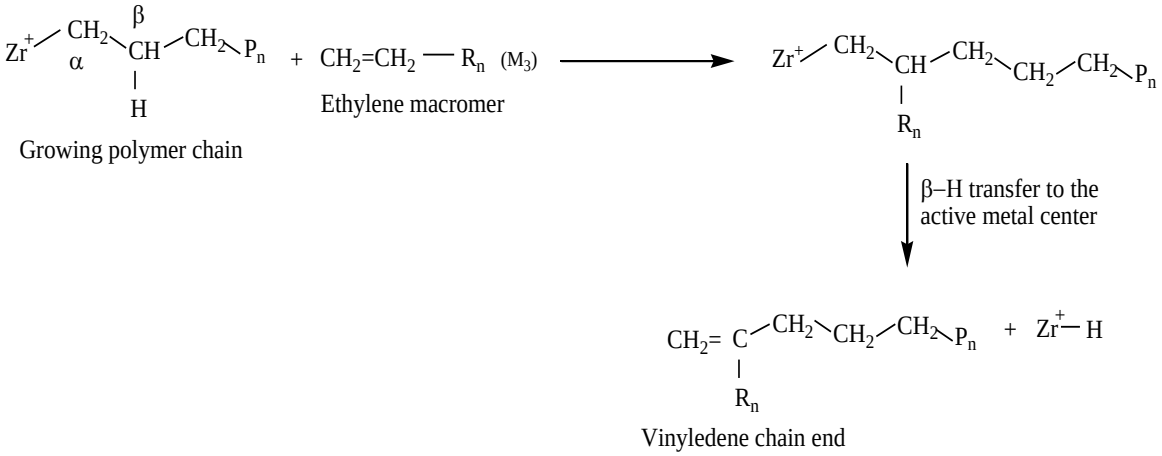

Scheme 4.9: Chain transfer to macromere followed by β-H transfer to metal center.

Where the terminal vinyl (CH_2=CHR) is formed when there is a β-H transfer from the growing polymer backbone end to the catalyst transition metal Zr and/or to the incoming ethylene monomer. This is called β-agostic interaction. In the first case, a metal hydride (Zr–H) species is produced while in the second case, a metal ethyl (Zr–C_2H_5) species is

generated [Thorshaug 1997, 1998, 2000; Wigum 2000; Lehmus 2000; Bruaseth 2005; Bialek 2010; Mehdabadi 2012; Britovsek 1999; Terao-Fujita 2006]. These routes are kinetically distinguishable. Whereas the former is a bimolecular reaction with a sterically bulkier six-centered transition state, the latter is a unimolecular reaction having a four-centered transition state. Therefore, β-H transfer to the incoming monomer is more sensitive to steric environments around the catalyst active site than β-H transfer to Zr [Britovsek 1999; Terao-Fujita 2006].

Kinetically controlled chain isomerization followed by β-H transfer to ethylene generates *trans*-vinylene unsaturation ($R_1CH=CHR_2$, $R_1 \neq R_2$) [Thorshaug 1997, 1998, 2000; Lehmus 2005; Bialek 2010] in the resulting homopolymer. See Scheme 2 (Thorshaug 1998, Scheme 7; Lehmus 2005, Scheme a). It should be noted that transfer of β-H prior to isomerization yields vinyl unsaturation. The chain isomerization occurs according to the following steps [Thorshaug 1998, 2000, Lehmus 2005]:

i. Transfer of β-H to the transition metal Zr;
ii. A partial detachment of the chain from Zr by breaking the Zr–CR bond (π-complexation);
iii. Relative rotation of the olefin and the metal hydride; and
iv. Reinsertion of hydrogen into the coordinated olefin, generating a structure with one primary and one secondary β-carbon.

4.2.2 Distributive Properties: MWD, LTD, SSA, CRYSTAF, SLD

Molecular weight distributions

Figure 4.2 illustrates the molecular weight distributions of solution homo- and copolymers synthesized with MAO anion Ia. With this MAO anion (Ia) the ethylene homopolymer produced has a narrow MWD. However, the ethylene/4-Methyl-1-pentene and ethylene/1-hexene copolymers contain low molecular weight fractions (or oligomers) which is seen their curves tailing towards the left.

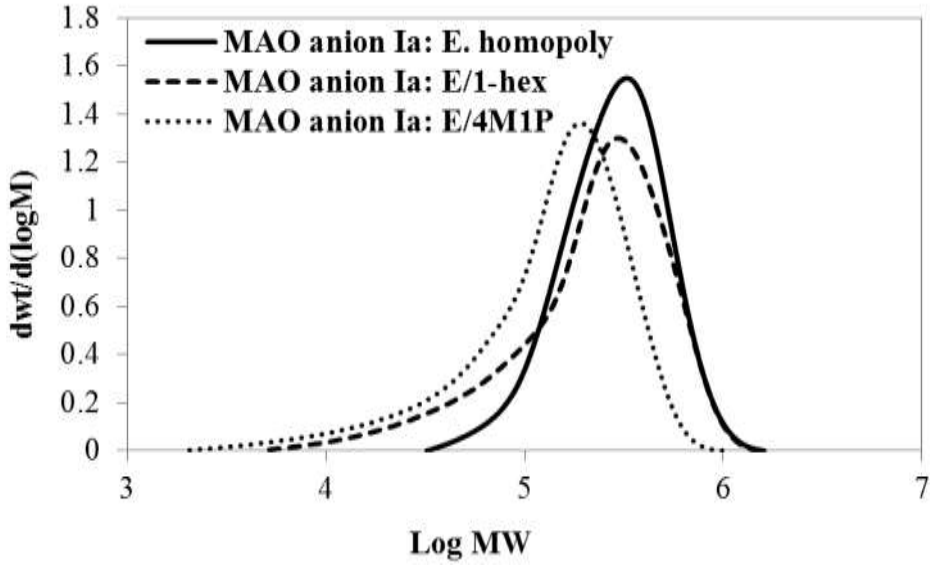

Figure 4.2: Molecular weight distributions for solution copolymers synthesized with MAO anion Ia.

Figure 4.3 below shows the molecular weight distributions for solution copolymers synthesized with MAO anion Ib. The trend in the MWD is not very different from that of MAO anion Ia. However, ethylene/1-hexene copolymer showed a higher fraction of the low molecular weight components (or oligomers).

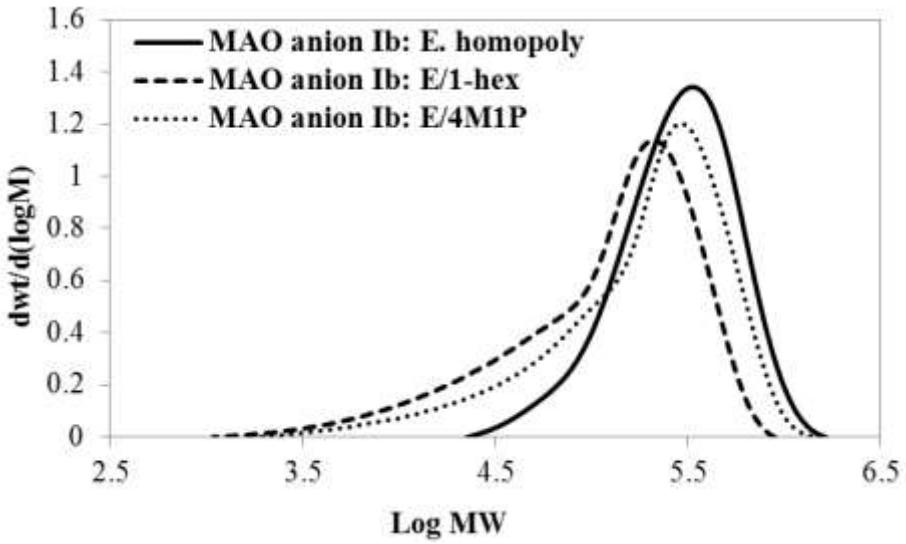

Figure 4.3: Molecular weight distributions for solution copolymers synthesized with MAO anion Ib.

Lamellar thickness distributions

Figure 4.4 shows the lamellar thickness distributions for solution homo- and copolymers synthesized with MAO anion Ia.

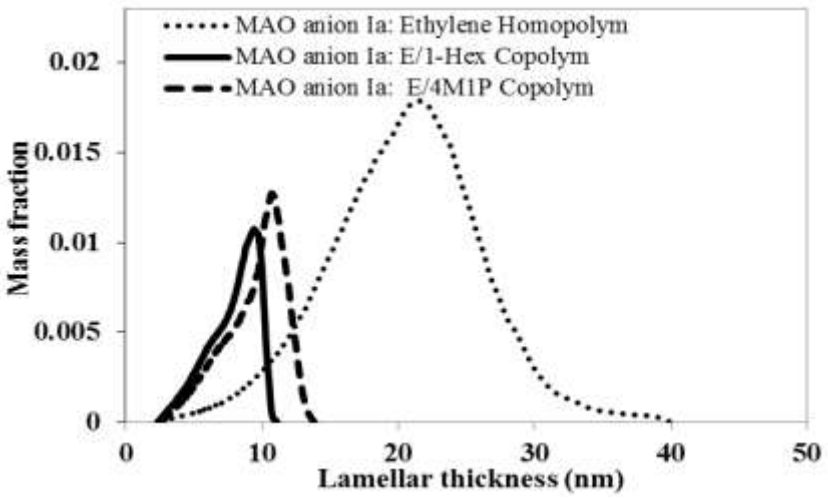

Figure 4.4: Lamellar thickness distributions for solution homo- and copolymers synthesized with MAO anion Ia.

Ethylene homopolym: $l_{lamellar\ wt.\ ave.}$= 20.53 *nm*; σ = 7.93; $l_{lamellar\ most\ probable.}$ = 21.13 *nm*;
E/1-hex. copolym: $l_{lamellar\ wt.\ ave.}$= 7.90 *nm*; σ = 2.48; $l_{lamellar\ most\ probable.}$ = 9.27 *nm*;
E/4M1P copolym: $l_{lamellar\ wt.\ ave.}$= 9.45 *nm*; σ = 3.03; $l_{lamellar\ most\ probable.}$ = 10.64 *nm*;

The lamellar thicknesses were calculated using Gibbs-Thomson equation (detailed in Chapter 3). In all cases, the average values of the lamellar thicknesses are less than the most probable ones. The span of each distribution as measured by standard deviation is given for each case. Ethylene homopolymer exhibited the widest span while ethylene-1-hexene and ethylene/4Methyl-1-pentene have much narrower distributions. This is also seen in their chemical composition distribution (CCD) plots. The bimodality is associated with non-uniform distribution of the side chain branching along the copolymer backbones.

Figure 4.5 shows the corresponding LTDs for homo- and copolymers of MAO anion Ib, with the average and most probable values as well as the span of the distributions.

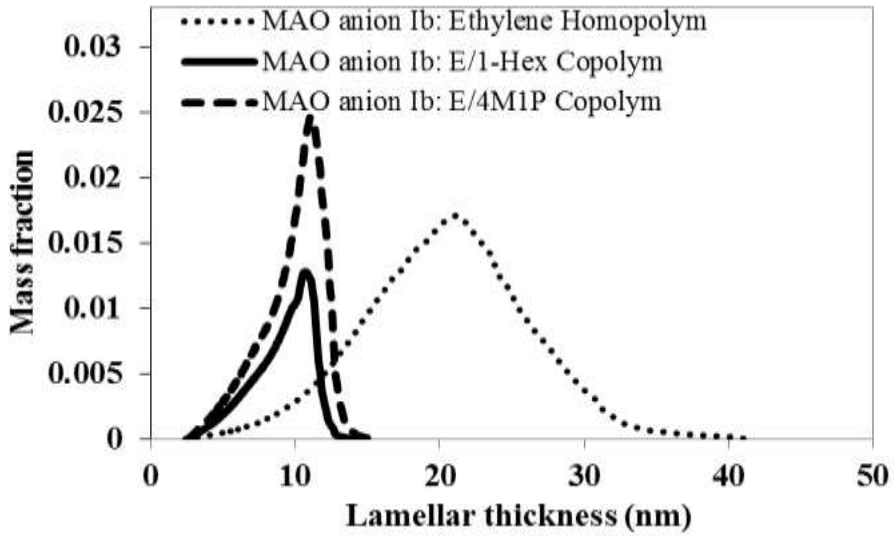

Figure 4.5: Lamellar thickness distributions for solution homo- and copolymers synthesized with MAO anion Ib.

Ethylene homopolym: $l_{lamellar\ wt.\ ave.}$= 20.49 *nm*; σ = 7.98; $l_{lamellar\ most\ probable.}$ = 21.13 *nm*;
E/1-hex. copolym: $l_{lamellar\ wt.\ ave.}$= 8.67 *nm*; σ = 2.58; $l_{lamellar\ most\ probable.}$ = 10.47 *nm*;
E/4M1P copolym: $l_{lamellar\ wt.\ ave.}$= 9.77 *nm*; σ = 3.99; $l_{lamellar\ most\ probable.}$ = 10.91 *nm*;

The trend is similar to that MAO anion Ia except that the width of the LTDs of the two copolymers concided. This conforms to to the similar results seen in their CCDs.

Successive Self-nucleation and Annealing (SSA)

The successive self-nucleation and annealing (SSA)- DSC experiment was pioneered by Fillon et al. [Fillon et al. 1993] for their isotactic polypropylene (PP). These experiments involved the partial melting of a semi-crystalline material, followed by recrystallization with the crystal fragments so produced as nuclei in the partial melting stage. The detailed procedure is described in the Chapter 3. Figure 4.6 illustrates the SSA thermogram for solution copolymers (MAO anion Ia).

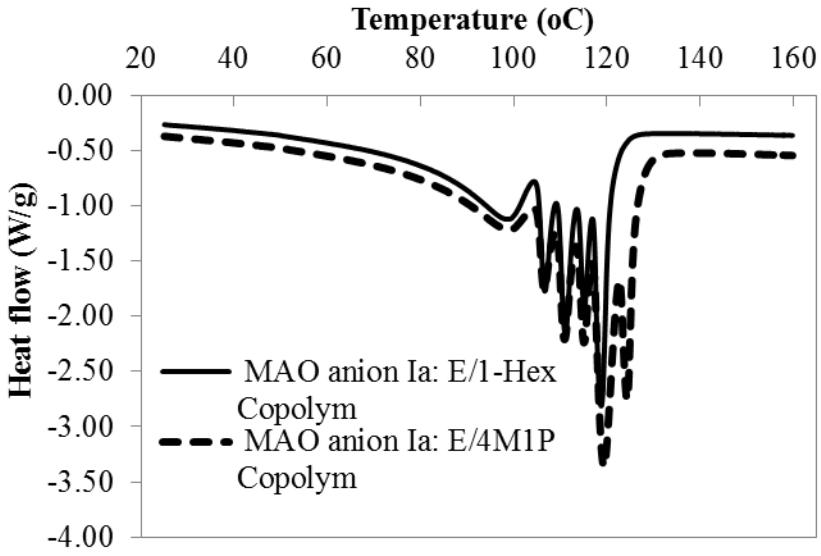

Figure 4.6: Successive Self-nucleation and Annealing thermogram for solution copolymers synthesized with MAO anion Ia.

With MAO anion Ia, the ethylene-1-hexene copolymers so obtained, showed five distinct melting peaks at (98.77, 106.49, 110.99, 115.01 and 118.71 °C), while ethylene/4-Methyl-1-pentene copolymer showed six melting peaks at (98.79, 106.07,

111.02, 114.86 and 124.21 °C). The additional peak covers the isomeric effect in the copolymerizations, while the coincidence in the rest of the peaks signify the similarity in the comonomers as well as the fact that same MAO anion was involved.

Each SSA peak denotes a population of backbones that have the same branch content, crystallinity, and lamellar thickness. These are illustrated in Figure 4.7 below.

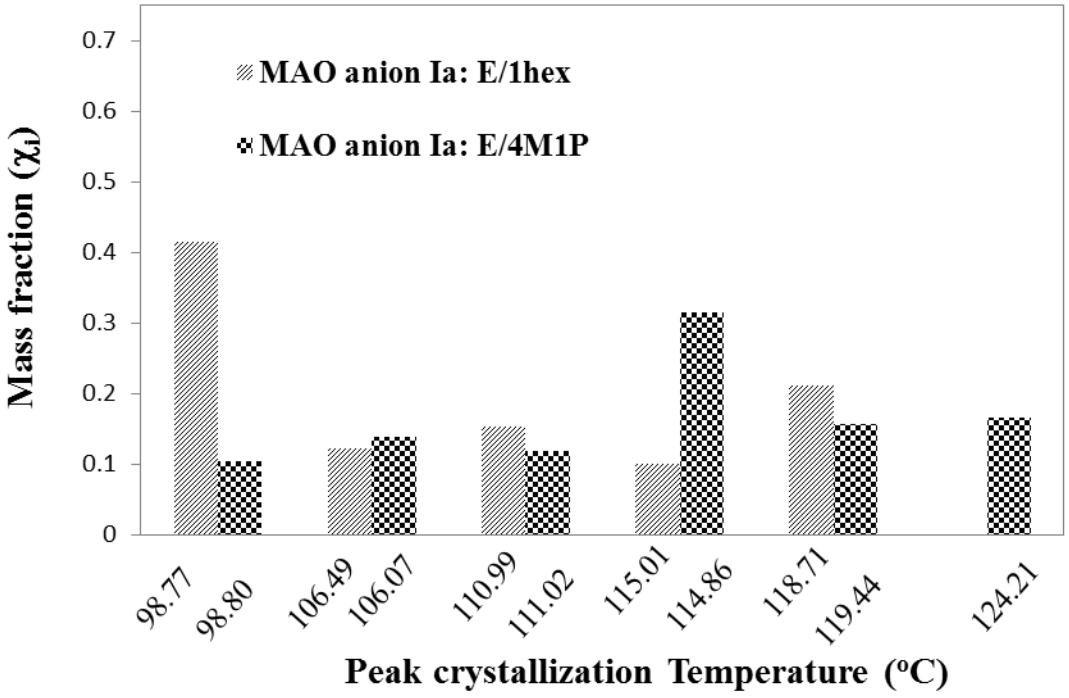

Figure 4.7: Mass fractions of the copolymer fractions with same branch content obtained with MAO anion Ia.

The SSA thermogram for MAO anion Ib is shown in Figure 4.8 below. Here, the catalysts did not produce LLDPEs with peaks around 98°C (unlike MAO anion Ia). However, both copolymers showed five distinct and coinciding peak fractionating temperatures.

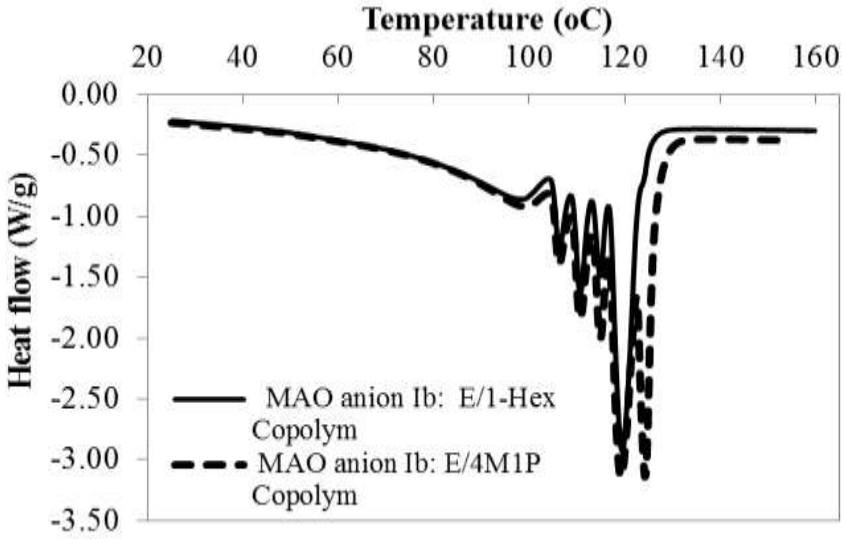

Figure 4.8: Successive Self-nucleation and Annealing thermogram for solution copolymers synthesized with MAO anion Ib.

Figure 4.9 shows the mass fractions of the copolymer fractions corresponding to the peaks of Figure 4.8.

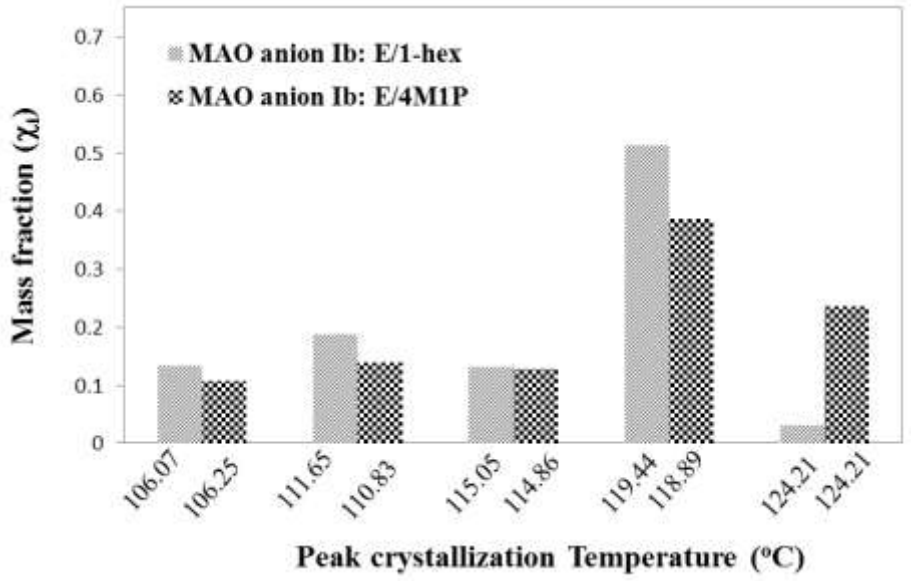

Figure 4.9: Mass fractions of the copolymer fractions with same branch content with MAO anion Ib.

The branch content at different peaks are varying significantly in E/1-hexene, while those obtained for E/4M1P at 106, 111 and 115°C are fairly uniform. Both copolymers, showed the highest fraction at 119.89 °C.

Crystallization analysis fractionation

Figure 4.10 illustrates the cystallization analysis fractionation for solution homo- and copolymers synthesized with MAO anion Ia. The chemical composition distribution of both ethylene/1-hexene and that of ethylene/4-Methyl-1-pentene copolymer are narrow with a small shoulder of a soluble fraction. These soluble fractions were observed only in the non-supported systems.

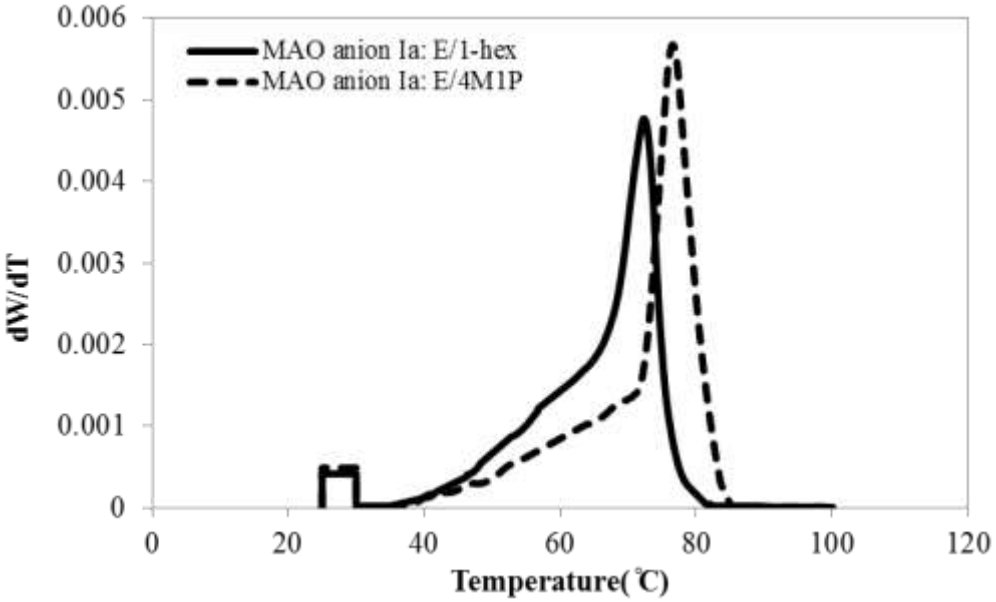

Figure 4.10: Cystallization analysis fractionation for solution copolymers (MAO anion Ia).

Figure 4.11 shows the corresponding CCD plots for solution copolymers (MAO anion Ib). Both distributions are narrow and without the shoulders. Therefore, soluble fractions or low molecular weight fractions are absent. The distributions are fairly uniform with high cystallizable fractions.

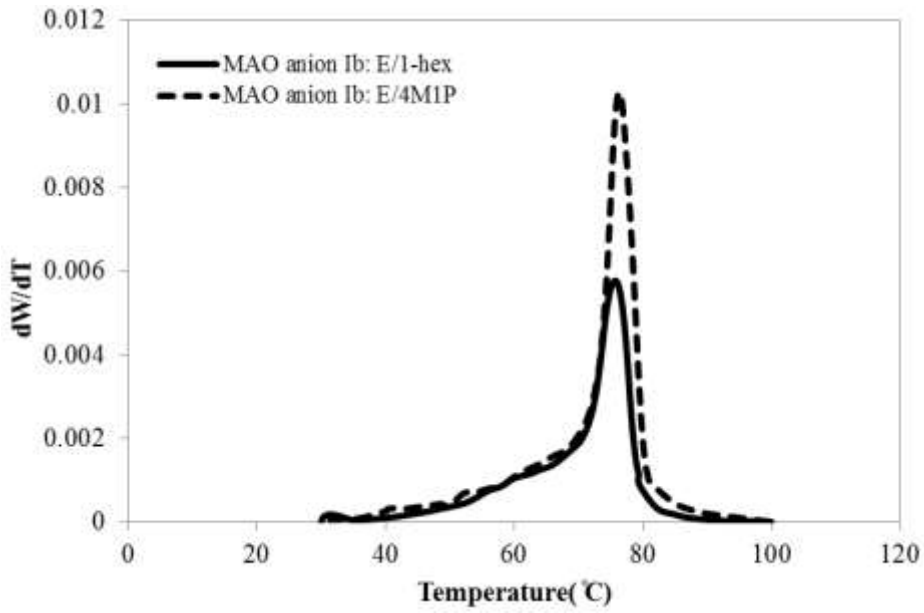

Figure 4.11: Cystallization analysis fractionation for solution copolymers (MAO anion Ib).

Ethylene sequence length distribution

The Figure above shows ethylene sequence length distribution along the copolymer backbone for solution copolymers (MAO anion Ia). E/4M1P copolymer has a wider distribution with most probable value of 36 ethylene units and a standard deviation of 51 units.

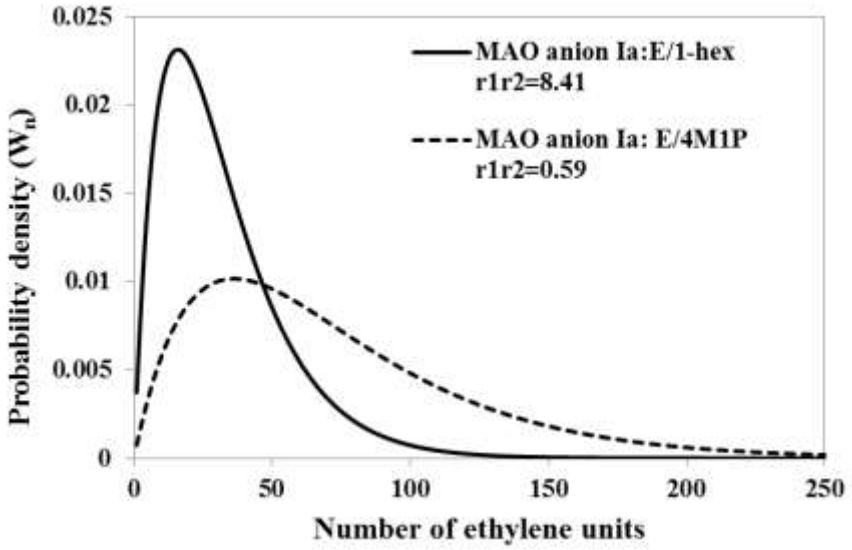

Figure 4.12: Ethylene sequence length distribution along copolymer backbones for solution copolymers (MAO anion Ia).

E/1-hex. copolym: $n_{ethylene\ units,\ wt.\ ave.}$= 32 *units*; σ = 22.47; $n_{ethylene\ units,\ most\ probable.}$ = 16 *units*;
E/4M1P copolym: $n_{ethylene\ units,\ wt.\ ave.}$= 72 *units*; σ = 51.13; $n_{ethylene\ units,\ most\ probable.}$ = 36 *units*;

Ethylene/1-hexene which has more comonomer incorporated (see Table 4.4) has a narrower distribution with most probable value of 16 ethylene units and a standard deviation of 22 units.

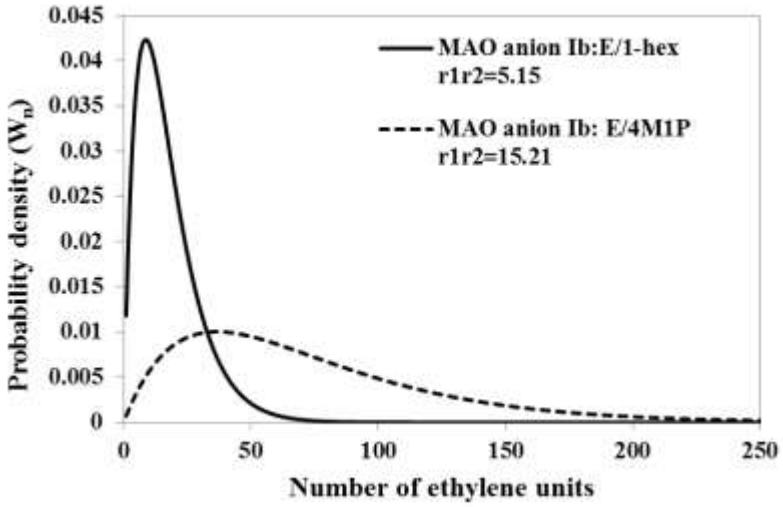

Figure 4.13: Ethylene sequence length distribution along copolymer backbones for solution copolymers (MAO anion Ib).

E/1-hex. copolym: $n_{ethylene\ units,\ wt.\ ave.}$= 17 *units*; σ = 12.29; $n_{ethylene\ units,\ most\ probable.}$ = 9 *units*;
E/4M1P copolym: $n_{ethylene\ units,\ wt.\ ave.}$= 73 *units*; σ = 51.44; $n_{ethylene\ units,\ most\ probable.}$ = 36 *units*;

E/4M1P copolymer has a wider distribution with most probable value of 36 ethylene units and a standard deviation of about 51 units. Ethylene/1-hexene which has more comonomer incorporated (see Table 4.4) has a narrower distribution with a most probable value of just 9 ethylene units and a standard deviation of 12 units.

4.3 In-situ Polymerization Results

4.3.1 Bulk properties: Mw, PDI, thermal properties, microstructural properties and vinyl unsaturations

Table 4.6 illustrates the catalyst productivity, weight average molecular weights and the polydispersity indices for the In-situ homo- and copolymers. Positive comonomer effects were observed in both E/1-hexene and E/4M1P copolymerizations. The low values of PDI indicate single site catalsyts.

Table 4.6: In-situ homo- and copolymers: Catalyst productivity, Mw and PDI.

Anion type	Polymer type	Catalyst productivity (gPE/gcat.hr)	M_w (g/mol)	PDI
MAO anion IIa	Ethylene homopolymer	46.36	318574.00	1.58
	E/1-hexene copolymer	67.00	229051.00	2.51
	E/4M1P copolymer	61.50	255864.00	2.22
MAO anion IIb	Ethylene homopolymer	55.00	416974.00	1.43
	E/1-hexene copolymer	63.00	244764.00	3.00
	E/4M1P copolymer	56.00	314908.00	3.87

Table 4.7 below shows the thermal properties of ethylene homo- and copolymers obtained during In-situ polymerization. With MAO anion IIa, 1-hexene units in the LLDPE backbone decreased the melting point and crystallinity from 134.08 to 114.08^{o}C and 65.7 to 41.92% respectively.

Table 4.7: In-situ homo- and copolymers: Thermal properties.

Anion type	Polymer type	T_{mp} (^{o}C)	T_{pc} (^{o}C)	Percent crystallinity (%)	Material density(g/cm^3)
MAO anion IIa	Ethylene homopolymer	134.08	117.36	65.7	0.953
	E/1-hexene copolymer	114.08	100.66	41.92	0.909
	E/4M1P copolymer	120.14	106.82	43.44	0.922
MAO anion IIb	Ethylene homopolymer	132.62	116.97	56.47	0.949
	E/1-hexene copolymer	114.81	101.32	36.6	0.911
	E/4M1P copolymer	120	108.5	43.36	0.922

Similar trend is seen MAO anion IIb, where the crystallinity was decreased to as low as 36.6%. In the case of copolymerization with 4-Methyl-1-pentene, the MAO anion had little effect as seen in constant values of these properties. However, the short chain branching impaired the high melting point, density and crystallinity values of ethylene homopolymer analogues. Thus, we conclude that while both copolymers will have better processing properties than PE homopolymer, ethylene/4-Methyl-1-pentene LLDPE will show a relatively higher use temperature than ethylene/1-hexene copolymer.

Table 4.8 below illustrates the corresponding microstructural properties of the copolymers. 12% 1-hexene was incorporated with MAO anion IIa, which led to an average ethylene sequence length of 12 units. Similarly, 3.3% of 4M1P incorporated with the same MAO anion (IIa) gave to an average ethylene sequence length of 31 units. With

MAO anion IIb, the percentage incorporation and average ethylene sequence length were 8% and 16 units respectively for E/1-hexene and 3.2% and 37 units respectively for E/4M1P. The experimental reactivity ratio products compare well with those calculated using First order Markov's copolymerization model. Therefore we conclude that the mechanism is well predicted by this model.

Table 4.8: In-situ copolymers: Microstructural properties.

Parameter	MAO anion IIa		MAO anion IIb	
	E/1-hexene copolymer	E/4M1P copolymer	E/1-hexene copolymer	E/4M1P copolymer
E	0.884	0.967	0.918	0.968
C	0.116	0.033	0.082	0.032
$\mathbf{r_E}$	20.60	35.62	20.87	45.66
$\mathbf{r_C}$	0.32	0.05	0.34	0.17
$\mathbf{<r_E r_C>}$	6.64	1.64	7.19	7.75
$\mathbf{r_E r_C}$ **Markov1**	6.29	1.65	6.90	7.99
$\mathbf{n_E}$	11.97	31.11	16.24	36.86
$\mathbf{n_C}$	1.57	1.06	1.45	1.22
$\mathbf{\chi R}$	0.72	0.98	0.75	0.85

Table 4.9 below shows the vinyl unsaturations for homo- and copolymers generated In-situ.

Table 4.9: In-situ homo- and copolymers: vinyl unsaturations (FTIR) (units per 1000 Carbon atoms).

MAO Anion	Polymer type	$N_{vinylidene\ unsat.}$	$N_{terminal\ vinyl\ unsat.}$	$N_{Transvinylene\ unsat.}$	N_{Total}	Vinylidene: *Trans*-vinylene : Terminal vinyl
MAO anion IIa	E-homop	0.04	1.21	0.15	1.39	0.03 : 0.11 : 1
	E/1-hex	1.41	0.08	0.01	1.50	17.84 : 0.12 : 1
	E/4M1P	1.57	0.15	0.03	1.75	10.58 : 0.22 : 1
MAO anion IIb	E-homop	0.10	1.39	0.20	1.69	0.07 : 0.14 : 1
	E/1-hex	1.39	0.39	0.06	1.84	3.51 : 0.16 : 1
	E/4M1P	2.30	0.80	0.05	3.15	2.90 0.06 : 1

Ethylene homopolymer showed negligible *trans*-vinylene and vinyledene unsaturation with both MAO anions IIa and IIb; while terminal vinyl unsaturation dominates in both cases. The copolymers on the other hand exhibited vinyledene as the most dominant type of chain end unsaturations. The total of these unsaturation fell in the range of about 1.4-2.0, except for ethylene/4-Methyl-1-pentene which led the list with about 3.5 units per 1000 Carbon atoms.

4.3.2 Distributive Properties: MWD, LTD, SSA, CRYSTAF, SLD

Molecular weight distributions

The Figure below shows the MWD of the In-situ homo- and copolymers synthesized with MAO anion IIa.

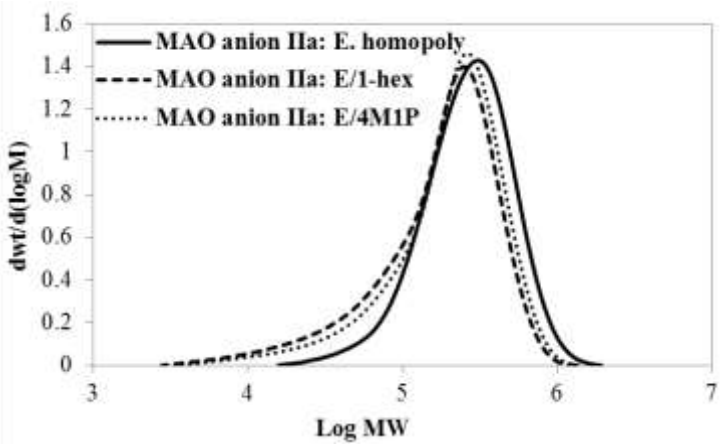

Figure 4.14: Molecular weight distributions for In-situ homo- and copolymers synthesized with MAO anion IIa.

The ethylene homopolymer has a narrow distribution, while ethylene/4-Methyl-1-pentene and ethylene/1-hexene copolymers have a broad distribution tailing towards the left, indicating the presence of low molecular weight fractions. This is due to chain transfer reactions.

Figure 4.15 shows the MWD of the In-situ homo- and copolymers synthesized with MAO anion IIb.

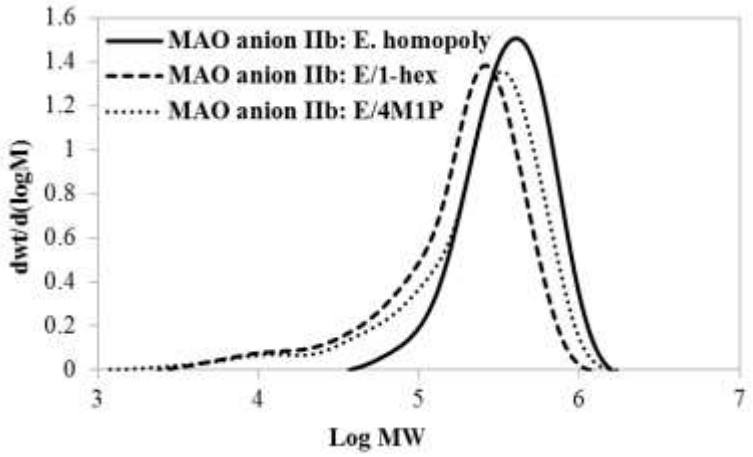

Figure 4.15: Molecular weight distributions for In-situ homo- and copolymers synthesized with MAO anion IIb.

Again, ethylene homopolymer shows a narrow distribution, while ethylene/4-Methyl-1-pentene and ethylene/1-hexene copolymers have broader distribution tailing towards the left, indicating the presence of low molecular weight components. This is due to chain transfer reactions.

Lamellar thickness distributions

Figure 4.16 shows the LTDs for homo- and copolymers of MAO anion IIa, with the average and most probable values as well as the spans of the distributions. Ethyelene homopolymer exhibits the widest distribution and the highest average LTD followed by ethylene/4-methyl-1-pentene and then ethylene/1-hexene copolymer. The bimodality exhibited by ethylene/4M1P copolymer justifies the non-uniformity of its chemical composition distribution (CCD).

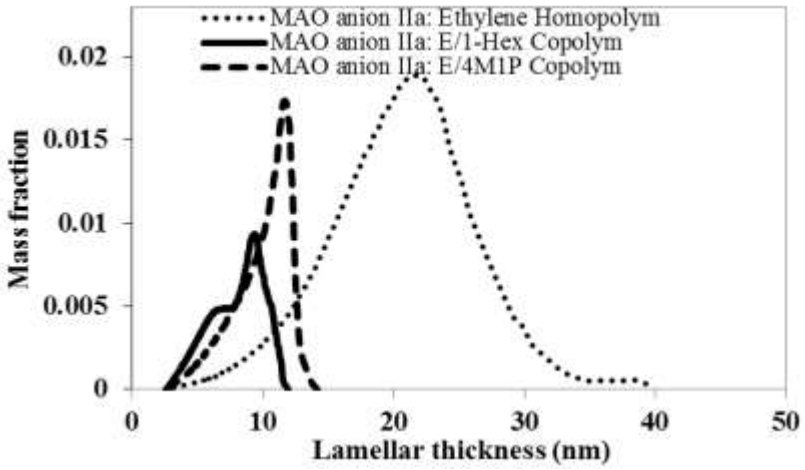

Figure 4.16: Lamellar thickness distributions for In-situ copolymers synthesized with MAO anion IIa.

Ethylene homopolym: $l_{lamellar\ wt.\ ave.}$= 20.72 *nm*; σ = 4.44; $l_{lamellar\ most\ probable.}$ = 21.47 *nm*;
E/1-hex. copolym: $l_{lamellar\ wt.\ ave.}$= 8.04 *nm*; σ = 2.56; $l_{lamellar\ most\ probable.}$ = 9.07 *nm*;
E/4M1P copolym: $l_{lamellar\ wt.\ ave.}$= 9.96 *nm*; σ = 3.03; $l_{lamellar\ most\ probable.}$ = 11.60 *nm*;

Figure 4.17 shows the corresponding LTDs for homo- and copolymers of MAO anion IIb, with the average and most probable values as well as the span of the distributions.

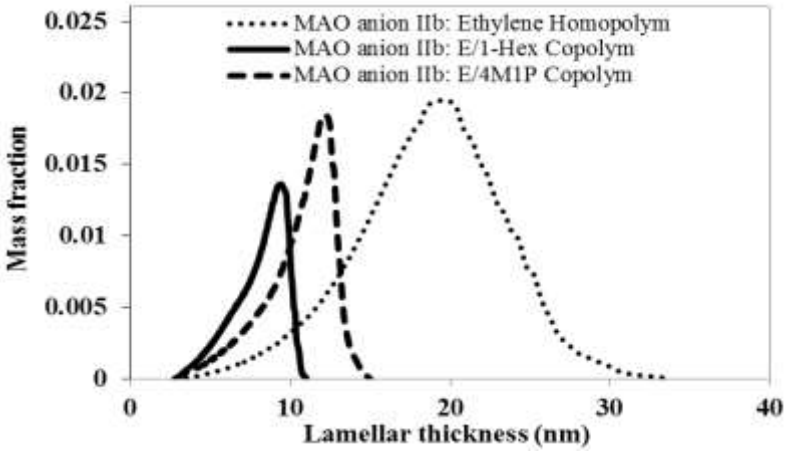

Figure 4.17: Lamellar thickness distributions for In-situ copolymers synthesized with MAO anion IIb.

Ethylene homopolym: $l_{lamellar\ wt.\ ave.}$= 18.78 *nm*; σ = 6.23; $l_{lamellar\ most\ probable.}$ = 19.54 *nm*;
E/1-hex. copolym: $l_{lamellar\ wt.\ ave.}$= 8.11 *nm*; σ = 2.11; $l_{lamellar\ most\ probable.}$ = 9.20 *nm*;
E/4M1P copolym: $l_{lamellar\ wt.\ ave.}$= 10.58 *nm*; σ = 3.10; $l_{lamellar\ most\ probable.}$ = 11.93 *nm*;

Again, ethyelene homopolymer shows the widest distribution and the highest average LTD followed by ethylene/4-methyl-1-pentene and then ethylene/1-hexene copolymer. Therefore the order of crystallinity of these materials decreases in this order.

Successive self-nucleation and annealing (SSA)

Figure 4.18 illustrates the SSA thermogram for In-situ copolymers (MAO anion IIa). Ethylene-1-hexene copolymers exhibited six distinct melting peaks at (98.56, 106.62, 110.02, 115.23, 118.71 and 123.84 °C), while ethylene/4-Methyl-1-pentene copolymer showed the same number of peak fractionating temperatures at (98.20, 106.62, 110.65, 114.86, 119.08 and 124.39 °C). The isomeric effect is seen in the varying side chain branching content, while the coincidence in the peak temperatures confirm that the that same MAO anion was used.

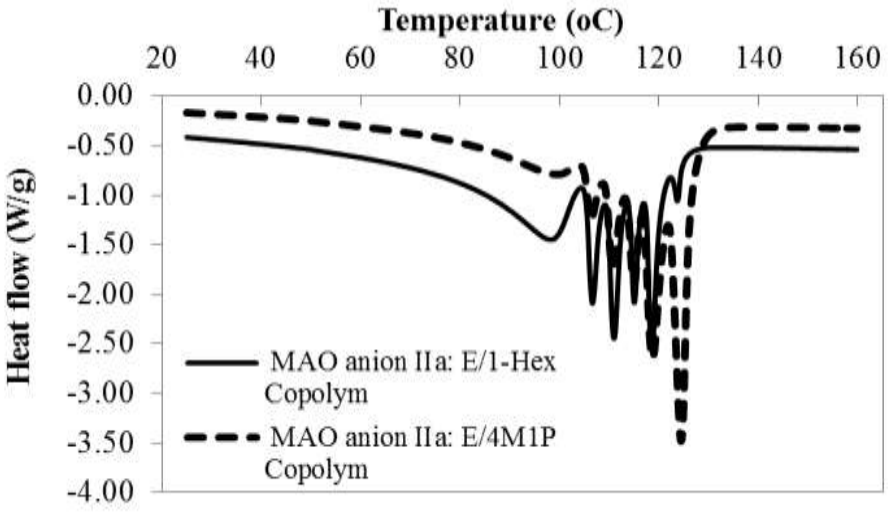

Figure 4.18: Successive Self-nucleation and Annealing thermogram for In-situ copolymers synthesized with MAO anion IIa.

Figure 4.19 below illustrates the population of backbones that have the same branch content, crystallinity, and lamellar thickness (i.e corresponding to each SSA peak).

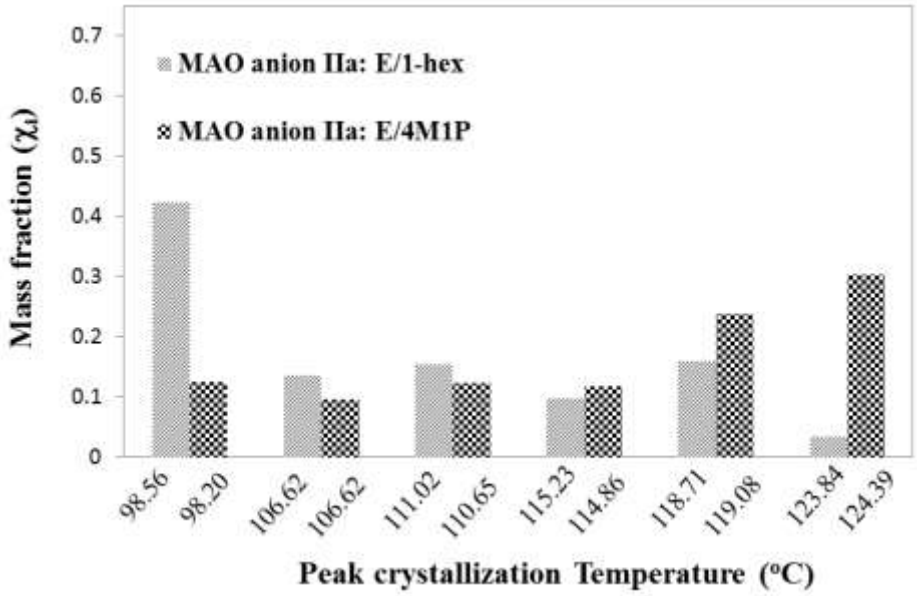

Figure 4.19: Mass fractions of the copolymer fractions with same branch content with MAO anion IIa.

The corresponding plots for MAO anion IIb copolymers are shown in the Figure below. For Ethylene/1-hexene copolymers, the peaks occurred at (98.74, 106.44, 110.83, 114.86, and 118.53 °C), while ethylene/4-Methyl-1-pentene copolymer showed same number of peak fractionating temperatures (106.62, 110.83, 115.23, 119.63 and 124.94 °C).

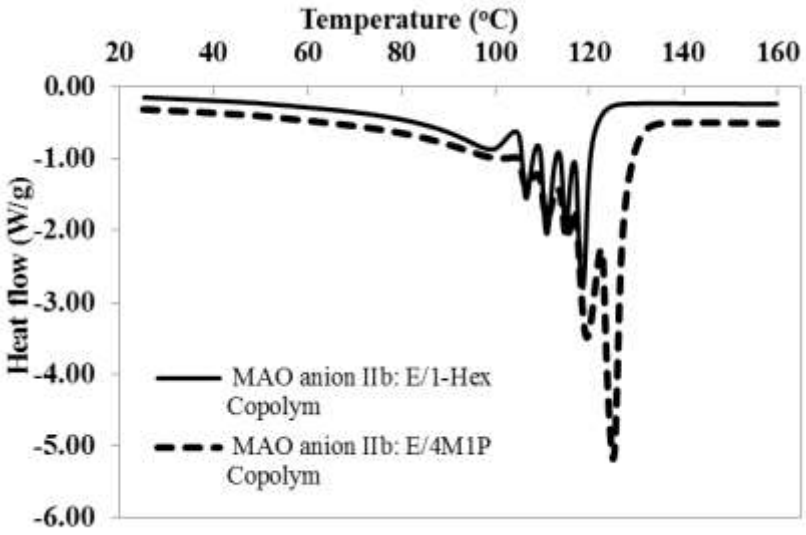

Figure 4.20: Successive Self-nucleation and Annealing thermogram for In-situ copolymers synthesized with MAO anion IIb.

Figure 4.21 illustrates the population of backbones that have the same branch content, crystallinity, and lamellar thickness (i.e corresponding to each SSA peak of Figure 4.20). Ethylene/1-hexene copolymers showed the highest fraction at 98 °C, while those at 106, 111 and 115 °C are not very different. For ethylene/4-Methyl-1-pentene copolymer, the highest fraction was obtained at 124 °C, while those at 106, 111 and 115 °C are comparable.

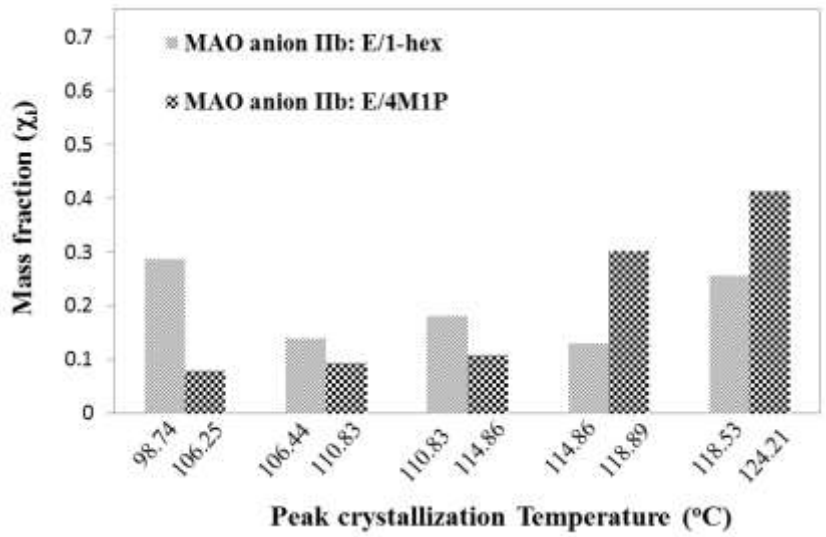

Figure 4.21: Mass fractions of the copolymer fractions with same branch content with MAO anion IIb.

Crystallization analysis fractionation

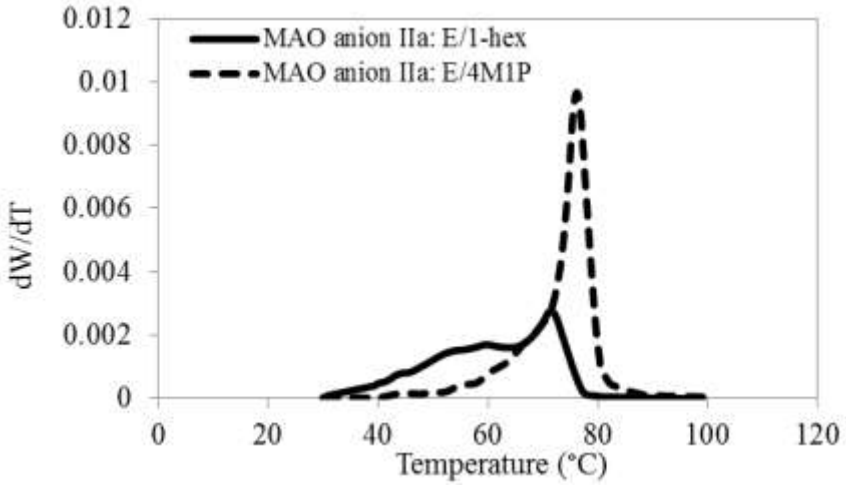

Figure 4.22: Cystallization analysis fractionation for In-situ copolymers (MAO anion IIa).

The chemical composition distribution of ethylene/1-hexene is non-uniform unlike that of ethylene/4-Methyl-1-pentene copolymer. This is the combined effect of MAO anion design and the branched comonomer used.

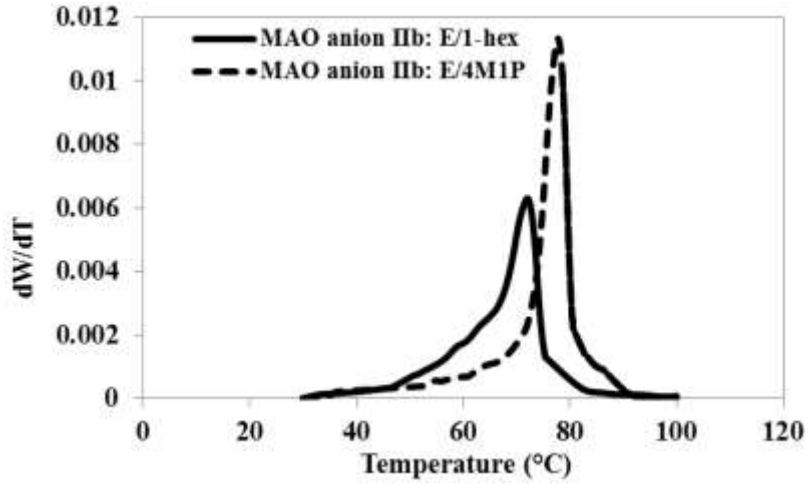

Figure 4.23: Cystallization analysis fractionation for In-situ copolymers (MAO anion IIb).

With MAO anion IIb, however (See Figure 4.23), both distributions are narrow. The microstructural properties generated by each of the catalyst used were investigated using 13C NMR and the method described by [Seger, 2004].

Ethylene sequence length distribution

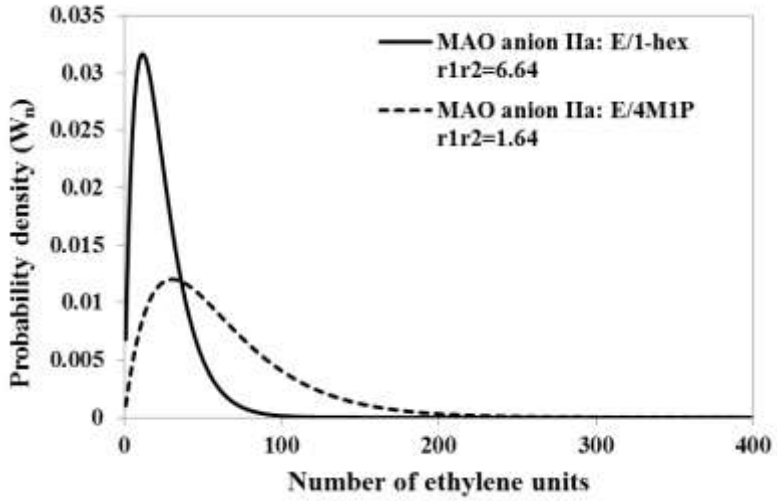

Figure 4.24: Ethylene sequence length distribution along copolymer backbones for In-situ copolymers (MAO anion IIa).

E/1-hex. copolym: $n_{ethylene\ units,\ wt.\ ave.}$= 23 *units*; σ = 23.29; $n_{ethylene\ units,\ most\ probable.}$ = 12 *units*;
E/4M1P copolym: $n_{ethylene\ units,\ wt.\ ave.}$= 61 *units*; σ = 43.33; $n_{ethylene\ units,\ most\ probable.}$ = 31 *units*;

The Figure above shows the ethylene sequence length distribution along copolymer backbones for In-situ copolymers (MAO anion IIa). Ethylene/4-Methyl-1-pentene shows a broader distribution with a standard deviation of about 43 ethylene units; while that of ethylene/1-hexene copolymer is more uniform with a standard deviation of about 23 ethylene units. The nature of the distributions is highly correlated to the level of comonomer incorporation in the copolymers. The corresponding plot for In-situ copolymers synthesized with MAO anion IIb is shown in Figure 4.25 below. Again ethylene/4-Methyl-1-pentene copolymer has a broader distribution with a standard deviation of about 51 ethylene units; while that of ethylene/1-hexene copolymers is almost the same as in MAO anion IIa at about 22 ethylene units.

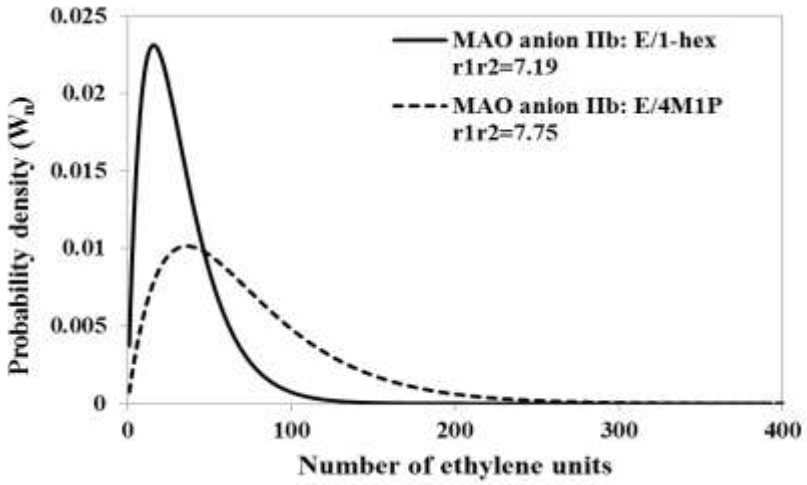

Figure 4.25 : Ethylene sequence length distribution along copolymer backbones for In-situ copolymers (MAO anion IIb).

E/1-hex. copolym: $n_{ethylene\ units,\ wt.\ ave.}$= 32 *units*; σ = 22.47; $n_{ethylene\ units,\ most\ probable.}$ = 16 *units*;
E/4M1P copolym: $n_{ethylene\ units,\ wt.\ ave.}$= 72 *units*; σ = 51.13; $n_{ethylene\ units,\ most\ probable.}$ = 36 *units*;

The linker, dichlorodimethylsilane has therefore improved the breadth of ethylene/1-hexene copolymer ethylene sequence length distribution but not that of ethylene/4-Methyl-1-pentene copolymer.

4.4 Slurry Polymerization Results

4.4.1 Bulk properties: Mw, PDI, thermal properties, microstructural properties and vinyl unsaturations

Table 4.10 illustratres catalyst productivity, weight average molecular weights and polydispersity indices of the homo- and copolymers obtained during slurry polymerization. Positive comonomer effects were observed in both E/1-hexene and E/4M1P copolymerizations. The low values of PDI in the homopolymerizations indicate that most of product was formed by the same or very similar active site types.

Table 4.10: Homo- and copolymers obtained during slurry polymerization: Catalyst productivity, Mw and PDI.

Anion type	Polymer type	Catalyst productivity (gPE/gcat.hr)	M_w (g/mol)	PDI
MAO anion IIIa	Ethylene homopolymer	101.82	228832.00	1.44
	E/1-hexene copolymer	116.36	190000.00	1.79
	E/4M1P copolymer	105.45	310075.00	1.76
MAO anion IIIb	Ethylene homopolymer	78.18	223370.00	1.54
	E/1-hexene copolymer	112.73	254422.00	1.71
	E/4M1P copolymer	88.18	221411.00	1.82

Table 4.11 illustrates the thermal properties of slurry homo- and copolymers. With MAO anion IIIa, 1-hexene units in the LLDPE backbone decreased the melting point, crystallinity and density from 127 to 112 oC, 54 to 32 % and 0.94 to 0.91 g/mL respectively. Similar trend is seen with MAO anion IIIb, where the crystallinity was decreased to as low as 26.6%.

Table 4.11: Homo- and copolymers obtained during slurry polymerization: Thermal properties.

Anion type	Polymer type	T_{mp} (^oC)	T_{pc} (^oC)	Percent crystallinity (%)	Material density(g/cm^3)
MAO anion IIIa	Ethylene homopolymer	126.92	109.95	54.06	0.937
	E/1-hexene copolymer	111.95	96.54	31.62	0.905
	E/4M1P copolymer	118.41	103.33	44.13	0.919
MAO anion IIIb	Ethylene homopolymer	120.48	105.54	48.41	0.923
	E/1-hexene copolymer	119.18	104.13	47.49	0.920
	E/4M1P copolymer	106.80	87.7	26.61	0.894

Comparing the copolymers, we observed that with MAO anion IIIa, ethylene/1-hexene showed the lowest thermal properties while ethylene homopolymer exhibits the highest values (as expected). Thus, while ethylene/4-Methyl-1-pentene LLDPE has higher use temperature, ethylene/1-hexene LLDPE will have better processing properties. However, with MAO anion IIIb, ethylene/4-Methyl-1-pentene showed the lowest thermal properties. Therefore ethylene/ 1-hexene LLDPE will in this case show higher use temperature, while ethylene/4-Methyl-1-pentene LLDPE will have better processing properties.

Table 4.12 below illustrates the microstructural properties of the copolymers. 14% 1-hexene was incorporated with MAO anion IIIa, which led to an average ethylene sequence length of 10 units. Similarly, 2.9% of 4M1P incorporated with the same MAO anion (IIIa) gave to an average ethylene sequence length of 55 units.

Table 4.12: Homo- and copolymers obtained during slurry polymerization: Microstructural properties

Parameter	MAO anion IIIa		MAO anion IIIb	
	E/1-hexene copolymer	E/4M1P copolymer	E/1-hexene copolymer	E/4M1P copolymer
E	0.860	0.970	0.936	0.966
C	0.140	0.029	0.064	0.034
$\mathbf{r_E}$	10.24	54.63	19.30	34.96
$\mathbf{r_C}$	0.59	0.64	0.89	1.14
$\mathbf{<r_E r_C>}$	5.99	35.17	17.23	39.71
$\mathbf{r_E r_C}$ **Markov1**	5.73	35.06	16.86	41.88
$\mathbf{n_E}$	10	55	25	52
$\boldsymbol{\chi}$**R**	0.860	0.970	0.936	0.966

With MAO anion IIIb, the percentage incorporation and average ethylene sequence length were 14% and 25 units respectively for E/1-hexene and 3.4% and 52 units respectively for E/4M1P. The experimental reactivity ratio products compare well with those calculated using First order Markov's copolymerization model.

Table 4.13 below shows the chain end unsaturations for slurry homo- and copolymers.

Table 4.13: Slurry Homo- and copolymers: vinyl unsaturations (FTIR) (units per 1000 Carbon atoms)

MAO Anion	Polymer type	$N_{vinylidene\ unsat.}$	$N_{terminal\ vinyl\ unsat.}$	$N_{Transvinylene\ unsat.}$	N_{Total}	Vinylidene: *Trans*-vinylene : Terminal vinyl
MAO anion IIIa	E-homop	0.02	0.22	0.95	1.19	0.88 : 4.21 : 1
	E/1-hex	2.58	0.10	0.37	3.04	26.30 : 3.73 : 1
	E/4M1P	0.79	0.02	0.32	1.14	45.53 : 18.62 : 1
MAO anion IIIb	E-homop	0.03	0.22	0.74	0.99	1.55 : 3.29 : 1
	E/1-hex	1.48	0.20	0.60	2.27	7.55 : 3.05 : 1
	E/4M1P	1.01	0.09	0.05	1.14	10.97 : 0.50 : 1

Ethylene homopolymer showed negligible vinyledene unsaturation with both MAO anions IIa and IIb; while *trans*-vinylene unsaturation dominates in both cases. The copolymers on the other hand exhibited vinyledene as the most dominant type of chain end unsaturation. The total of these unsaturations fell in the range of about 1.0 unit per 1000 carbons; except for ethylene/1-hexene which showed a total of 3.04 with MAO anion IIIa, but decreased to 2.27 units per 1000 Carbon atoms when the silica was treated with $ClMe_2SiCl$.

4.4.2 Distributive Properties: MWD, LTD, SSA, CRYSTAF, SLD

Molecular weight distributions

The MWDs of the slurry homo- and copolymers synthesized with MAO anion IIIa are illustrated in Figure 4.26 below.

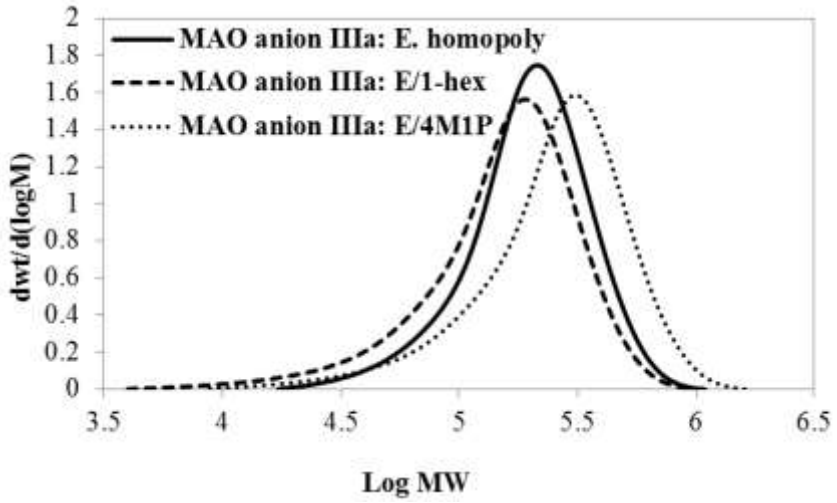

Figure 4.26: Molecular weight distribution for slurry catalyst homo- and copolymers synthesized with MAO anion IIIa.

All the polymers showed uniform distributions. Unlike the case of MAO anions Ia, Ib, IIa and IIb, the copolymers here show insignificant amounts of low molecular weight

fractions. It is also interesting that ethylene/4-Methyl-1-pentene has a higher average of the distribution than the homopolymer.

The Figure below shows the MWDs of the Slurry homo- and copolymers synthesized with MAO anion IIIb. Here, the MWDs of the copolymers (ethylene/4-Methyl-1-pentene and ethylene/1-hexene) coincide with each other and are almost the same with that of ethylene homopolymer. Therefore, introduction of dichlorodimethylsilane has suppressed the chain transfer reactions in the supported catalysts polymerizations.

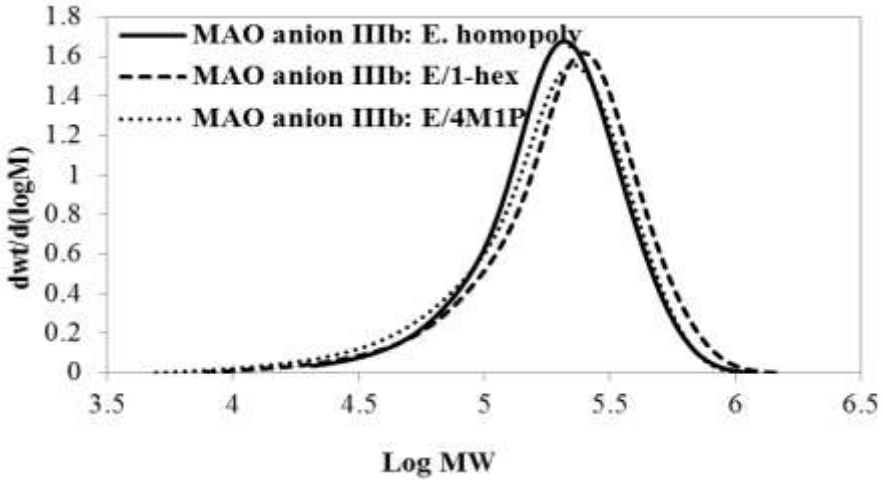

Figure 4.27: Molecular weight distribution for slurry homo- and copolymers synthesized with MAO anion IIIb.

Lamellar thickness distributions

Figure 4.28 shows the LTDs for homo- and copolymers of MAO anion IIIa. In all cases, the average values of the lamellar thicknesses are less than the most probable ones.

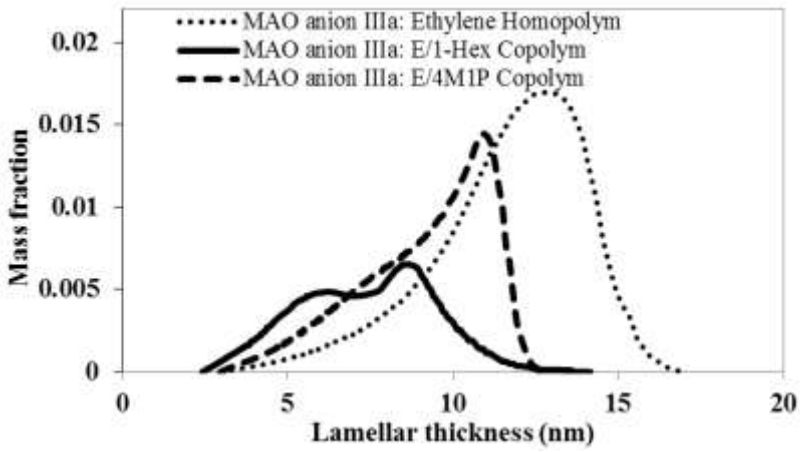

Figure 4.28: Lamellar thickness distributions for slurry homo- and copolymers synthesized with MAO anion IIIa.

Ethylene homopolym: $l_{lamellar\ wt.\ ave.}$= 11.683 *nm*; σ = 3.19; $l_{lamellar\ most\ probable.}$ = 12.68 *nm*;
E/1-hex. copolym: $l_{lamellar\ wt.\ ave.}$= 7.413 *nm*; σ = 2.43; $l_{lamellar\ most\ probable.}$ = 8.47 *nm*;
E/4M1P copolym: $l_{lamellar\ wt.\ ave.}$= 9.179 *nm*; σ = 2.59; $l_{lamellar\ most\ probable.}$ = 10.83 *nm*;

The span of each distribution as measured by standard deviation is given for each case. Ethylene homopolymer exhibited the widest span while ethylene-1-hexene shows a bimodal curve. The bimodality is associated with non-uniform distribution of the side chain branching along the copolymer backbones.

Figure 4.29 shows the LTDs for homo- and copolymers of MAO anion IIIb. In this case however, ethylene/4M1P exhibits the bimodality. So we conclude similarly that this is in conformity with its non-uniform CCD.

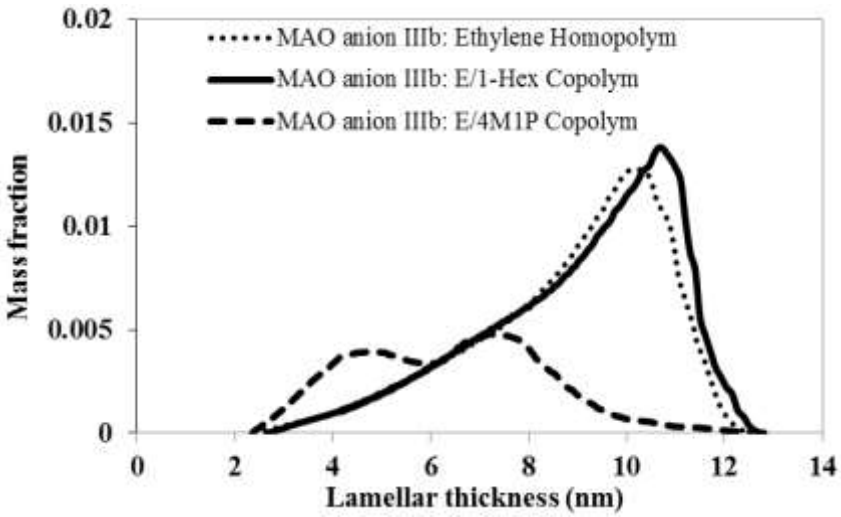

Figure 4.29: Lamellar thickness distributions for slurry homo- and copolymers synthesized with MAO anion IIIb.

Ethylene homopolym: $l_{lamellar\ wt.\ ave.}$= 8.863 *nm*; σ = 2.67; $l_{lamellar\ most\ probable.}$ = 10.30 *nm*;
E/1-hex. copolym: $l_{lamellar\ wt.\ ave.}$= 9.082 *nm*; σ = 2.70; $l_{lamellar\ most\ probable.}$ = 10.64 *nm*;
E/4M1P copolym: $l_{lamellar\ wt.\ ave.}$= 6.443 *nm*; σ = 2.17; $l_{lamellar\ most\ probable.}$ = 7.28 *nm*;

Successive self-nucleation and annealing (SSA)

Figure 4.30 illustrates the SSA thermogram for In-situ copolymers (MAO anion IIIa). Ethylene-1-hexene copolymers exhibited five different melting peaks at (106.48, 111.12, 115.40, 119.48 and 124.69 °C), while ethylene/4-Methyl-1-pentene copolymer showed same number of peak fractionating temperatures at (106.85, 110.75, 115.02, 118.93 and 124.32 °C).

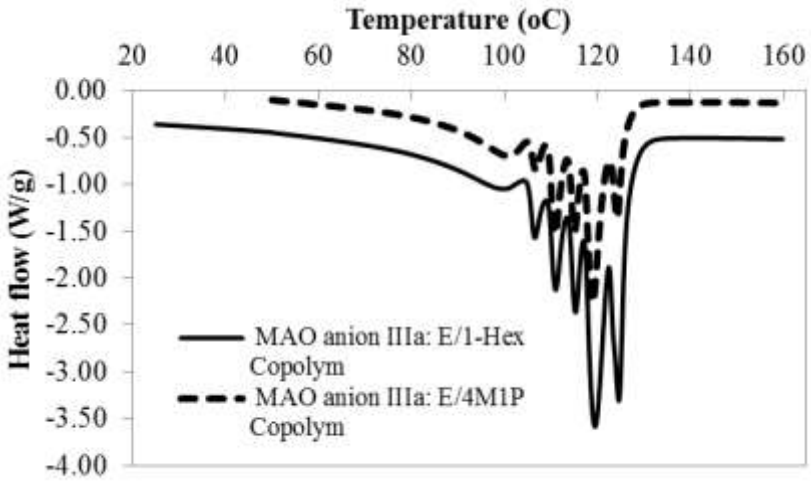

Figure 4.30: Successive Self-nucleation and Annealing thermogram for slurry copolymers (MAO anion IIIa).

The isomeric effect is seen in the varying side chain branching content (Figure 4.31), while the coincidence in the peak temperatures is the result of using the same MAO anion in the synthesis.

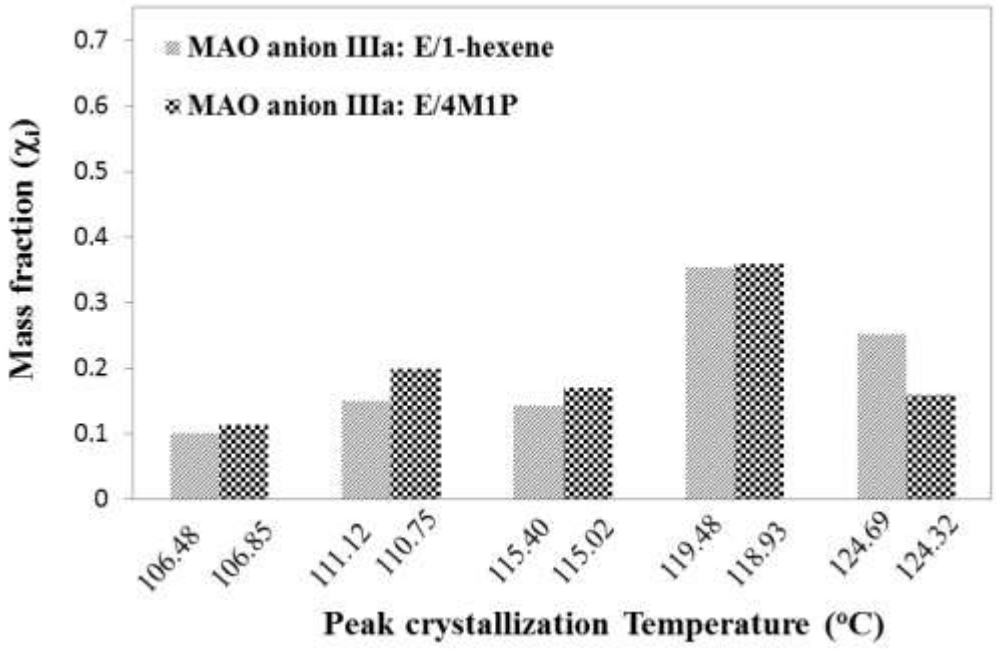

Figure 4.31: Mass fractions of the copolymer fractions with same branch content with MAO anion IIIa.

The corresponding SSA-DSC thermogram for MAO anion IIIb copolymers is shown in Figure 4.32.

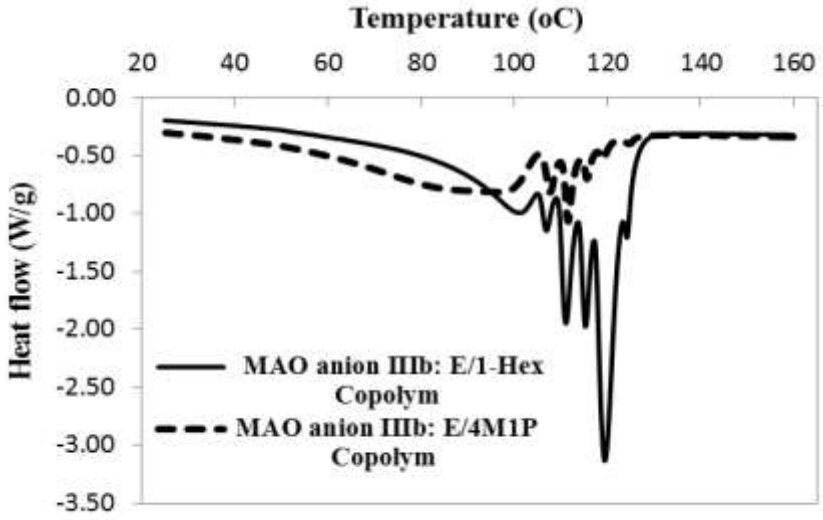

Figure 4.32: Successive Self-nucleation and Annealing thermogram for slurry copolymers (MAO anion IIIb).

For Ethylene-1-hexene copolymers, the peaks occurred at (96.14, 106.81, 110.99, 115.34, and 119.35°C), while ethylene/4-Methyl-1-pentene copolymer showed its own number of peak fractionating temperatures (99.17, 107.52, 111.24, 115.51, 118.74 and 124.43 °C).

Figure 4.33 illustrates the population of backbones that have the same branch content, crystallinity, and lamellar thickness (i.e corresponding to each SSA peak).

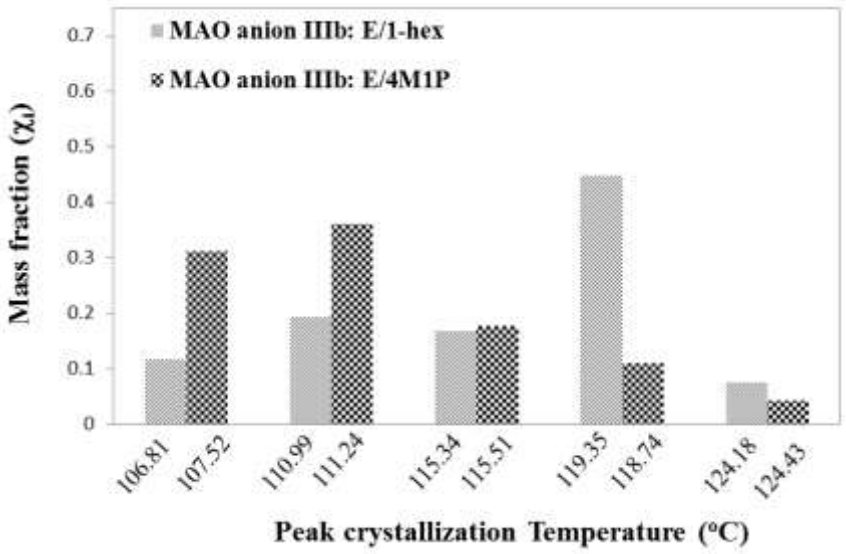

Figure 4.33: Mass fractions of the copolymer fractions with same branch content with MAO anion IIIb.

Crystallization analysis fractionation

Figure 4.34 illustrates the cystallization analysis fractionation for slurry copolymers (MAO anion IIIa).

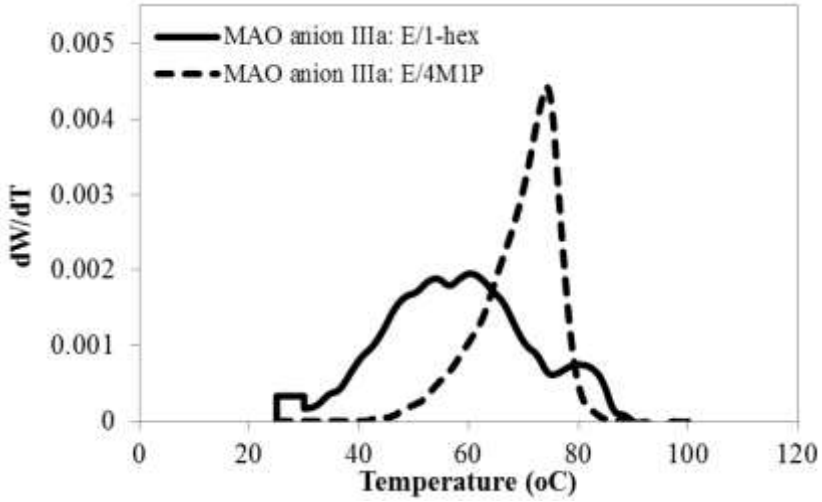

Figure 4.34: Cystallization analysis fractionation for slurry copolymers (MAO anion IIIa).

The chemical composition distribution of ethylene/1-hexene is non-uniform unlike that of ethylene/4-Methyl-1-pentene copolymer. This is the combined effect of MAO anion design and the branched comonomer (4-Methyl-1-pentene) used.

Figure 4.35 below shows the corresponding crystallization analysis fractionation plot for slurry copolymers (MAO anion IIIb).

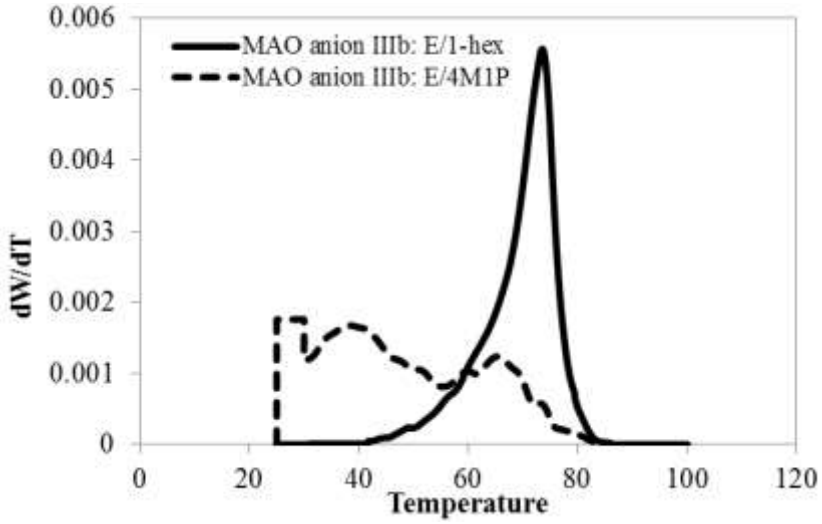

Figure 4.35: Cystallization analysis fractionation for slurry copolymers (MAO anion IIIb).

The trend here is the reverse of that of Figure 4.34. That is, the chemical composition distribution of ethylene/1-hexene copolymer is uniform unlike that of ethylene/4-Methyl-1-pentene copolymer. For this reason, we deemed that the crystallization kinetics for these copolymers is worth investigating (See section 4.5).

Ethylene sequence length distribution

Figure 4.36 illustrates ethylene sequence length distribution along copolymer backbones for slurry copolymers synthesized with MAO anion IIIa.

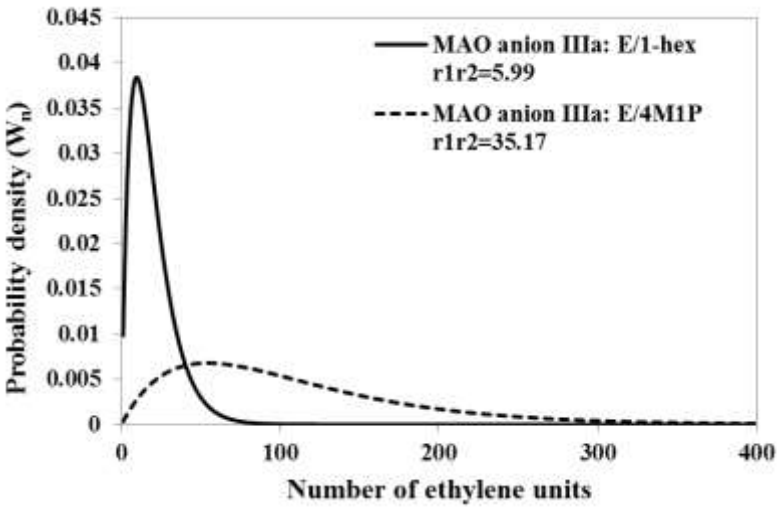

Figure 4.36: Ethylene sequence length distribution along copolymer backbones for slurry copolymers (MAO anion IIIa).

E/1-hex. copolym: $n_{ethylene\ units,\ wt.\ ave.}$= 19 *units*; σ = 13.55; $n_{ethylene\ units,\ most\ probable.}$ = 10 *units*;
E/4M1P copolym: $n_{ethylene\ units,\ wt.\ ave.}$= 104 *units*; σ = 75.31; $n_{ethylene\ units,\ most\ probable.}$ = 54 *units*;

Ethylene/4-Methyl-1-pentene shows a broader distribution with a standard deviation of 75 ethylene units; while that of ethylene/1-hexene copolymer is more uniform with standard deviation of just 14 ethylene units. The nature of the distributions is highly correlated to the level of comonomer incorporation in the copolymers.

The corresponding plot for Slurry copolymers synthesized with MAO anion IIIb is shown in Figure 4.37 below.

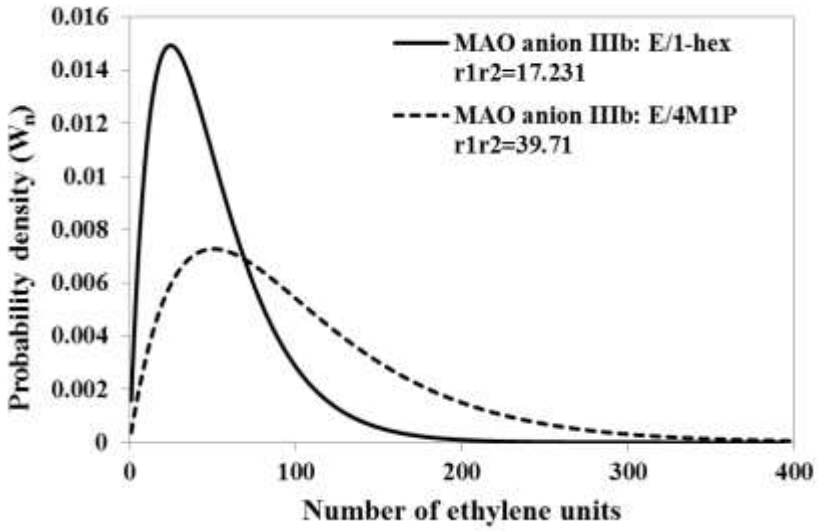

Figure 4.37 : Ethylene sequence length distribution along copolymer backbones for slurry copolymers (MAO anion IIIb).

E/1-hex. copolym: $n_{ethylene\ units,\ wt.\ ave.}$= 49 *units*; σ = 34.83; $n_{ethylene\ units,\ most\ probable.}$ = 25 *units*;
E/4M1P copolym: $n_{ethylene\ units,\ wt.\ ave.}$= 98 *units*; σ = 70.71; $n_{ethylene\ units,\ most\ probable.}$ = 51 *units*;

Here, both ethylene/4-Methyl-1-pentene and ethylene/1-hexene copolymers show broad distributions. However, that of ethylene/4-Methyl-1-pentene copolymer has a higher standard deviation of about 71 ethylene units (not too different from that of MAO anion IIIa); while that of ethylene/1-hexene copolymers is about half at about 34 ethylene units. Dichlorodimethylsilane has therefore improved the breadth of ethylene/1-hexene copolymer ethylene sequence length distribution but not that of ethylene/4-Methyl-1-pentene copolymer.

4.5 Polymer Crystallization Kinetic Studies

4.5.1 Crystallization Kinetic Model

The multiple cooling rate experiments were conducted at 10, 12.5, 15, 17.5, and 20 °C/min. The procedure is reported in (Atiqullah et al., 2012).

The *nonisothermal* Avrami-Erofeev crystallization rate equation is given by:

$$\frac{d\alpha(T)}{dT} = \frac{k_0}{\beta} \times exp\left[-\frac{E_a^A}{R}\left(\frac{1}{T} - \frac{1}{T_0}\right)\right] \times n(1-\alpha(T))[-ln(1-\alpha(T))]^{\frac{n-1}{n}} \quad (4.1)$$

We define

$$f(\alpha(T)) = n(1-\alpha(T))[-ln(1-\alpha(T))]^{\frac{n-1}{n}} \quad (4.2)$$

$$k'(T) = k_0 \times exp\left[-\frac{E_a^A}{R}\left(\frac{1}{T} - \frac{1}{T_0}\right)\right] \quad (4.3)$$

$$E_a^A(\text{apparent crystallization energy}) = E_{grow} - E_{nucl} \quad (4.4)$$

$$k_0 = \left(\frac{K_s N_0}{V_0}\right)\frac{k_{grow,0}}{k_{nucl,0}} \quad (4.5)$$

$$k_{grow}(T) = k_{grow,0} \times exp\left[-\frac{E_{grow}}{R}\left(\frac{1}{T} - \frac{1}{T_0}\right)\right] \quad (4.6)$$

$$k_{nucl}(T) = k_{nucl,0} \times exp\left[-\frac{E_{nucl}}{R}\left(\frac{1}{T} - \frac{1}{T_0}\right)\right] \quad (4.7)$$

$f(\alpha(T))$ is called Avrami-Erofeev nonisothermal crystallization function. n represents the dimension of the growing crystal. N_0 represents the number of germ nuclei, (that is the potential nucleus formation sites/defects). V_0 is the initial volume of the molten polymer. K_s gives the shape factor for the growing nuclei. $k_{grow}(T)$ and $k_{nucl}(T)$ in equations 4.6 and 4.7 follow the Arrhenius form reported elsewhere in the literature (Routray and Deo., 2005; Fogler, 2006; Hossain and de Lasa 2007). $k_{grow,0}$ and $K_{nucl,0}$ are the frequency factors for crystal growth and nucleation respectively. E_{grow} and E_{nucl} represent the corresponding activation energies. T_0 is the reference temperature.

The suitability of the above type of Arrhenius relation in the numerical treatment of a typical sigmoidal relative crystallinity versus T curve is well documented (Kanervo and Krause 2002). The use of this form of Arrhenius expression (with T_0) facilitates searching the kinetic parameters (k_0, and E_a) by eliminating the stiffness of the problem; and therefore greatly minimizing the statistical correlation between the kinetic parameters (k_0, and E_a) (Hossain and de Lasa 2007; Kanervo and Krause, 2002; Watts, 1994).

Equation 4.1 is characterized by the following features:

- It is a kinetic equation which is based on conservation laws.
- The kinetic parameters k_0, E_a, and n can be determined using a single constant cooling rate DSC experiment (α-T data).
- The statistical cross-correlation coefficient measures the interdependence among the parameters k_0, E_a, and n.
- The effect of polymer microstructure on crystallization can be deduced from the plots of $f(\alpha(T))$ versus $\alpha(T)$ and $\frac{1}{T}$.

The relation between $\alpha(T)$ and the weight fraction relative crystallinity $\alpha_w(T)$ is presented in Lorenzo and Arnal, (2007) as:

$$\alpha(T) = \frac{\alpha_w(T)}{\alpha_w(T) + {\rho_c}/{\rho_a}[1-\alpha_w(T)]} \tag{4.8}$$

where ρ_c and ρ_a represent the the densities of the crystalline and amorphous phases, respectively. The values reported for polyethylene are ρ_c = 1.004 g/mL and ρ_a = 0.853 g/mL (Atiqullah et al. 2012).

$\alpha_w(T)$ can be obtained from equation 4.9 using the data of a typical constant cooling rate (second cycle) of nonisothermal DSC experiment.

$$\alpha_w(T) = \frac{\Delta H(T)}{\Delta H_{total}} = \frac{\int_{T_0}^{T}\left(\frac{dH}{dT}\right)dT}{\int_{T_0}^{T\infty}\left(\frac{dH}{dT}\right)dT} \tag{4.9}$$

where ΔH_{total} is the maximum enthalphy obtained at the end of the nonisothermal crystallization process and $\Delta H(T)$ is the enthalpy corresponding to temperature T of crystallization. T_0 and T_∞ represent the initial and the final temperatures of crystallization, respectively. ΔH_{total} and $\Delta H(T)$ both can be acquired through the software of a standard differential scanning calorimeter (DSC). Using Equation 4.8, volume fraction $\alpha(T)$ can be obtained from the DSC-generated $\alpha_w(T)$.

Four copolymers namely ethylene/1-hexene and ethylene/4-Methyl-1-pentene synthesized with IIIa and IIIb were selected for this studies. This combination will give us insight into both the branch-induced isomeric effect (1-hexene and 4-Methyl-1-pentene) and effect of MAO anion design on the crystallization kinetic parameters. The basis for this selection is because the chemical composition distributions of the aforementioned samples are significantly different.

4.5.2 Numerical Solution of the Crystallization Kinetic Model and Parameter Estimation

Equation 4.1 representing the nonisothermal Avrami-Erofeev polymer crystallization rate, was solved by separation of the variables into a function of $\alpha(T)$ on the LHS and a function of T on the RHS, and integrating. The result is:

$$LHS = (-Log[1-\alpha])^{\frac{1}{n}} \tag{4.10}$$

$$RHS = \frac{exp\left(\frac{\mathrm{Ea}}{RT_0 k_0}\right)}{\beta}\left(T\, exp\left(-\frac{\mathrm{Ea}}{RT}\right)T + \frac{\mathrm{Ea\ ExpIntegralEi}\left(-\frac{\mathrm{Ea}}{RT}\right)}{R}\right) \tag{4.11}$$

Equation 4.11 shows how the challenge in evaluating the temperature integral was overcome by evaluating it in the complex plane. The non-linear model in this algebraic form was then used with the NonLinearModelFit of MATHEMATICA to formulate the regression scheme. All the preexponential factors, k_0s were evaluated at 370 K, the chosen reference temperature. Equation 4.10, is discontinuous at $\alpha(T) = 1$. Therefore, the model was evaluated up to $\alpha(T) \cong 0.9999$. Enough experimental data points were used for estimation of the kinetic parameters (k_0, E_a, and n) at each heating rate to ascertain the suitability of the model.

The performance of the crystallization kinetic model was evaluated based on the following:

- 95% confidence interval;
- Coefficient of determination (R^2);
- Estimated variance; and

- Standard error.

The kinetic parameters so obtained were tabulated above.

Table 4.14: Estimated parameters for the Avrami-Erofeev crystallization model.

Heating Rate (^oC/min)	SAMPLES				
	Parameter	**MAO anion IIIa E/4M1P**	**MAO anion IIIa E/1-hexene**	**MAO anion IIIb E/1-hexene**	**MAO anion IIIb E/4M1P**
10.0	n	2.75	2.4	2.5	2.2
	k_0	0.343±0.0275	0.343±0.0275	0.347±0.0287	0.538±0.0299
	E_a	38.04±3.36	30.22±2.68	38.20±3.30	30.967±1.53
	R^2	0.971	0.971	0.973	0.989
12.5	n	2.6	2.8	2.7	2.2
	k_0	0.448±0.0404	0.513±0.0429	0.435±0.0389	0.667±0.0376
	E_a	38.05±3.65	30.58±2.58	38.45±3.49	30.51±1.46
	R^2	0.961	0.967	0.972	0.988
15.0	n	2.4	2.7	2.15	2.4
	k_0	0.509±0.0383	0.610±0.0411	0.410±0.020	0.806±0.0448
	E_a	38.07±2.88	30.42±1.84	38.53±2.04	30.974±1.47
	R^2	0.978	0.984	0.990	0.987
17.5	n	2.8	2.75	2.2	2.2
	k_0	0.659±0.0540	0.745±0.0560	0.410±0.020	0.973±0.054
	E_a	38.81±3.42	30.70±1.84	38.64±2.06	30.18±1.36
	R^2	0.970	0.980	0.990	0.990
20.0	n	2.4	2.6	2.3	2.2
	k_0	0.710±0.0535	0.644±0.04673	0.728±0.0529	1.158±0.0619
	E_a	36.46±2.55	30.89±2.19	37.96±2.61	30.62±1.30
	R^2	0.972	0.975	0.981	0.991

The values of n between 2 to 3 for all the samples, suggested that the nucleation is heterogeneous and cystal growth is bi- or tridimensional.

The crystallization activation energies remained constant for each sample at different cooling rates. That is independent of the heating rates. This conforms to the concept of

invariance of activation energy articulated by Galwey and co-thinkers (Galwey, 2003a; Galwey, 2003b), and offers a different opinion about the concept of *variable/instantaneous activation energy* (Sahay et al., 2005; Vyazovkin et al., 2002; Supaphol et al., 2003; Chrissafis et al., 2007; Papageorgiou et al., 2010a; Papageorgiou et al., 2010b; Muraleedharan 2011; Papadimitriou et al., 2008; Xia 2005; Eloussifi et al., 2012; Vyazovkin, 1997) which is under practice in handling nonisothermal kinetic data.

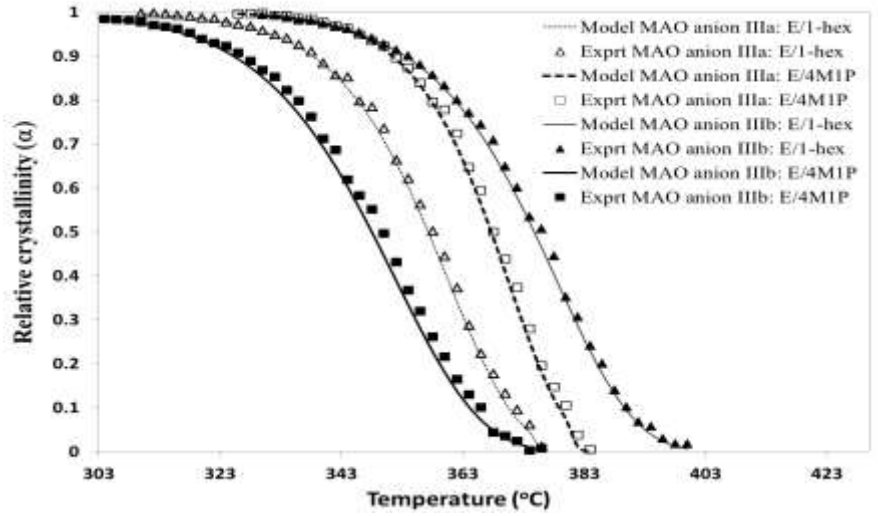

Figure 4.38: Relative crystallinity versus temperature slurry copolymers (MAO anion IIIa and IIIb).

Figure 4.38 compares the rigorous nonisothermal Avrami-Erofeev model predictions with the experimental DSC relative crystallinity profiles of all the data polymers. We observed that for all the polymers, the model (developed using a set of phenomenological assumptions) matched the entire relative crystallinity curve with high values of coefficients of determination, R^2 between 0.961–0.991. This result is physically significant. This means that the mechanism of nucleation and crystal growth used in the development of the constitutive model equation is the same for all the cooling rates, throughout the crystallization process. Therefore, the model overcomes the drawbacks

and limitations of the existing nonisothermal crystallization models. Therefore, the concept of change in crystallization mechanism, as reported by [Papageorgiou et al., 2010b; Zhang et al., 2006; Acar et al., 2007; Olmos et al., 2009; Adhikari and Lozano, 2011], does not appear to be necessary.

This conclusion originates from the appropriate application of the current nonisothermal Avrami-Erofeev crystallization model and the calculation algorithm that we have used. This is how we addressed the subject of mathematical artifact in this study.

CONCLUSIONS

This thesis has been carried out successfully and the following scientific advancements in the field are part of its outcomes:

1. The MAO anion design affected the distributive (e.g molecular weight distributions, ethylene sequence length distributions, lamellar thickness distributions etc.) as well as the bulk properties (e.g. weight average molecular weights, polydispersity indices, density Mw, PDI, thermal properties, microstructural properties and vinyl unsaturations) of the polymers. This understanding leads to the production of specific application-oriented polymers.

2. The copolymerization mechanism was well predicted by first order Markovian (terminal) model, in which the insertion of a comonomer into a growing polymer chain depends on the last added species.

3. Dichlorodimethylsilane ($ClMe_2SiCl$) suppresses chain transfer reactions in supported catalyst.

4. ^{13}C NMR/SSA-DSC can elaborate how supported MAO anions architect copolymer backbones and regulate compositional heterogeniety. This provides road map to design novel heterogeneous metallocene catalysts.

5. The Avrami-Erofeev model predicted degree of crystallinity that well matched the experimental DSC crystallinity profiles notably for Avrami-Erofeev index of 2 to 3, which implies bi- and tri-dimensional crystal growth.

6. The concept of *instantaneous variable crystallization activation energy*, articulated in the literature, is refuted.

7. The crystallization kinetic model successfully elaborates the influence of compositional heterogeniety on copolymer crystallization behavior.

The following product development niches emerged from the application of supported MAO anions and the concept of isomeric copolymerization, around which this work is centered:

1. Improvement in processability, as demonstrated by the very low melting temperature and crystallinity of MAO anion IIIa (E/4M1P copolymer).
2. Stability, that is less susceptibility to degradation as seen in the ethylene homo- and 4-Methyl-1-pentene copolymers of supported MAO anions IIIa and IIIb
3. Load bearing application as demonstrated by our high molecular weight (300,000-420,000) products: *MAO anion Ia (E. Homopoly, E/1-hex), MAO anion Ib (E. homopoly), MAO anion IIa (E. homopoly), MAO anion IIb (E. homopoly, E/4M1P), MAO anion IIIa (E/4M1P)*
4. Production of blocky copolymer through the use of supported catalysts and alpha-olefins as exhibited by our supported catalysts copolymers with the order of blockiness as: E/4M1P > E/1-hexene

RECOMMENDATIONS

The following are recommended for future work

1. MAO has multiple structures which are in dynamic equilibrium with one another. Therefore, the concept supported cocatalyst anion should be further investigated using borane/borate cocatalysts which have a defined single structure.

2. Mechanism, kinetics of polymerization, copolymer backbone heterogeneity, thermal behaviors, etc. of the system in (1) above, should be compared with the supported MAO anion analogues.

3. The effect of hydrogen as a chain transfer agent should be studied on the above polymerization systems.

4. Study the effects of other functionalizing linkers on catalysts activity and polymerization mechanism, polymer compositional heterogeneity and properties.

5. Study the properties of the blends of the homo- and copolymers synthesized.

6. Carry out molecular dynamics studies of the structure and properties of the homo- and copolymers obtained.

7. Use other comonomers like 1-butene, 1-octene, and their branched analogues to synthesis novel LLDPEs with same catalyst synthesis methodology.

REFERENCES

Acar I, Durmuş A, Özgümüş S. Journal of Applied Polymer Science. 2007; 106:4180–4191.

Adhikari A., Lozano K. Journal of Polymer Research. 2011, 18:875–880.

Alghyamah AA, Soares JBP. *Macromol Rapid Commun*. 2009;30:384–393.

Alghyamah AA, Soares JBP. *Macromol Symp*2009;285:81–89.

Anantawaraskul S, Bongsontia W, Soares JBP. *Macromol React Eng.* 2011; 8:549–562.

Anantawaraskul S, Bongsontia W, Soares JBP. *Macromol Symp.* 2009;282:167–174.

Angermund K, Fink G, Jensen VR, Kleinschmidt R.*Chem Rev.* 2000;100:1457-1470.

Anton E, Adams TA, Arnaud R.*Polymer*. 1994;35:433–434.

Atiqullah M, Akhtar MN, Faiz M, Moman AA, Abu-Raqabah AH, Khan JH, Wazeer MI. Surf. Interf. Anal. 38 (2006) 1319–1327.

Atiqullah M, Akhtar MN, Moman AA, Abu-Raqabah AH, Palackal SJ, Al-Muallem HA, Hamed OM. *Applied Catalysis A: General*. 2007;320:134-143.

Atiqullah M, Hossain MM, Kamal MS, Al-Harthi MA, Hossaen A, Khan MJ, Hussain I. AICHE Journal. 2012; DOI 10.1002/aic.13806.

Atiqullah M, Tinkl M, Pfaendner R, Akhtar MN, Hussain I.*Polymer Reviews*. 2010;50:178-230.

Atiqullah M, Winston MS, Bercaw JE, Hussain I, Fazal A, Al-Harthi MA, Emwas AHM, Khan MJ, Hossaen A. Polym. Degrad. Stab. 97 (2012) 1164–1177.

Atiqullah M,Nauman EB. *Chemical Engineering Science*. 1990;45:1267.

Atiqullah M. *European Polymer Journal*. 1993;29:1581.

Atiqullah M. in: D.L. Marmaduke (Ed.), Nova Science, New York, 2008. Chen EYX, Marks TJ. Chem. Rev. 100 (2000) 1391-1434.

Atiqullah M. PhD Thesis, Rensselaer Polytechnik Institute, Troy, New York. 1988.

Atiqullah M. Progress in Heterogeneous Catalysis (Ed: Marmaduke DL) New York: Nova Science, 2008.

Awudza JAM and Tait PJT. Journal of Polymer Science: Part A: Polymer Chemistry, Vol. 46, 267–277 (2008)

Babushkin DE, Semikolenova NV, Zakharov VA, Talsi EP. Macromol. Chem. Phys. 201 (2000) 558–567.

Białek M, Czaja K, Sacher-Majewska B. *Thermochimica Acta.* 2005;429:149–154.

Białek M, Czaja K. *Macromol Chem Phys.* 2006;207:1651–1660.

Blom R, Follestadb A, Noel, O.*Journal of Molecular Catalysis*. 1994; 91: 237-249.

Bochmann M. Organometallics. 29 (2010) 4711–4740.

Brintzinger HH, Fischer D, Mülhaupt R, Rieger B, Waymouth RM. Angew. Chem. Int. Ed. Engl., 1995; 34:1143.

Chai CK, Frye CJ. USP 6,642,339 B1 (2003).

Chang HS, Song WD, Chu KJ, Ihm SK. *Macromolecules*. 1992;25:2086–2092.

Chen EYX, Marks TJ. *Chem Rev* 2000;100**:**1391−1434.

Chen Y-X Tobin J. Marks TJ. *Organometallics.* 1997; 16:3649-3657

Chernyshov K, Gen D, Shemouratov Y,Prokhorov K, Nikolaeva G, Sagitova E, Pashinin P, Kovalchuk A, Klyamkina A, Nedorezova P, Shklyaruk B, Optov V. *Macromol. Symp*. 2010; 296: 505–516

Choi Y, Soares JBP. *The Canadian Journal of Chemical Engineering*. 2012;90:646-671.

Chrissafis K, Paraskevopoulos KM, Stavrev SY, Docoslis A, Vassiliou A, Biakiaris DN. Thermochemica Acta. 2007; 465:6–17.

Chu K-J, Soares JBP, Penlidis A, Ihm S-K. *European Polymer Journal*. 2000;36:3–11.

Chu KJ, Soares JBP, Penlidis A. *Macromol Chem Phys*. 2000;201:340.

Coates GW. *Chem Rev*. 2000;100:1223-1252.

Czaja K, Sacher B, Białek M *Thermal Analysis and Calorimetry*. 2002;67:547–554.

D. Coevoet, H. Cramail, A. Deffieux, Macromol. Chem. Phys. 199 (1998) 1451–1457.

D. Coevoet, H. Cramail, A. Deffieux, Macromol. Chem. Phys. 199 (1998) 1459–1464.

de Freitas AJD, dos Santos JHD, Meneghetti SMP, Meneghetti MR. Jour Appl. Polym. Sci. 119 (2011) 3051–3057.

de Ga´scue BR, Herna´ndez JLPG, Valle´s EM. *J Therm Anal Calorim*. 2011;103:669–678.

Descour C, Duchateau R, Mosia MR, Gruter G-JM, Severnc JR, Rastogi S. *Polym. Chem*. 2011; 2, 2261.

DesLauriers PJ, McDaniel MP, Rohlfing DC, Krishnaswamy RK, Secora SJ, Benham EA, Maeger PL, Wolfe AR, Sukhadia AM, Beaulieu WB. Polym. Eng. Sci. 45 (2005) 1203–1213.

DesLauriers PJ, Tso C, Youlu Y, Rohlfing DL, McDaniel MP. Appl. Catal. A: Gen. 388 (2010) 102–112.

Dong J-Y, Hu Y. *Coordination Chemistry Reviews.* 2006; 250:47–65

Eisch JJ, Caldwell KR, Werner S, Kruger C. Organometallics. 10 (1991) 3417–3419.

Eisch JJ, Mackenzie K, Windisch H, Krüger C. Eur. Jour. Inorg. Chem. 1 (1999) 153–162.

Eisch JJ, Piotrowski AM, Brownstein SK, Gabe EJ, Leet FL. Jour. Am. Chem. Soc. 107 (1985) 7219–7221.

Eloussifi H, Farjas J, Roura J. Journal of Thermal Analysis and Calorimetry. 2012; 108:597–603.

Ewen JA. *J Am Chem Soc*. 1984;106:6355-6364.

Farjas J, Roura P. AICHE Journal. 2008:2145–2154.

Ferraris G, Corno C, Priola A, and Cesca S. *Macromolecules.* 1977; 10(1): 188-197.

Fillon B, Whittmann JC, Lotz B, Thierry A. J Polym Sci Part B: Polym Phys 1993;31(10):1383–93.

Fink G, Steinmetz B, Zechlin J, Przybyla C, Tesche B. *Chem Rev*. 2000;100:1377-1390.

Flory PJ. *J Am Chem Soc.* 1936;58:1877–1885.

Flory PJ. Journal of Chemical Physics. 1949; 17:223–240.

Fogler HS. New Jersey: Prentice Hall International, 2006.

Fusco R, Longo L, Proto A, Musi F, Garbassi F. Macromol. Rapid Commun. 19 (1998) 257–262.

Gajan D, Cope´ret C. *New J. Chem.* 2011;35:2403–2408.

Galimberti M, Piemontesi F, Alagia L, Losio S, Boragno L, Stagnaro P, Sacchi MC. J*ournal of Polymer Science: Part A: Polymer Chemistry*. 2010; 48(10)2063-2075

Galland GB, Seferin MS, Mauler RS, dos Santos JHZ. Polym. Intl. 48 (1999) 660–664.

Galwey AK. Thermochimica Acta. 2003; 397:249–268.

Galwey AK. Thermochimica Acta. 2003; 399:1–29.

Gao H, Pan J, Guo L, Xiao D, Qing Wu Q. *Polymer*. 2011; 52:130-137.

Giannetti E, Nicoletti GM, Mazzocchi R. *Jour Polym Sci Part A: Polym Chem Ed*. 1985;23:2117-2134. (b)

Grieken RV, Carrero A, Suarez I, Paredes B. Eur. Polym. Jour. 43 (2007) 1267–1277.

Grieken RV, Carrero A, Suarez I, Paredes B. *Macromol Symp* 2007;259:243–252.

Groppo E., Lamberti C., Bordiga S., Spoto G., Zecchina, A. *Chem. Rev*. 105, 115 (2005).

Guo L, Gao H, Li L, Wu Q. *Macromol. Chem. Phys*. 2011; 212: 2029–2035

Helmut GA, Köppl A. *Chem. Rev.* 2000;100:1205-1221.

Hlatky GG. *Chem Rev* 2000;100:1347−1376.

Hoff RE and Mathers RT. New Jersey: John Wiley & Sons, 2010.

Hosoda S, Nozue Y, Kawashima Y, Utsumi S, Nagamatsu T, Wagener K, Berda E, Rojas G, Baughman T, Leonard J. Macromolecular Symposium. 2009; 282:50–64.

Hossain MM, de Lasa HI. AICHE Journal. 2007; 53:1817–1829.

http://en.wikipedia.org/wiki/4-Methyl-1-pentene

http://en.wikipedia.org/wiki/ethylene

http://www.tosoh-finechem.com/poly/poly_metallocene_e.html

IDES:http://www.ides.com/info/generics/38/Polyolefin-Polyolefin

Irwin LJ, Reibenspies JH, and Miller SA.*J. AM. Chem. Soc*. 2004, 126, 16716-16717.

Ivanchev SS, Badaev VK, Ivancheva NI, Budtov VP, Khaikin S.Ya, Lemenovskii D. *Polymer science. Series A, Chemistry, physics*,2000; 42(2):126-131

Jaber IA, Ray HRW, Jour. Appl. Polym. Sci. 49 (1993) 1709–24.

Janiak C. In *Kirk-Othmer Encyclopedia of Chemical Technology*; Seidel, A. (Ed.). 2006;16:79–125.

John J, Eisch JJ, Pombrik SI, Zheng GX. Organometallics. 12 (1993) 3856–3863.

Johnson LK, Killian CK, Brookhart M. *J. Am. Chem. Soc.*, 117, 6414 (1995).

Kaivalchatchawal P, Samingprai S, Shiono T, Praserthdam P, Jongsomjit B, Eur. Polym. Jour. 48 (2012) 1304–1312.

Kakinuki K, Fujiki M, Nomura K. *Macromolecules* 2009; 42: 4585–4595

Kaminsky W. *J. Chem. Soc*., *Dalton Trans*. 1998; 9:1413–1418

Kaminsky W. *Macromol. Chem. Phys.*, 1996, **197**, 3907.

Kaminsky W, Kulper K, Brintzinger HH, Wald ER. *Angew Chem Int Ed Engl.* 1985; 24:507-508.

Kamnisky W, Miri M.*Jour Polym Sci Polym Chem Ed.* 1985;23:2151-2164(a)

Kanervo J, Krause AOI. Journal of Catalysis. 2002; 207:57–65.

Karol J, Sun-Chueh SC, Kao KJ. Cann, Jour. Polym. Sci. Part A: Polym. Chem. 31 (1993) 2541–2553.

Kim I, Ha CS. Polym. Bull. 52 (2004) 133–139.

Kim I, Chang-Sik Ha. *Applied Catalysis A: General.* 2003;251:167–180.

Kissin YV, Mink RI, Nowlin TE, Brandolini AJ. Springer, 1999; 60–75.

Kissin YV. Elsevier Science, New York, 2008.

Koivumiiki J, Seppala JV. Macromolecules. 26 (1993) 5535–5538.

Koppl A, Babel AI, Alt HG. Jour. Mol. Catal. A: Chem. 153 (2000)109–119.

Lasdon LS, Waren AD, Jain A, Ratner M. *ACM Trans Math. Soft.* 1978;4:34–50.

Lee JS, Yim J-H, Jeon J-K, Ko YS. *Catalysis Today*. 2012; doi:10.1016/j.cattod.2011.12.003.

Leone G,Losio S, Piovani D, Sommazzi A, Giovanni Ricci G. The Royal Society of Chemistry 2012: 1-4

Li J, DiVerdi JA, Maciel GE. Jour Am Chem Soc. 128 (2006) 17093–17101.

Linnolahti M, Severn J.R., T.A. Pakkanen, Angew Chem. Int. Ed. 47 (2008) 9279–9283.

Lobón-Poo M, Barcina JO, Martínez AG, Expósito MT, Vega JF, Martínez-Salazar J, Reyes MI. *Macromolecules*. 2006;39:7479-7482.

Lorenzo AT, Arnal ML, Müller AJ, Albuerne J. Journal of Polymer Testing. 2007; 26:222–231.

Lorenzo AT, Arnal ML, Müller AJ, de Fierro AB, Abetz V. *Macromol Chem Phys.* 2006;207:39–49.

Losio S, Boccia AC, Boggioni L, Sacchi MC, Ferro DR. *Macromolecules.* 2009; 42:6964–6971.

Losio S, Boccia AC, Sacchi MC. *Macromol. Chem. Phys*. 2008, 209, 1115–1128.

Losio S, Stagnaro P, Motta T, Sacchi MC. *Macromolecules* 2008; 41:1104-1111.

Losio S, Tritto I, Zannoni G, Sacchi MC. *Macromolecules*.**2006;** 39:8920-8927

Macchioni A. Chem Rev. 105 (2005) 2039–2073.

Malpass DB. Processes.Scrivener Publishing LLC Salem, Massachusetts. 2010. pp 79-82

Mauler RS, Galland GB, Scipioni RS, Quijada ZR. *Polymer Bulletin*, 1996; 37:469-474

Mayo FR, Lewis FM. Copolymerization. I. *J Am Chem Soc.* 1944;66:1594–1601.

Monrabal B. *J Appl Polym Sci*. 1994;52:491-499.

Monrabal B. *Macromol Symp*. 1996;110: 81-86.

Mosia MR. Eindhoven: Technische Universitie Eindhoven, 2004. ISBN 90-386-2766-1

Müller AJ, Arnal ML. *Progress in Polymer Science (Oxford)*. 2005;30:559–603.

Müller AJ, Hernández ZH, Arnal ML, Sánchez J. Journal of Polymer Bulletin. 1997; 39:4650–472.

Müller AJ, Progress in Polymer Science (Oxford). 2005; 30:559–603.

Muraleedharan K, Pasha L. Journal of Serbian Chemical Society. 2011. 76:1015–1026.

Naga N, Mizunuma K, Sadatoshi H, Kakugo M*Polymer*. 2000; 41:203–209

Negureanu L, Hall RW, Butler LG, Simeral LA. *J Am Chem Soc.* 2006;128:16816-16826.

Negureanu L, Hall RW, Butler LG, Simeral LA. Jour. Am. Chem. Soc. 128 (2006) 16816–16826.

Nomura K, Itagaki K. *Progress in Olefin Polymerization Catalysts and Polyolefin Materials.* 2006. 179-184.

Olabisi O, Atiqullah M, Kaminsky W.*Journal of Macromolecular Science–Reviews in Macromolecular Chemistry and Physics*. 1997;C37(3):519.

Olmos D, Dominguez C, Castrillo PD, Gonzalez-Benito J. Polymer. 2009; 50:1732–1742.

Panchenko VN, Semikolenova NV, Danilova IG, Paukshtis EA, Zakharov VA. Jour. Mol. Catal. A: Chem. 142 (1999) 27–37.

Papadimitriou SA, Papageorgiou GZ, Bikiaris DN. European Polymer Journal. 2008; 44:2356–2366.

Papageorgiou G, Bikiaris DN, Chrissafis K. Polymer International. 2010; 59:1630–1638.

Papageorgiou GZ, Achilias DS, Karayanndis GP. Polymer. 2010; 51:2565–2575.

Paredes B, Grieken RV, Carrero A, Suarez I, Soares JBP.*Macromol Chem Phys.* 2011;212:1590–1599.

Paredes B, Soares JBP, Grieken RV, Carrero A, Suarez I. *Macromol Symp.* 2007;257:103–111.

Pasquet V, Spitz R, Die Makromol. Chem. 194 (1993) 451–461.

Pédeutour J-N, Radhakrishnan K, Cramail H, Deffieux A. *Polym Intl.* 2002;51:973-977.

Pédeutour J-N, Radhakrishnan K, Cramail H, Deffieux A. *Macromol Rapid Commun.* 2001;22:1095-1123.

Pédeutour JN, Radhakrishnan K, Cramail H, Deffieux A. Macromol. Rapid Commun. 22 (2001) 1095–1123.

Pédeutour JN, Radhakrishnan K, Cramail H, Deffieux A. Polym. Intl. 51 (2002) 973–977.

Przybyla C, Tesche B, Fink G. *Macromol Rapid Commun.* 1999;20**:**328–332.

Przybyla C, Tesche B, Fink G. Macromol. Rapid Commun. 20 (1999) 328–332.

Quijada R, Rojas R, Mauler RS, Galland G B, Scipioni RB. *J Appl Polym Sci*. 1997;64:2567–2574.

Rappe AK, Skiff WM, Casewit CJ. *Chem Rev.* 2000;100:1435-1456.

Rappe AK, Skiff WM, Casewit CJ. Chem. Rev. 100 (2000) 1435–1456.G.W. Coates, Chem. Rev. 100 (2000) 1223–1252.

Routray K, Deo G. AICHE Journal. 2005; 51:1733–1746.

Sagel E, Director Polypropylene Foro Pemex. Polyethylene Global Overview *IHS*. 2012.

Sahay SS, Krishnan K. Thermochemica Acta. 2005; 430:23–29.

Sarzotti DM, Soares JBP, Penlidis A. *J Polym Sci Part B: Polym Phys*. 2002;40:2595-2611.

Schaverien CJ, Ernst R, Schut P, Dall'Occo T. Organometallics. 20 (2001) 3436–3452.

Schneider MJ, Suhm J, Mülhaupt R, Prosenc M-H, Brintzinger HH. *Macromolecules*. 1997;30:3164-3168.

Seger MR, Maciel GE. *Anal Chem.* 2004;76:5734–5747.

Severn JR, Chadwick JC, Duchateau R, Friederichs N. *Chem Rev.* 2005;105:4073–4147.

Severn JR, Chadwick JC. Germany:Wiley-VCH Verlag GmbH & Co. KGaA, Weinheim, 2008.

Severn JR, Duchateau R, van Santen RA, Ellis DD, Spek AL. *Organometallics,* 2002; 21:4-6

Simha R, Branson H. *J. Chem. Phys.* 1944;12:253-267.

Sinn H.. Tailor-Made Polymers: Via Immobilization of Alpha-Olefin. *Macromol. Symp.*, 1995, **97**, 27.

Skupinski W, Nicinski K, Jamanek D, Wieczorek Z. *Molecules.* **2005**;10*:* 659-671.

Smit M, Zheng X, Brüll R, Loos J, Chadwick JC, Koning CE. Jour. Polym. Sci. Part A: Polym. Chem. 44 (2006) 2883–2890.

Soares JBP, Hamielec AE. *Polymer*. 1995;36:2257–2263.

Soares JBP. *Macromol Symp*2007;257:1–12.

Stockmayer WH. *J. Chem. Phys.* 1945;13:199-207.

Supaphol P, Dangseeyun N, Srimoaon P, Nithitanakul M. Thermochemica Acta. 2003; 406:207–220.

Talsi EP, Semikolenova NV, PanchenkoVN, Sobolev AP, Babushkin DE, Shubin AA, Zakharov VA. *J Mol Cat A: Chemical*, 1999;131–137.

Thomas JM, Raja R, Lewis DW. *Angew. Chem Int Ed.* 2005;44:6456–6482.

Tsutsui T, Kashiwa N.*Polym Commun*. 1988;29:180-183.

Usami T, Takayama S. *Polymer Journal*. 1984;16:731-738.

Ustynyuk LY, Fushman EA, Lalayan SS, Nifantév IE. Jour. Organomet. Chem. 700 (2012) 166–179.

Vyazovkin S, Burnham AK, Criado JM, Perez-Maqueda LA, Popescu C, Sbirrazzuoli N. Thermochemica Acta. 2011; 520:1–19.

Vyazovkin S, Sbirrazzuoli N. Macromolecular Rapid Communication. 2002; 23:766–770

Vyazovkin S. J. Computer Chemistry. 2001; 22:178–183.

Vyazovkin SJ. Computer Chemistry. 1997; 18:393–402.

Wahner UM, Tincul I, Joubert DJ, Sadiku ER, Forlino F, Losio S, Tritto I, Sacchi MC. *Macromol Chem Phys*. 2003;204:1738-1746.

Wang Q, Song L, Zhao YL. Macromol. Rapid Commun. 22 (2001) 1030–1034.

Wang, B (2006). *Coordination Chemistry Reviews***250**: 242.

Wannaborworn M, Praserthdam P, Jongsomjit B. Molecules. 16 (2011) 373–383.

Watts DG. Canadian Journal of Chemical Engineering. 1994; 72:701–710.

Wilkinson G, Rosenblum M, Whiting MC, Woodward RB.*Journal of the American Chemical Society*. 1952; **74**(8): 2125–2126.

Wood-Adams PM, Dealy JM, deGroot AW, Redwine OD. *Macromolecules*. 2000;33:7489–7499.

www.bp.com/chemicals

www.ceresana.com

www.newworldencyclopedia.org/entry/Polyethylene

www.polymer.hacettepe.edu.tr/.../polymertechnologylesson/

Xia X, Xie C, Cai S. Thermochemica Acta. 2005; 427:129–135.

Xu G, Cheng D. *Macromolecules.* 2001; 34:2040-2047.

Yano A, Sone M, Yamada S, Hasegawa S, Akimoto A. *Macromol Chem Phys*. 1999;200:924-932.

Ystenes M, Eilertsen JL, Jianke LIU, Matthias OH, Rytter E, Stovneng JA. Jour. Polym. Sci. Part A: Polym. Chem. 30 (2000) 3106–3127.

Zhang C, Wu HF, Ma CA, Sumita M. Material Letters. 2006, 60: 1054–1058.

Zhuravlev LT. CRC Press, Taylor & Francis Group, 2006;131:261–266.

Zurek E, Woo TK, Firman TK, and Ziegler T. *Inorg Chem.* 2001a;40:361-370.

Zurek E, Ziegler T. *Inorg Chem.* 2001b;40:3279-3292.

Zurek E, Ziegler T. *Organometallics.* 2002;21:83-92.

Zurek E. MS Thesis, University of Calgary, Canada. 2002.

VITAE

Name: Sagir Adamu

Nationality: Nigerian

Date of Birth: January 2, 1984

Email: cesa2020@yahoo.com

Address: Department of Chemical Engineering, Ahmadu Bello University Zaria.

Academic Background: Ahmadu Bello University Zaria
(Bachelor Degree in Chemical Engineering, 2009)